HOKKAIDO UNIVERSITY

Title	Photoelectric Studies of Organized Bacteriorhodopsin Films at the Solid/Liquid Interface
Author(s)	Koyama, Koichi
Citation	. ( ) 5295
Issue Date	1998-03-25
DOI	10.11501/3137258
Doc URL	http://hdl.handle.net/2115/51488
Type	theses (doctoral)
File Information	000000322448.pdf

Instructions for use

Photoelectric Studies of Organized Bacteriorhodopsin Films at the Solid/Liquid Interface

Koichi Koyama

Photoelectric Studies of Organized Bacteriorhodopsin Films at the Solid/Liquid Interface

Koichi Koyama

Contents

Chapter 1   General Introduction

The photoelectric properties of organic molecules have been studied extensively using their thin dry films placed at the interface of conductive electrodes. In electrochemistry, photographic dye sensitization has been applied by exploiting various sensitizing dyes at the interface of a conductive or semiconductive electrode and a liquid electrolyte. Eventually, dye-sensitized electrochemical cells were proposed as a potential model for photosynthetic energy conversion. These photocells bearing a light-sensitive thin organic film produce a photocurrent due to electron transfer across the solid/liquid interface. This interface serves as an effective potential barrier to rectify the electron flow. As long as the chromophore of a molecule under electronic excitation is made to contact an electrode or a medium containing an electron donor or acceptor, the possibility arises that the chromophore undergoes electronic oxidation or reduction as a result of carrier exchange. This is the essential reason why photoelectric conversion using organic dyes more or less carries the risk of photodegradation of the chromophore, often caused by photooxidation involving singlet oxygen.

One rare exception to such cases is likely to be bacteriorhodopsin (bR), a sort of photosensitive chromoprotein that contains retinal as a chromophore in its protein cavity. Further, bR is not a redox-active molecule and its reaction site, retinal, is well protected by the surrounding close-packed helices of protein. This is not the case for photosynthetic reaction centers, other important photosensitive proteins; they perform redox reactions involving the chromophore (chlorophyll) and surrounding donors and acceptors, thus allowing for the possibility of oxidative degradation of the chromophore and under unfavorable reaction conditions. In the bR molecule, light energy is first converted to a geometrical change of the chromophore, which subsequently provides a chemical energy to transport a proton.

Structure and Function of Bacteriorhodopsin

Bacteriorhodopsin is a protein (MW 26,000) found in the plasma membrane of *Halobac-terium salinarium* [1]. The bR protein assembled into 2-dimensional crystalline arrays in the so-called purple membrane (PM) [2]. This rhodopsin-like protein uses light energy to translocate protons across the cell membrane from the cytoplasmic side to the extracel-lular side, thereby generating a substantial electrochemical gradient which is used in the synthesis of ATP, as has been described by Mitchell [3].

A spatial model ($\sim$0.7 nm resolution) of bR was published by Henderson and Unwin in 1975 [4]. Recently, improved images of bR at 0.35 nm resolution [5, 6] were obtained. In the work they made use of a unique feature of bR which is arranged in purple sheets in a very regular way, forming two-dimensional crystals. With the aid of electron microscopy and the electron diffraction technique, they revealed structures shown in Fig. 1.1.
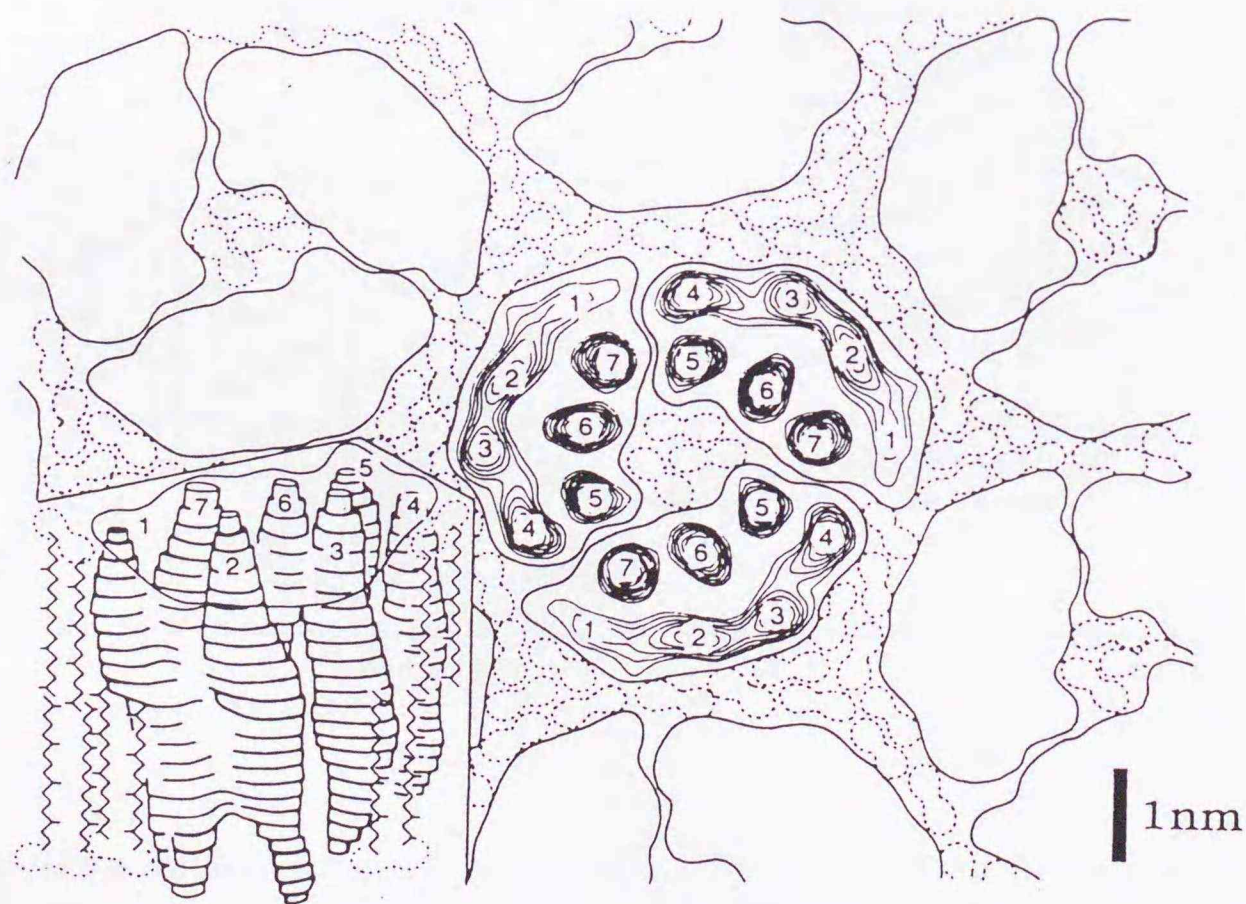
Figure 1.1: Spatial arrangement of bR. Scattering density map of the purple sheet at 0.35 nm resolution (projection onto the plane of the membrane). Reconstitution of the three-dimensional structure of a single bR molecule. Side view of the model (*Lower left*).

According to Henderson et al., a bR polypeptide chain crosses the membrane seven times,

forming seven α-helical columns, each about 3.5 nm in height and built of hydrophobic amino acid residues.

The primary structure of bR was determined by Khorana and his collaborators [7]. The protein was found to be composed of 248 amino acids forming seven hydrophobic sequences of about 24–28 residues each, interrupted by six, short, hydrophilic sequences. Moreover, there is a hydrophilic "tail" including about 20 amino acids at the C-end of the polypeptide (Fig. 1.2). The movement of protons takes place during the photocycle of bR, which operates for a time frame of 10^{-12} to 10^{-2} s. Photon absorption by a bR chromophore results in a cyclic event which involves about several stages. Each of
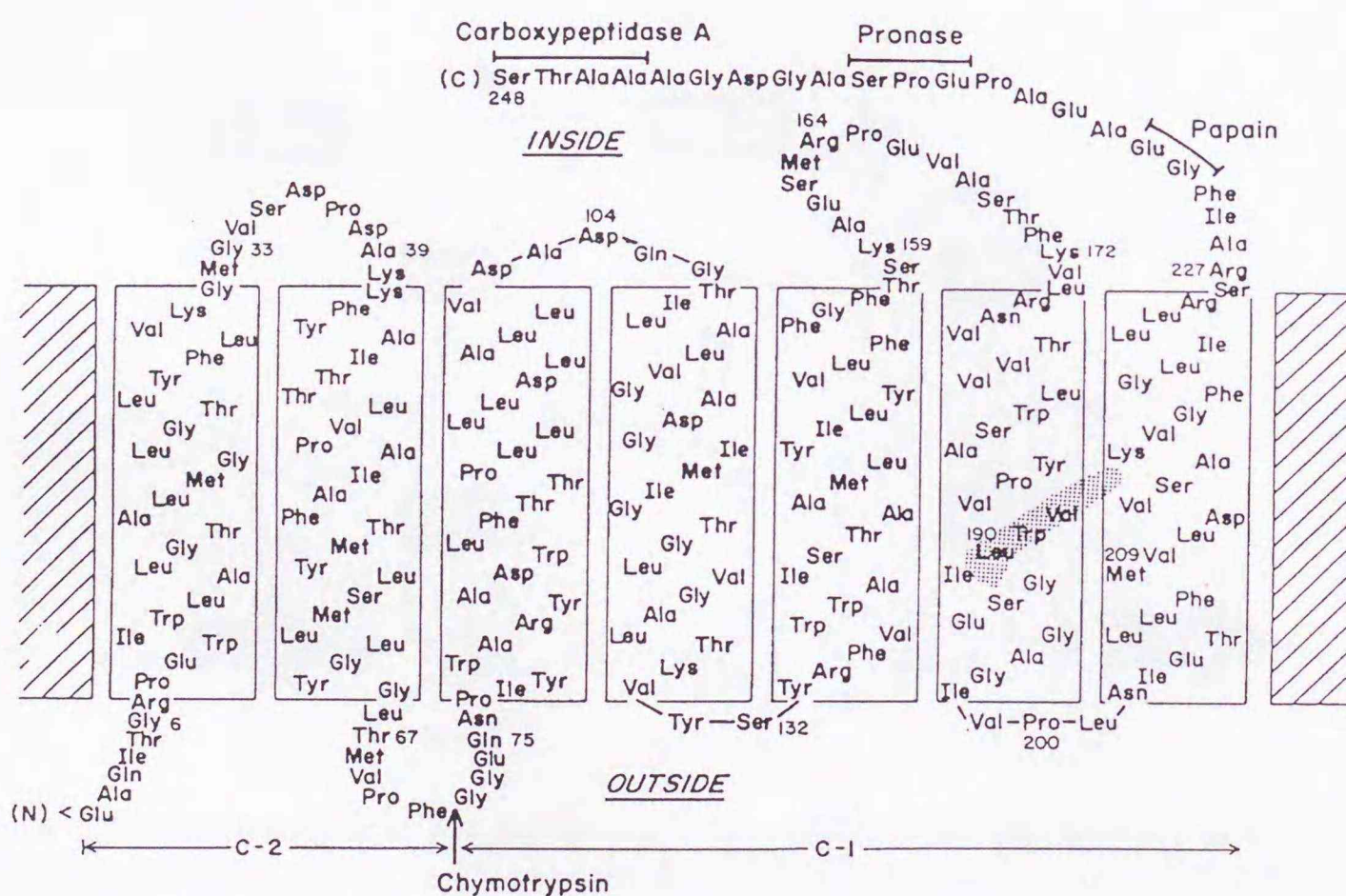
Figure 1.2: The secondary structure model of bR. BR consists of one polypeptide chain of 248 amino acids, whose sequence was determined by gene sequencing. The polypeptide is believed to traverse membrane seven times in the form of α-helical rods. A single retinal molecule linked as a Schiff base to the ϵ-amino group of Lys-216 serves as the chromophore. The shaded area represents the location and approximate orientation of retinal in the protein. Chymotrypsin cleaves bR to two fragments, C-1 (72–248 amino acids) and C-2 (1–71 amino acids). Papain removes about 17 amino acids, Pronase removes 10 amino acids, and carboxypeptidase A removes three to four amino acids from the COOH terminus of bR[8].

them can be identified by characteristic spectral shift. As early as 1971 Oesterhelt and Stoeckenius [1] described the key intermediate of the bR photocycle, absorbing at a much shorter wave length (412nm) than the parent form (568nm). This intermediate was named M. Thus, the cycle was written as $\mathbf{bR} \longrightarrow \mathbf{K} \longrightarrow \mathbf{L} \longrightarrow \mathbf{M}$, where $\mathbf{bR}$ denotes the ground state of bR, as shown in Fig. 1.3. It was suggested that the $\mathbf{M} \longrightarrow \mathbf{bR}$ transition also includes two intermediates ($\mathbf{M} \longrightarrow \mathbf{N} \longrightarrow \mathbf{O} \longrightarrow \mathbf{bR}$). The primary and sole light-driven event, $\mathbf{bR}$ to $\mathbf{K}$ transition, occurs extremely fast ($\leq$ps) [9] and is accompanied by isomerization of retinal chromophore from the all-trans to 13-cis form. All subsequent steps are thermal relaxations with characteristic absorption maxima in the visible and UV region, similar to the reaction cycle of vertebrate rhodopsin.
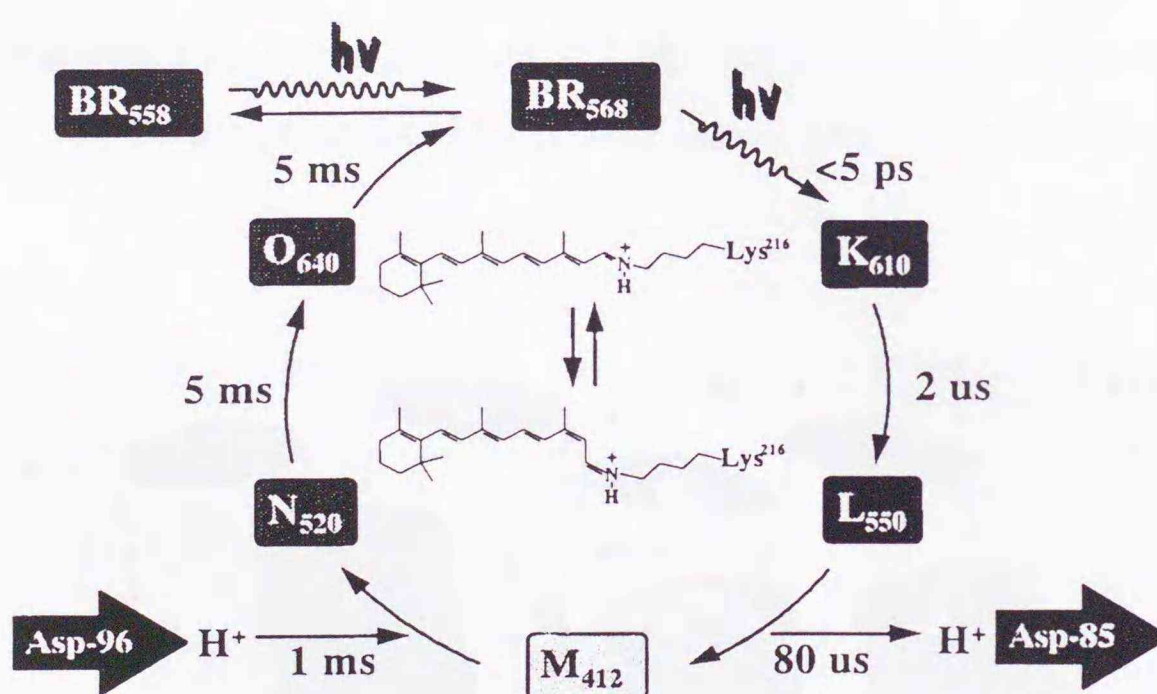
Figure 1.3: Intermediates of bR photocycle. The parent pigment, light-adapted bR (bR$_{568}$) contains an all-trans retinal residue attached to Lys-216 with a protonated Stiff base linkage. Photon absorption converts bR to $\mathbf{K}$ which regenerates bR$_{568}$ via $\mathbf{L}$, $\mathbf{M}$, $\mathbf{N}$ and $\mathbf{O}$ intermediates. Trans-cis photoisomerization of retinal about the $C_{13}{=}C_{14}$ bond translocates the Schiff base to a new environment inside the membrane. The $\mathbf{M} \longrightarrow \mathbf{O}$ transition is accompanied by proton transfer from a protolytic group of the protein to the Stiff base nitrogen. In the dark, bR$_{568}$ slowly converts to a dark-adapted form bR$_{558}$ which contains approximately equal amounts of all-trans and 13-cis retinals. Subscripts refer to absorption maxima.

Storage of bR for several hours in the dark gives rise to dark adaptation of this protein when about 50% of the all-trans bR$_{568}$ molecules convents to bR$_{558}$ which contains a 13-cis retinal residue. The Stiff base in Illumination induces a fast bR$_{558}$ $\longrightarrow$ bR$_{568}$ transition

(light adaptation) [10, 11].

To describe the relationship between the function and the structure of bR, a number of models for the proton transfer mechanism have been proposed [12]. Site-specific mutangenesis of bR in combination with refined electron diffraction studies [5] made it possible to specify the key amino acids working as proton channel in the retinal pocket. These experiments revealed that only three or four key amino acid residues affects the photocycle and proton transfer of bR [13, 14]. Most recent proton pumping mechanism is shown in Fig. 1.4. After excitation by light (**bR** to **K**), (1) Schiff base proton is transferred to Asp-85 (**L** to **M**). When Asp-85 is protonated, the pKa of Glu-204, which has recently been identified as a proton releasing group at the extracellular side [15], is decreased [16]. As a result, (2) a proton is released to the extracellular side. This is followed by the trans to cis reisomerization and (3) proton transfer from Asp-96 to Stiff base occurs (**M** to **N**). After that, (4) Asp-96 is reprotonated by picking up a proton in the cytoplasmic side (**N** to **O**).
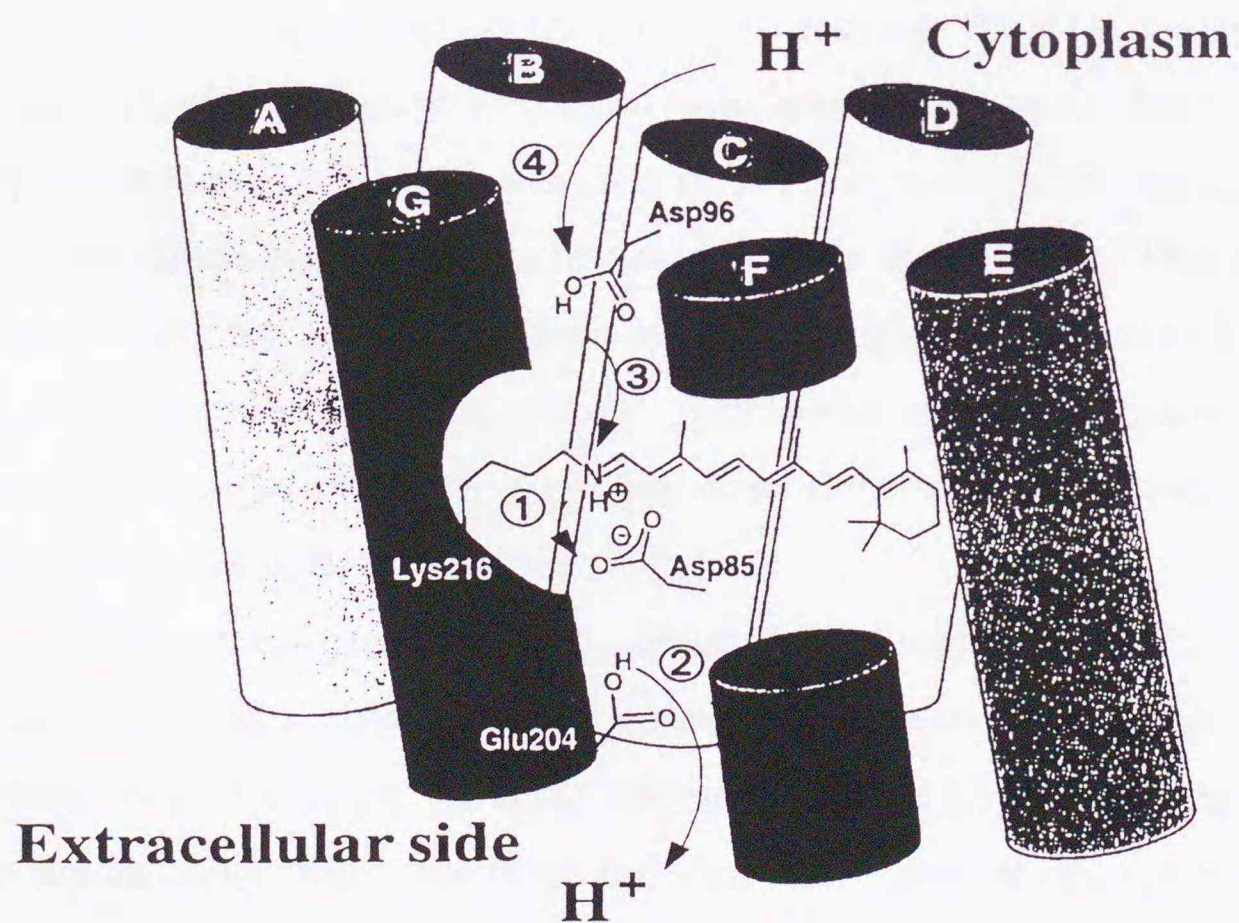
Figure 1.4: Schematic structure of the proton transfer pathway in bR including the key amino acid residues.

Photoelectric Aspects of Bacteriorhodopsin

The intrinsic properties of bR are most suitable for optical and optoelectronic applications due to (1) long term stability of the protein against thermal and photochemical degradation, (2) fast photochemical reactions with displacement of electric charges, (3) large shifts in the absorption spectrum accompanying the photocycle, which permits accurate and reproducible assignment of the states, and (4) the ability to form thin, ordered films by using the Langmuir–Blodgett (LB) method or other versatile techniques for molecular organization that allow these materials to be incorporated into devices.

In the early years after the discovery of the photoelectrochemical conversion power of bR, experimental systems were developed to prove Mitchell's chemi-osmotic hypothesis [17] or to construct solar energy cells optimized for highest quantum yields to generate a steady photocurrent [18, 19]. Later, it was pointed out that air-dried thin films of PM might be used to construct "biochips" [20]. Even the application of bR's photoelectric effects for constructing "computational elements" have been considered [21].

For long time there were a number of photoelectric studies, from which no strong conclusions can be drawn, because either the apparatus response function was not properly taken into account, or important experimental parameters were missing (like temperature, pH), or the experimental conditions were not suited to establish well defined microconditions (like membrane filters). Only a few studies made strong cases. This unbalanced situation can be ascribed to the difficulties of designing photoelectric experimental systems that allow for undistorted measurement of molecular charge displacements, as well as for kinetic spectroscopy with high resolution. Even the proof for undistorted recording of electrical signals was difficult to achieve [22].

Since photoelectric measurements rely on the topological asymmetry of PMs, the membranes must be oriented with respect to the electrodes. A variety of method have been used to obtain oriented samples, including electric fields, and all kinds of interfaces—like immiscible liquids, solid/water interfaces and thin films. Several quite different experimental systems are currently in use. Five experimental systems can be distinguished according to the way the PMs or vesicle preparations are oriented. Typical references referring to the laboratories in which the techniques were established are given:

1. Orientation by adsorption at hydrophobic/hydrophilic interfaces like air/water [23].

2. Orientation by adsorption to thin supporting films. The films may consist of membrane filters [24], or phospholipid membrane [25].

3. Orientation by small electric fields in samples of large dimensions. PMs can be oriented by immobilization in polymers [26].

4. Orientation by electric fields in measuring cells of flat dimensions where the two electrodes close enough to form a capacitor. The PMs can be transiently oriented by short voltage pulses if the solvent is water [27] or permanently oriented by sedimentation in dc fields before drying the sample [28].

5. Transmembrane incorporation into liquid bilayer membranes, allowing for application of transmembrane gradients in the pH or the voltage [29].

From the polarity of the photovoltage and the fact that a positive charge, H^+, is transported from the cytoplasm to the extracellular side, the sidedness of orientation becomes unequivocally defined in such experiments. However, observations made in the various experimental systems are contradictory: at near neutral pH, the cytoplasmic side appears to carry more negative surface charges than the extracellular side as concluded from adsorption to cationic ion exchange films [30], from orientation in electric fields [27], and from sedimentation onto metal electrodes [28]. The opposite direction of adsorption was found when PMs adhered to lipid bilayer membranes which were positively charged by the addition of small amount of octadecylamine [31].

By using dry PM films deposited on a conductive glass, Nagy first measured photoelectric response [32]. Váró later studied the photovoltaic effects of electrodeposited PM films by vacuum depositing a counterelectrode on the PM film [28]. Both methods required a unidirectional orientation of PM to elicit efficient photoresponse. Many other photoelectric measurements have been conducted, including dry and wet systems, as reviewed by Trissl [33].

Such work has stimulated investigation on many potential applications [34], such as spatial light modulators for optical computing systems [35] and real-time holography us-

ing a bR mutant [36]. In photocells using thin films of PM, it was believed that the degree of photoelectric response depends significantly on the orientation of the PM fragments because of the highly directional nature of this membrane protein. Photoelectric measurements showed that PM films prepared by conventional techniques described above seem to be non-randomly oriented, although it has not yet been possible to determine quantitatively the extent of orientation achieved by these techniques.

In this thesis, the author would like to describe a unique photoelectric response obtained by a bR immobilized electrochemical cell and its application for optoelectronic devices in Chapter 2 and 3. Chapter 4 and 5 will deal with the determination for orientation of bR molecules on a solid substrate and a rational method to control the orientation of PM films by antibody techniques. In Chapter 6 and 7, we will discuss a possible mechanism for generation of photoelectric response from the bR-based electrochemical cell using various mutant proteins of bR in combination with a laser technique.

Chapter 2   Photoelectric Response from Bacteriorhodopsin Films at the Electrode-Electrolyte Interface

2.1   Introduction

In vitro photophysics of bacteriorhodopsin (bR) has stimulated a number of potential studies in the design of light conversion systems based on the photoreactions of this retinal analogue. Occurrence of vectorial charge transfer and proton pumping in the photoexcited bR enables the design of bR-based dry photovoltaic cells with relatively high output voltage and sufficient durability [33]. An extended study for image detection using bR photovoltaic cells has currently been attempted as an approach to an artificial visual receptor [37]. Membrane preparation for the photovoltaic cells has mainly employed the electrodeposition technique [28] that yields a relatively thick layer of purple membrane PM. A two-dimensional array of PMs can be formed at the air-water interface [23] and its LB films have successfully been incorporated in a photovoltaic sandwich cell by Furuno et al. [38]. Use of the photovoltaic cells with electrode/PM/electrode junctions, however, involves disadvantages due to dry PM films such as instability of the electrical outputs against ambient humidity and high electric resistivities suppressing the production of photocurrents.

The LB technique enables molecular-order assembling of functional proteins essential for the design of bioelectronic devices. We have established a method to obtain efficient and stable photocurrent response from a PM film as thin as a single monolayer, using an electrochemical system under potentiostatic regulation of electrode. The present study shows light conversion characteristics of the bR-based photoelectrochemical cell.

2.2   Materials and Methods

PM was purified from the plasma membrane of *Halobacterium salinarium* (S-9 strain) by
the conventional method [39] and was suspended in pure water to give an optical density
of 5–7 (570 nm).

The suspension was mixed with hexane and DMF (dimethyl formamide) at the volume
ratio H_2O/hexane/DMF of 10 : 10 : 2 and vigorously agitated on a Voltex mixer to yield an
opaque reddish emulsion. The emulsion was then carefully applied on an aqueous surface
(neutral pH, room temperature) set in a Langmuir film balance to form a monolayer film
of PM. This method caused no dissolution of PM into the aqueous subphase, allowing
direct measurement of pressure-area isotherms for the monolayer. The monolayer film
thus formed was compressed at a rate of approx. 10 cm^2/min. Transmission electron
microscopy [40] has revealed that the PM monolayer is a 2-dimensional array of randomly
dispersed fragments of PM (approx. 0.5–1.0 μm in size).

The PM monolayer was deposited and built up on the surface of an SnO_2 electrode
(4500 Å thick SnO_2 layer with an effective area for electrolysis of 0.5 cm^2, specific re-
sistance of $4 \times 10^{-4} \Omega$cm) by the modified horizontal transfer method [41] under a surface
pressure of 20 mN/m. The PM-LB film thus prepared had a characteristic broad absorp-
tion spectrum of bR with its maximal absorbance at around 570 nm being proportional
to the number of monolayers with the slope of 0.002/monolayer.

In the three electrodes system, the PM coated SnO_2 electrode was set in an electro-
chemical cell containing 0.1 M KCl as a supporting electrolyte, together with a counter
electrode (platinum) and a standard calomel reference electrode (SCE). For photocur-
rent measurement, the electrode potential of SnO_2 was regulated with respect to SCE by
means of a Toho Technical Research Model 2020 potentiostat and photocurrent outputs
recorded on a Gould Model 420 digital storage oscilloscope or a Graphtec Model WX2400
XY recorder.

In two electrodes system, a small amount of an aqueous electrolyte, which was typically
an aqueous gel comprising 4% carboxymethylchitin and 1 M KCl (pH 7 to 8), was then
applied on the PM film, and the electrolyte was sandwiched with a counterelectrode (an

Au-sublimated glass plate) by use of a Teflon spacer (200 μm thick) (Fig. 2.2(A)). The photocurrent was monitored by a Gould Model 420 or a Hewlett Packard Model 54520C digital storage oscilloscope.

All electrochemical measurements were performed under aerated conditions at room temperature. A 150 W xenon arc lamp was used as a light source in combination with a green band-pass filter and IR-cut filter, which provided green light irradiation with an intensity maximum at 530 nm, a half band width of 65 nm, and an incident power at the electrode of 10 cm^2.

2.3   Results and Discussion

2.3.1   Characterization of PM Monolayers

The PM monolayer formed on neutral water gave stable surface pressures up to >40 mN/m. Figure 2.1 shows a typical pressure–ares (π–A) isotherm for the monolayer, where the area was formally given as the film area per bR molecule based on a known total amount of bR added on the water surface.

2.3.2   Photoelectric Response and Action Spectrum

Irradiation of green light onto the PM film through the SnO$_2$ electrode by a 150 W xenon lamp caused a photocurrent response with the time profile shown in Fig. 2.2(B). Positive and negative transient photocurrents are generated when light is switched on and off, respectively; these pulses are followed by rapid relaxation to the background level [42].

This characteristic response is attributed to a charge displacement occurring in the photoexited bR molecule. Excitation of a light-adapted bR causes a rapid trans to cis isomerization of the chromophore retinal accompanied by a change of dipole moment, which is followed, via thermal intermediates named **K** and **L**, by the vectorial transfer of protons (proton pumping) within the bR molecule. Excitation of bR ultimately brings about charge displacement that induces an electric current on an electrode adjacent to the molecule. The action spectrum of the transient photocurrent (Fig. 2.3) coincides with
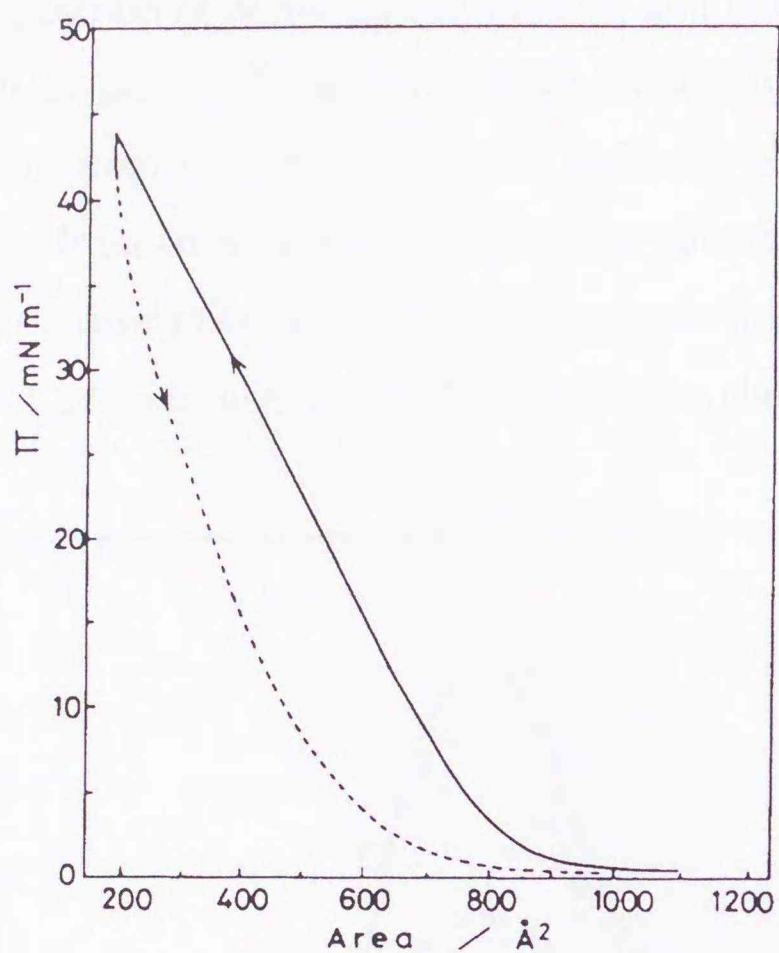
Figure 2.1: Surface pressure (π)–area isotherm of a PM monolayer film at approx. 25°C at the air-water interface. The aqueous phase contained 10^{-3} M phosphate buffer (pH 6.4). Cyclic scanning of the isotherm was reproducible. The abscissa represents film area per bR molecule.
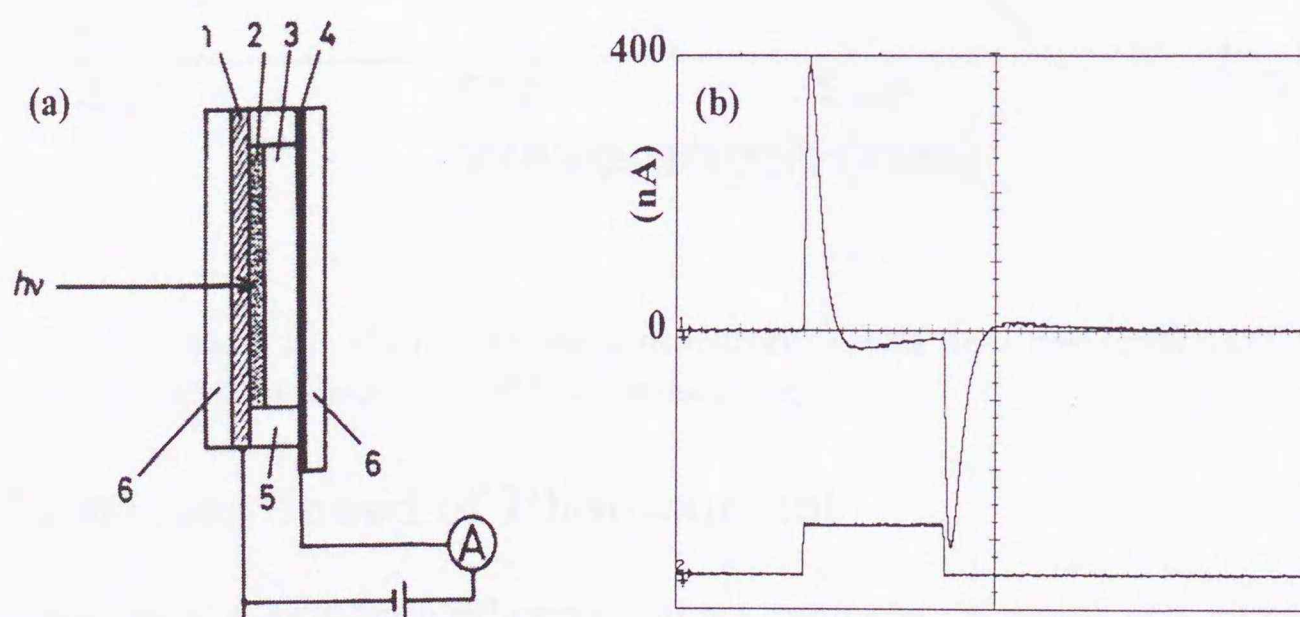
Figure 2.2: (A) Structure (cross section) of a bR-immobilized photocell; 1. SnO_2 transparent conductive layer; 2. PM-LB film (typically six to ten layers); 3. aqueous electrolyte gel layer comprising 6% carboxymethylchitin and 1 M KCl; 4. Au layer as counterelectrode; 5. Teflon ring spacer; 6. glass substrate. (B) Typical profile of the time response of bR-induced photocurrent.

the broad absorption spectrum of bR (at 450 to 650 nm) and indicates that the origin of photoresponse is bR. In the photocell, the photocurrent induced by bR is strongly rectified in the cathodic direction (from the electrolyte to the electrode side). Rectification of the photocurrent may result from an electric field established spontaneously at the interface of an oxide electrode (negatively charged) and an aqueous electrolyte phase including the thin PM film, which is a phenomenon characteristic of electrochemical interfaces.
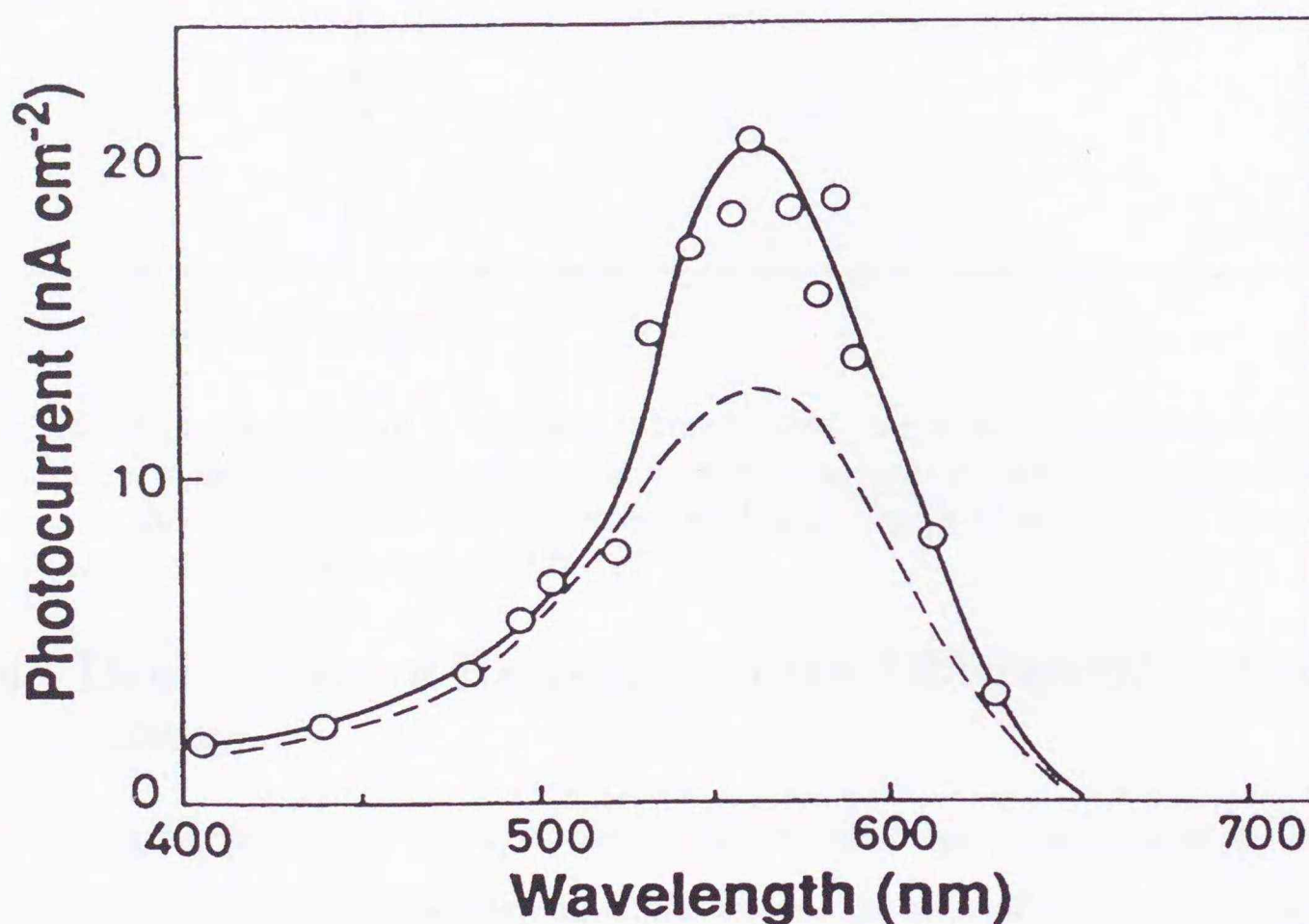
Figure 2.3: Action spectrum of bR-induced photocurrent (*solid line*) measured with a film of two PM layers, and optical absorption of bR (*dashed line*).

2.3.3   Response Speed of Photocurrent

The time response of a light-induced signal output from the photocell was examined by a digital storage oscilloscope under flush excitation with a light pulse of $\sim$50 μs. Figure 2.4 shows the response profile of a signal and a reference light pulse monitored by a photodiode. The transient response takes place within a time range of about 200 μ. This supports that the photocurrent is associated with the proton transfer process (**L** to **M** transition, $\sim$100 μs) in the photocycle of bR.
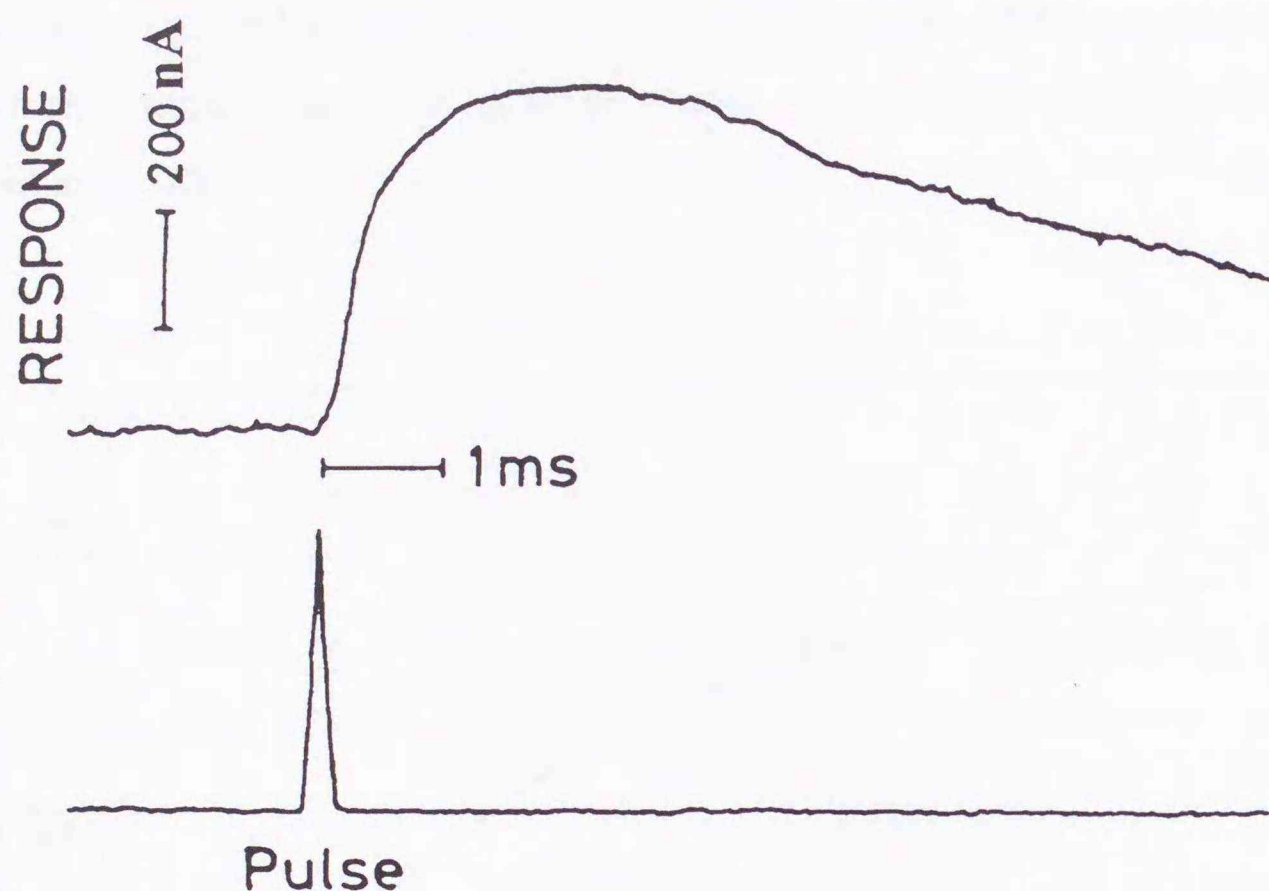
Figure 2.4: Time response of a transient photocurrent under flush excitation of a stack of PM-LB film, monitored by use of a digital storage oscilloscope. In order to reduce the external electric noise this measurement was performed with a sandwich type photocell (two electrode system) bearing a thin electrolyte gel[42].

2.3.4 Dependence of Response on the Differential of Light Intensity

The photoelectric output of the bR-based photoreceptor was examined as a function of the differential of the light intensity, in other words, the rate of change in imaging light intensity. The measurement demonstrates how sensitively the photoreceptor responds to the rapidity of motion when a moving object is sensed. A rotating sector equipped with an optical wedge was adopted to generate various gradients in light intensity at the photoreceptor plane. A 150 W xenon arc lamp in combination with a long pass filter was used as the light source, which gave a maximum intensity of 5–10 mW/cm^2. Figure 2.5 shows a typical result obtained with a photoreceptor comprising of a LB film of 6 PM layers in which the abscissa represents the intensity differential, dI/dt. The relation between the output (peak value of transient photocurrent) and the intensity differential was eventually found to be a nonlinear and appear to fit a hyperbola. The mechanism for this nonlinear relationship is not clear at the present stage of investigation. It was

confirmed from the result that the photoreceptor is capable of sensing the rapidity of motion of an optical image; the faster an object moves, the larger the photoreceptor output becomes [43].
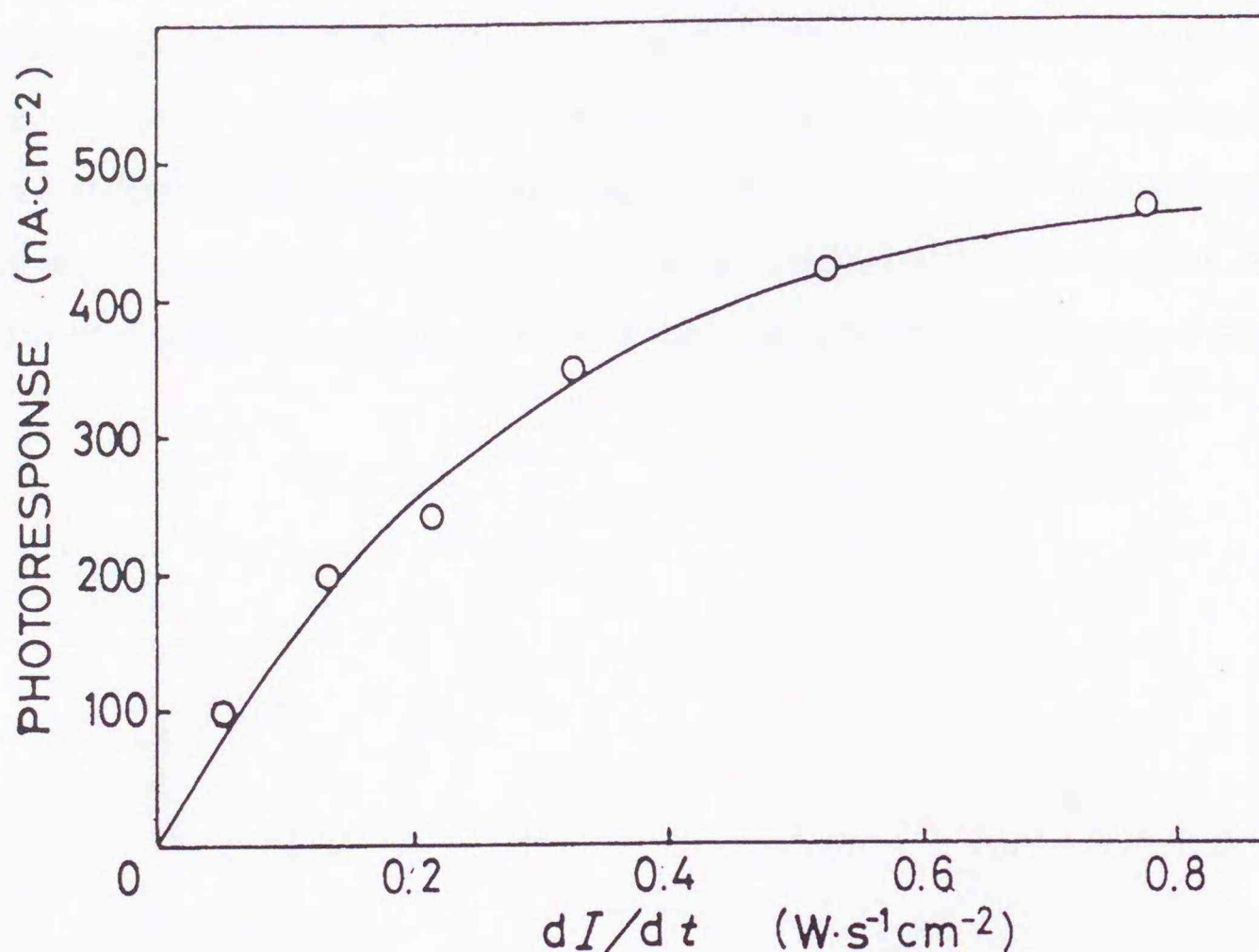
Figure 2.5: Plot of the photoeletric output of the bR-based photoreceptor against the differential of light intensity. Peak photocurrents were obtained from 6 PM monolayers on an SnO_2 electrode under irradiation of visible light ($>$470 nm) as a function of the slope (dI/dt) of change of light intensity. The dI/dt value was obtained based on the light intensity change monitored by a commercial radiophotometer.

2.3.5 The Quantum Efficiency and the Light Intensity Dependence of Photocurrent

Quantum conversion efficiency of the present photocell was determined by the photocurrent measurement under monochromic excitation of a PM film in the electrochemical cell. An electrode bearing 6 PM monolayers, which absorbs about 2% of incident light, was irradiated at 550 nm using an interference filter (half-band width, 8 nm). This gave pho-

tocurrents of >60 nA/cm^2 under an incident photon flux of 4×10^{15} photons/s per cm^2 determined by means of a radiophotometer (EG&G) calibrated with ferroxalate chemical actinometry. The result shows that the quantum efficiency for the present system was in the order of 1.0×10^{-2}, which is regarded as much higher than those previously attainted with bR-mounted dry photocells as estimated from their experimental conditions [44].

The bR-based photocell showed a linear relation between the output photocurrent and the light intensity, as is exhibited in Fig. 2.6. The linearity covers an intensity region of at least 3 orders of magnitude ranging from 10^{-4} to 10^{-1} W/cm^2. This excellent linearity in light sensing makes it possible to detect small changes in brightness that occur even when the photoreceptor is being exposed to the high-intensity irradiation of sunlight.
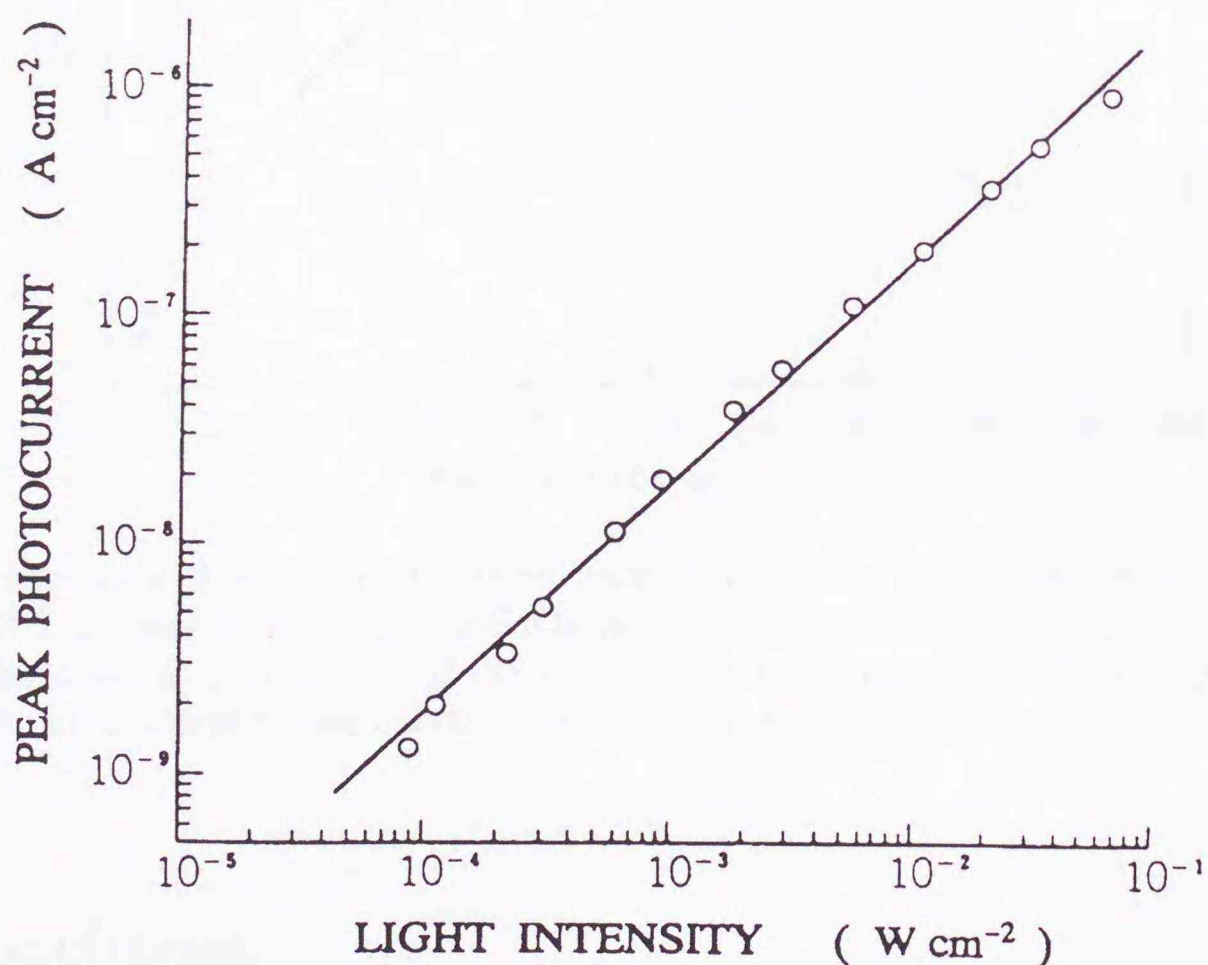
Figure 2.6: Relation between the bR-induced photocurrent (transient peak value) and the light intensity incident to the PM film. Light intensity represents the quantity of a transient charge that occurred in the intensity from a ambient intensity level, to which the photocell can respond.

2.3.6 Relation between Photocurrent and the Number of PM Layers

Photocurrent tends to be saturated in magnitude as the number of PM monolayers built up on the electrode is increased. This tendency is shown in Fig. 2.7, which plots the peak photocurrent versus the number of layers of PM-LB film, i.e., film thickness (one PM monolayer is approx. 4 nm thick). The result implies that the contribution of bR to photocurrent is limited to the PM layer positioned close to the electrode surface where the field effect becomes more significant.
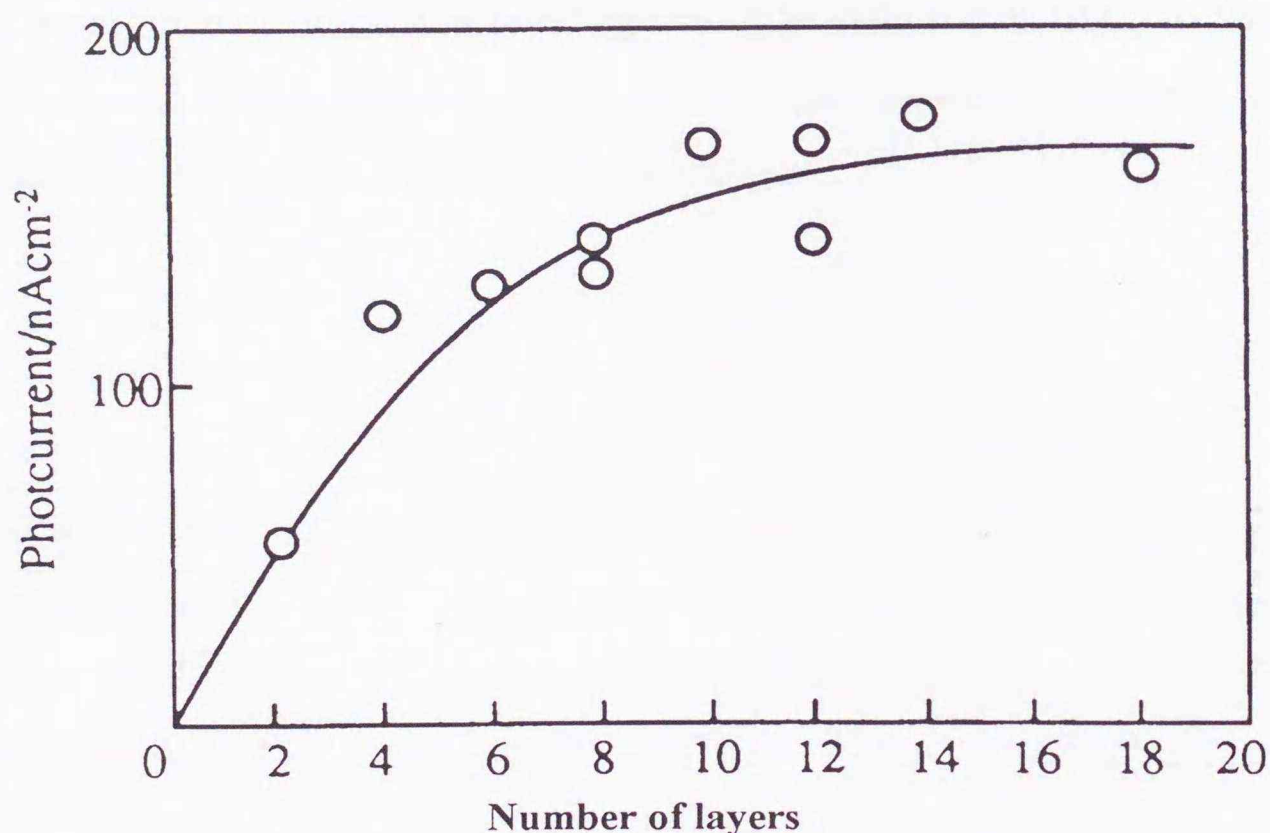
Figure 2.7: Magnitude of bR-induced photocurrent as a function of the number of PM monolayers. PM-LB films were build up on the SnO_2 electrode surface and their photocurrents were measured under cathodic polarization of the electrode potential (around -0.5 V vs SCE, three electrodes system) in a neutral electrolyte solution (0.1 M KCl).

2.4 Conclusion

A photoelectrochemical cell which adopted for the first time the membrane of bR as a light-sensitive eletrode-electrolyte interfacial layer was demonstrated here. It is proved that efficient bR-induced photocurrents are produced by this system under optimized elec-

trochemical conditions without using any redox compound or additional sensitizing agent in the electrolyte. Quantum conversion of light to electric current by the bR membrane, which has been practically restricted in the case of dry photovoltaic cells, is achieved by the present electrochemical method. The characteristic differential responsivity of the photocurrent resembles the function of biological photoreceptors in their light sensing behavior. Use of bR as a light-sensing material is thus highly promising for the design of future bioelectronic devices.

Based on the present technique, we have in fact attempted the construction of a bR-based image sensing system with a simplified sandwich cell structure [42]. This system proved to be capable of processing input optical information according to the response function illustrated in Fig. 2.2(b). An extension of this system to development of a bR-based artificial retina is described in the next Chapter.

Chapter 3

Image Sensing and Processing by a Bacteriorhodopsin-based Artificial Photoreceptor

3.1 Introduction

Device implementation and architecture for visual information processing provides a key solution to overcoming the recent extensive need for pattern recognition and image compression in transaction of high-density information. Silicon-based analog very-large-scale-integration technology combined with high-speed parallel computation circuitry revealed itself to be an immediate means to mimic the functions of a visual system. Silicon-based technology however necessitates the loading of integrated devices and circuits onto a chip. In the human retina, photoreceptors laterally arrayed in the receptive field perform real-time parallel processing of visual information. Retinal photoreceptors are endowed with differential responsivity to light, which, as a spatial filter, enables rapid extraction of edge profiles from images at the materials level, which is necessary primarily for pattern recognition. Material-level implementation of visual functions with minimal hardware is highly sought after for real-time parallel processing of images but is difficult to realize in the range of existing solid-state technology.

Bacteriorhodopsin (bR) is a protein analog of the visual pigment and and performs a unique light-driven cyclic reaction. This molecule demonstrates enormous potential when incorporated as the photoreceptive element of an optoelectonic device. The high responsivity and excellent stability of bR enable the design of multifunction optical devices and memories that are useful for information processing. The rapid reversible chromism of bR has recently been applied for a real-time holographic memory [45] and spatial light modulators for optical computation [35], both of which ensured the protection of bR from laser irradiation.

The photoelectric responsivity of bR has been studied extensively for light sensing

applications [33]. An extremely rapid photoelectric response within a time range of picoseconds can be obtained that is generally ascribed to the initial charge displacement of bR on its extinction to the so-called **K** intermediate [46]. This rapidity, surpassing those of solid-state photodiodes, implies a potential advantage of bR for the design of real-time image processing systems. The first application of bR to image processing was undertaken by Lewis and co-workers who attempted implementation of bR-immobilized reception fields to mimic the edge detection mechanism of the retina [37] and proposed a neural network architecture that uses a bR-based dry photovoltaic cell [47].

We have developed an electrochemical photocell that immobilizes a bR thin film at the solid-liquid interface [42]. It was found that this wet-type photocell intrinsically possesses differential responsivity to light intensity. This material-level differential responsivity allowed us to design an artificial photoreceptor that is capable of detecting motion and edge information of images in real time. Here we describe the image processing capability of a bR-based artificial photoreceptor that has been developed as a retina model [48].

3.2   Results and Discussion

3.2.1   Photoelectric Aspect of the BR-Based Artificial Photoreceptor

We previously fabricated a bR-based photoreceptor, using a thin bR membrane immobilized at the interface of the electrode and aqueous electrolyte in an electrochemical sandwich-type photocell [42]. When a thin film of bR was placed on a metal oxide electrode such as SnO_2 and had contact with an aqueous electrolyte, light-excited bR molecules caused a photocurrent that responds differentially to change in light intensity. A typical profile of such a response is depicted in Fig. 3.1. The photocurrent originates from the light absorption of the bR molecule as has been confirmed by its action spectrum [42] that coincides with the broad spectral absorption of bR over wavelengths of 450–650 nm with a peak around 560 nm. Generation of the differential photocurrent was always rectified in the cathodic direction, i.e., from the electrolyte to electrode side. The bR-based photoreceptor is thus characterized as a differentially responsive photodiode for

visible light detection and is regarded as a simple model for retinal ganglion cells having a similar responsivity. In order to examine the image sensing and processing abilities of bR, we attempted two-dimensional implementation of this photoreceptor as described below.
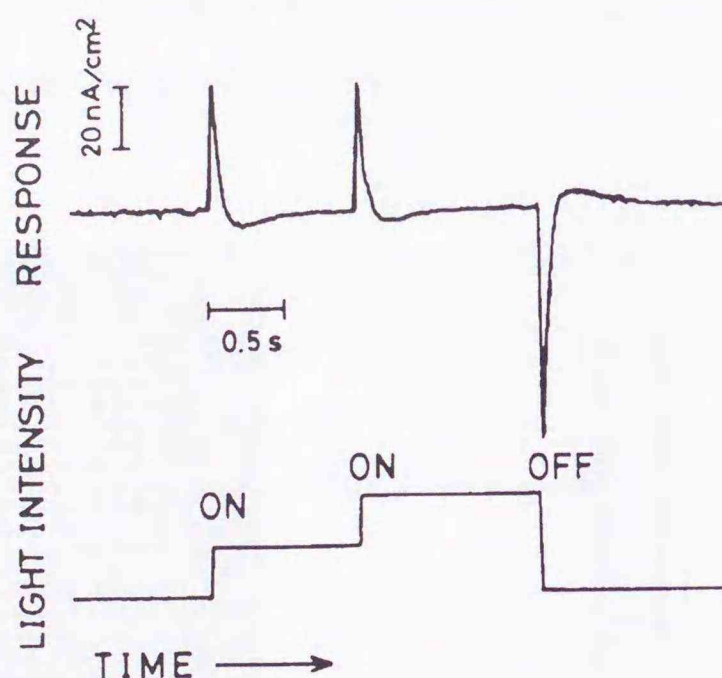
Figure 3.1: Response profile of photoelectric signals from a bR-based photoreceptor. The light intensity was changed stepwise during irradiation by use of neutral density filters. Its pattern as monitored by a photodiode is shown at the bottom at which each step corresponds to an equivalent change in light intensity of approx. 2 mW/cm^2. The response apparently takes place in a differential mode against light intensity change.

3.2.2 Fabricating BR-Based 256-Pixel Image Sensor

Implementation of BR-Based Photoreceptor

Purple membrane (PM) that contains two-dimensionally crystallized bR molecules was isolated from S-9 strains of *Halobacterium salinarium* using the conventional method [39], and fragments of PM were suspended in pure water.

The PM-immobilized (bR-based) photoreceptor was fabricated fundamentally by following the previously described method; it had a sandwich structure comprising the electrochemical junctions of working electrode/PM film/aqueous electrolyte gel/counter electrode. As a working electrode that immobilizes thereon a thin film of PM, an optically transparent indium tin oxide (ITO) electrode was prepared that has a two-dimensionally arrayed 256 square pixel (1.3×1.3 mm) ITO layer (100 nm thick) on a glass plate (50×50 mm). Figure 3.2(a) shows the pixel pattern of the ITO electrode. Each pixel had an inde-

pendent wire (70 μm width) leading to the terminals aligned at four edges for connection with an external parallel circuit for signal amplification. The wire region that excludes the pixels was covered with an insulting and colored coating of Si in order to keep the wire from contact with the electrolyte as well as from exposure to incident light. The light receptive area made of the pixel network was 31×31 mm in size.
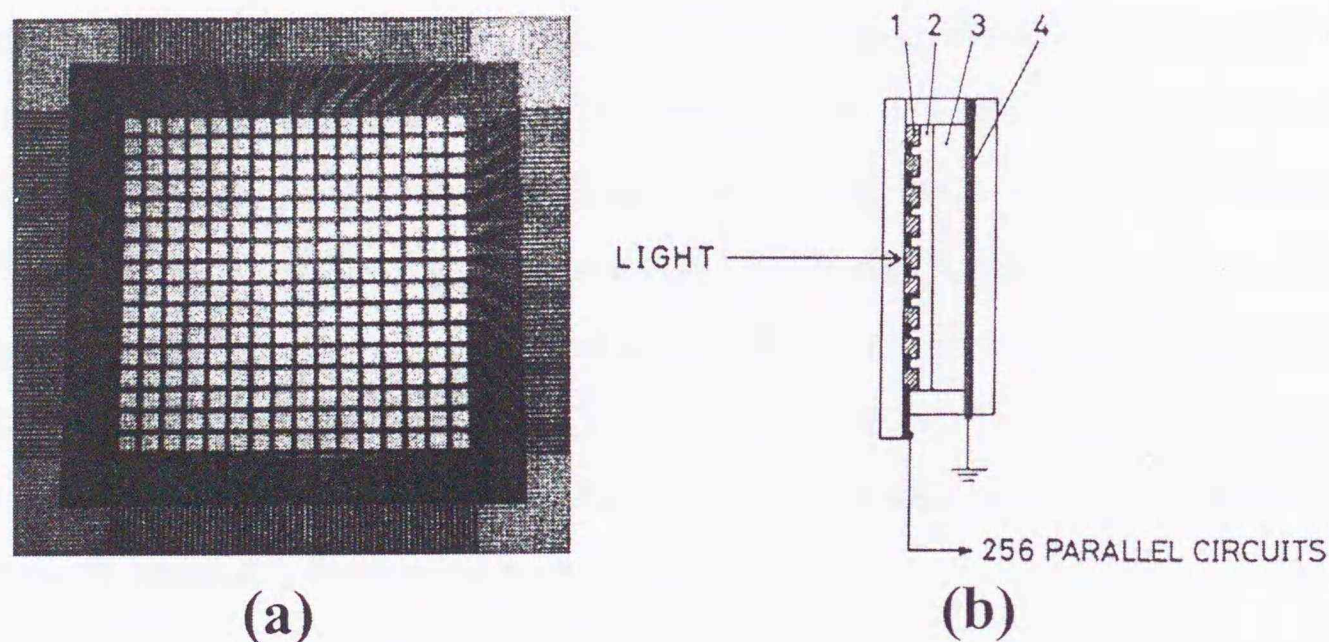
Figure 3.2: (a) 256-pixelized network pattern of an ITO electrode. (b) Junction structure of the bR-based pixelized photoreceptor; 1, 256-pixel ITO electrode; 2, bR film; 3, electrolyte gel comprising 4% carboxylmethylchitin and 2 M KCl; 4, gold counterelectrode.

The entire surface of the pixel-bearing side of the ITO substrate was coated with a Langmuir-Blodgett (LB) film of PM by the LB technique as described in Chapter 2. The LB film typically consisted of a stack of 10–14 layers of PM, each PM layer corresponding to one monolayer of bR molecules. A portion of the LB film on the edge terminals was wiped away and the film that remained on the pixel region was dried under air. A Teflon ring spacer (300 μm thick) was placed on the electrode so as to surround the pixel array, and the internal cavity was filled with a viscous gel of an aqueous electrolyte composed of 4% carboxylmethylchitin and 2 M potassium chloride (pH 7.4). A gold-coated glass plate that served as a counterelectrode was finally superposed onto this gel layer, and the outer joints of the sandwich cell were shielded with an epoxy adhesive agent. An image sensor of a sandwich-type structure thus fabricated is sketched in Fig. 3.2(b), which comprises a 256-pixel bR-based photoreceptor.

Signal Transmission and Image Display

The image sensor was electrically combined at its edge terminals with edge connectors that are combined to parallel circuits for signal amplification. Figure 3.3 shows the amplification circuit that includes the display device. Light induced small currents from each pixel were converted to a dc voltage, amplified by an operational amplifier and resistors, and finally output to light-emitting diodes (LED's, 6×6 mm), which constituted a display panel composed of 256 image units. The LED we used has a threshold voltage for emission of 1.5 V, which corresponds to an initial photocurrent at each pixel of 5 nA. With the use of 1 MΩ resistance in signal amplification and 10 nF capacitance for noise reduction, the *RC* time constant of the signal conversion circuit was theoretically limited to 10 ms. The whole sensing system was composed of the bR image sensor, circuit-integrated body, and the LED display panel (10×10 cm). As a consequence, the light response generated at each pixel in the image sensor was simultaneously displayed as light emitted by each LED through parallel information transaction.
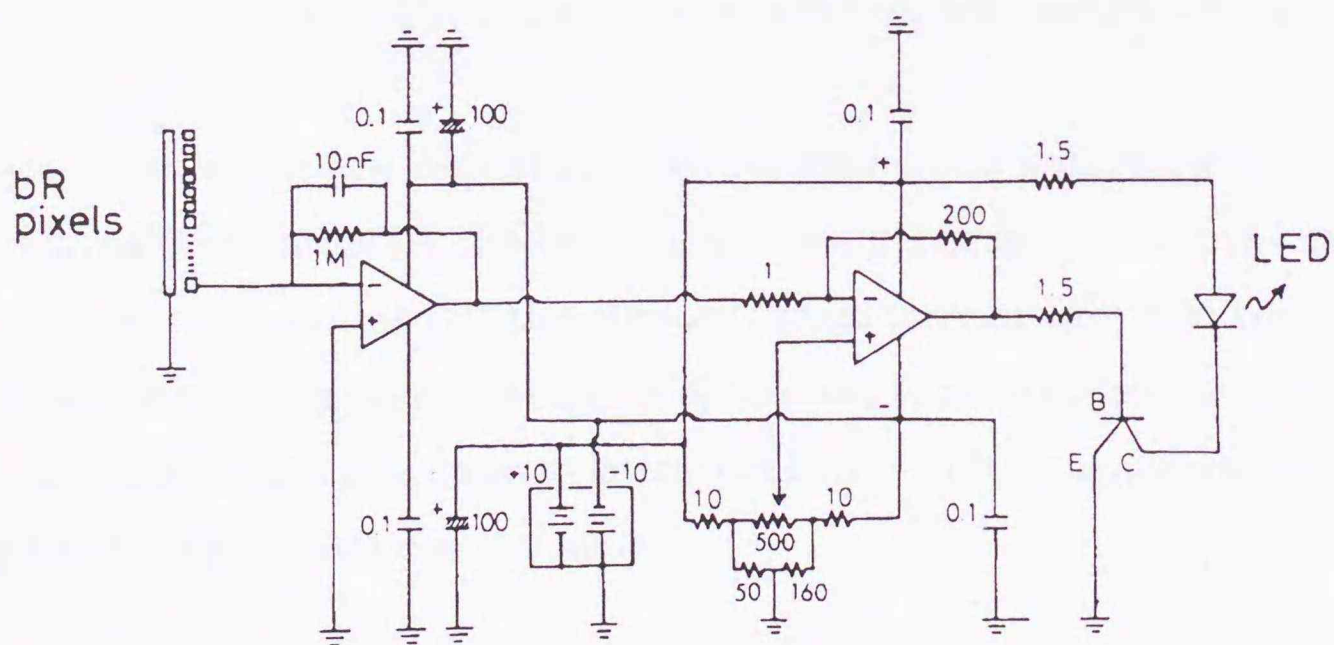
Figure 3.3: Signal transmission and amplification circuit for image display. Photocurrent produced at the photoreceptor (*left*) are converted and amplified in the voltage mode by a dual operational amplifier to output to a LED (*right*) for display of images. The circuit takes place the form of parallel signal processing.

Image Projection and Optical Modulation

A commercial 150 W slide projector was used as a light source, and its white light that passes through a slide of various optical images and patterns was irradiated to the photoreceptive plane of the image sensor.

Two types of optical modulation were applied to the image that is incident upon the sensor. For detection of the entire form of an image, we mechanically chopped incident light, using a rotating sector with a light-cutting frequency of 20–50 Hz and an exposure-to-non exposure time ratio of 1 : 3. This intensity modulation was adopted for sensing still images, which are normally ignored in the presence of differential resposivity. Other more important modulation employed in this study is geometrical oscillation of the optical axis that is incident upon the photoreceptor.

Alternatively the photoreceptor itself can be oscillated, which directly corresponds to the small involuntary movements of the human eye, an established physiological phenomenon. Such spatial oscillation of optical images causes a light intensity fluctuation at the edge portion of the image. A combination of this modulation with the differential responsive photoreceptor enables real-time edge detection from images typical of visual information processing.

A motor-driven mechanical oscillator, which performs linear oscillations of an optical lens in vectorial and horizontal directions at a constant frequency (vertically 340 rpm, horizontally 590 rpm), was used for this purpose. Image-carrying light from the projector passes across the oscillating lens set along the optical axis to reach the photoreceptor plane in which a focused image is to undergo lateral oscillation with an amplitude adjusted to the length of the signal-pixel size (1.3 mm).

3.2.3 Image Sensing and Processing Experiments

Selective Detection of Motion of the Optical Image

The unique sensing function of our bR-based artificial photoreceptor was first identified by its rapid detection of the moving component of an image. The motion-detection ability is characteristic of the visual system found in humans and animals. In the retina,

the motion detectors present in the ganglion cells [49] of the receptive field output a differential response to adjacent neurons that are combined to the visual cortex in the cerebrum. Ganglion cells also behave as an edge detector.

Figure 3.4 shows an example of detecting a hand motion in which experiment a liquid-crystal video projector was used to project an image, which is being monitored simultaneously by a commercial CCD video camera. Figure 3.4 includes a picture that was taken at the moment the hand movement stopped. Apparently, the photoreceptor detects a mobile object alone and ignores still objects. The extraction of moving objects is achieved virtually in real time, actually in the time range of less than 1 ms.

(a)   **(b)**
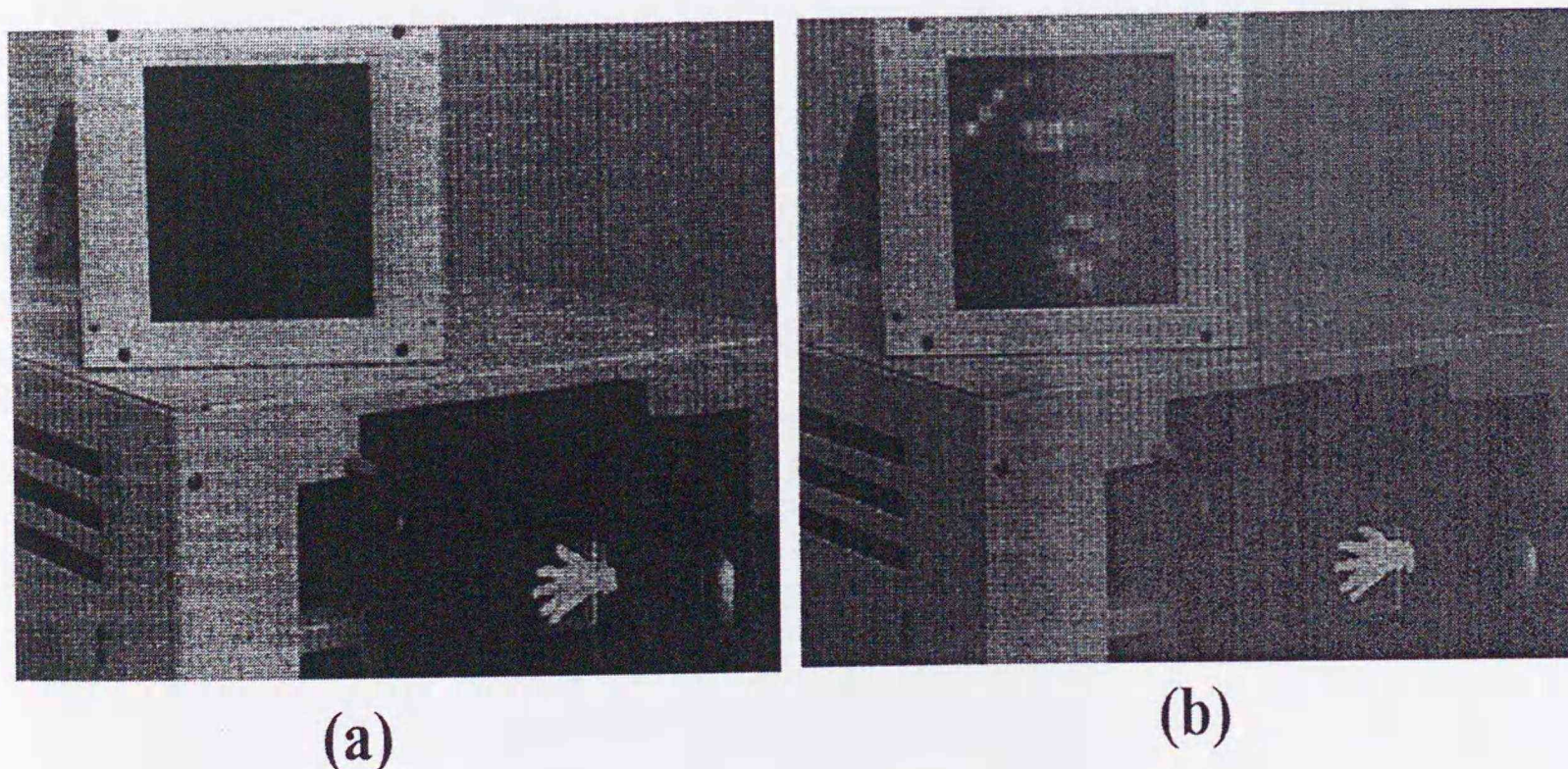
Figure 3.4: Detection of a moving hand by the 256-pixel bR-based photoreceptor. (a) The photoreceptor is insensitive to still images when the hand stopped its motion (b) but starts detecting the hand images at the moment the hand starts to jiggle.

Figure 3.5 exhibits a typical example of a pixelized image detected from a motion of a human face (illustration) when the face image was projected and scanned horizontally across the photoreceptor. The photoreceptor detected the edge profile of the face only at the moment of optical scanning. It is seen that, depending on the direction of motion, the edge profile being extracted is clearly discernible. In addition intensity (contrast) of the detected image, which is expressed as the brightness of the LED pixel, was found to reflect the rapidity of the motion.
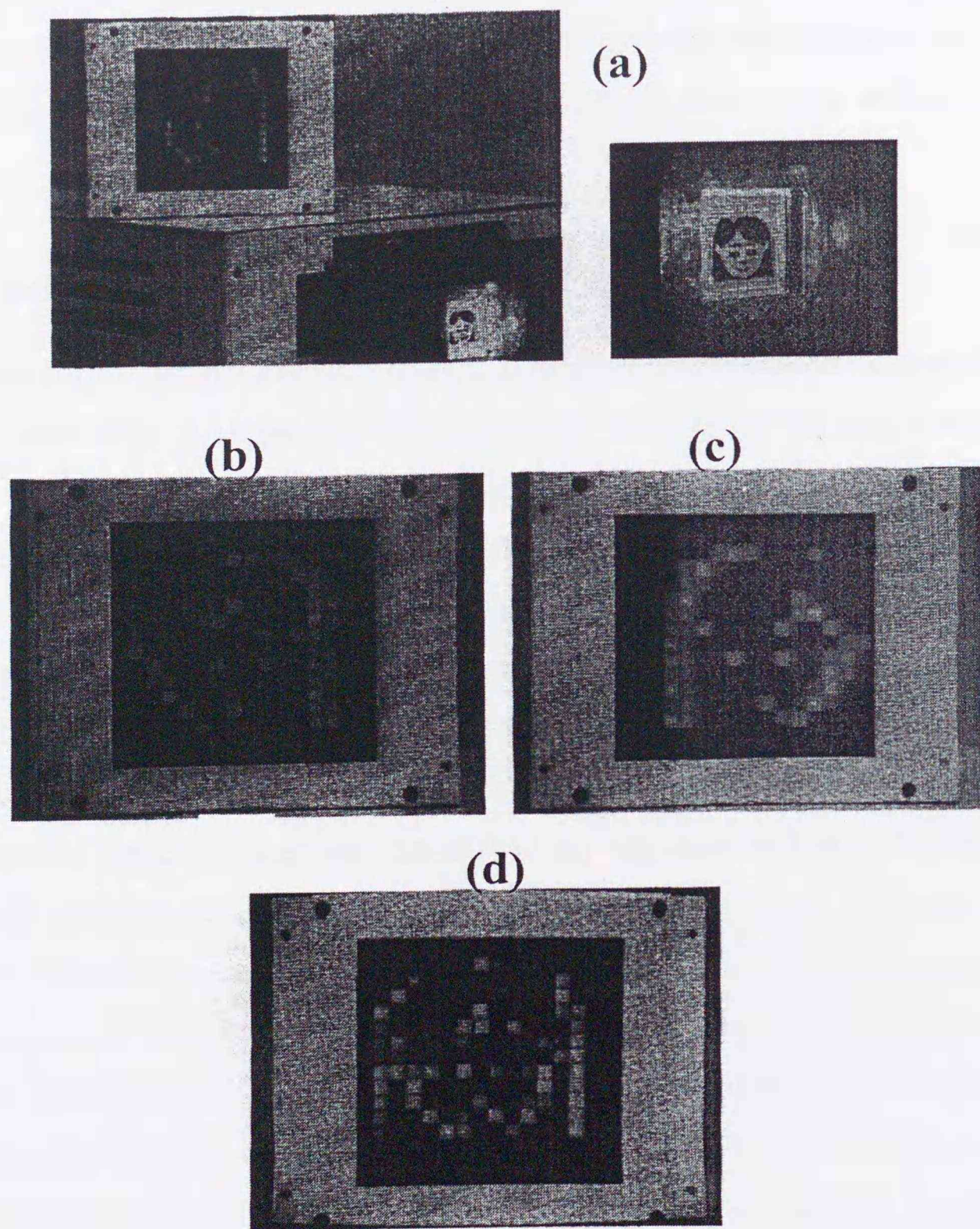
Figure 3.5: Detection of human face pattern by the 256-pixel bR-based photoreceptor. (a) A face image (illustration) supplied by a slide projector is scanned on the photoreceptor (*lower right*) and the detected pixelized image appears simultaneously on the LED display panel (*upper half*) placed on the circuit body. The original image incident to the 256-pixel photoreceptor is enlarged on the right. (b), (c) Face profiles detected by scanning the protected image from the right to the left side and from the left to right side (direction on this display panel), respectively. Nothing was detected when stopped the movement of the image stopped. For moving images the photoreceptor simultaneously extracts their edge profiles with the pattern detected depending on the direction of movement. (d) An example of the whole face profile extracted by oscillating the image on the photoreceptor plane.

In both examples, when the projected image starts a swinging motion (or the optical axis of the images is randomly oscillated), the whole profile of the image appears in an edge-enhanced form. The photoreceptor can thus perform selective sensing of moving components, acting as the same time as an edge profile detector as well as a direction sensor.

3.2.4   Edge Detection and Outline Extraction

Our 256-pixel artificial photoreceptor was subjected to experiments to examine the image-processing capability. A target was an alphabetical letter projected with a slide bearing a positive image. The entire image was detected under chopping modulation of the optical system as described above. To detect the edge component of the letter image, we set an oscillator in the optical axis to cause spatial oscillation of the image. This operation corresponds to physiological eye movements that makes the human photoreceptor always perceptive to still objects. The oscillation was performed in either the vertical or horizontal direction at a frequency of 340 or 590 rpm, respectively. Under this spatial modulation, the detected image was simultaneously displayed on the LED panel.

Figure 3.6 exhibits the edge detection data that were obtained for letter image T. The arrow indicates the direction of the optical axis oscillation. As can be clearly seen, the horizontal and vectorial components of the letter image are selectively detected under vertical and horizontal oscillation, respectively, of the optical axis. Under cyclic oscillation in both directions, whole edge components that constitute the horizontal and vertical profiles of images were visible in reality as a video picture. On the other hand, the data shown in Fig. 3.6 are an extraction of a single image picked up from a television monitor. The same results were obtained, as a simulation of eye movements, by oscillation of the photoreceptor itself with respect to a still image.

These results demonstrate that the bR-based photoreceptor is able to detect edge components of images of a desired vectorial direction immediately (virtually in real time) under the appropriate optical modulation. Edge detection in the present system proceeds by parallel information transaction without the need for computation circuitry. This simple bioelectronic system holds enormous potential for advanced visual processing if better
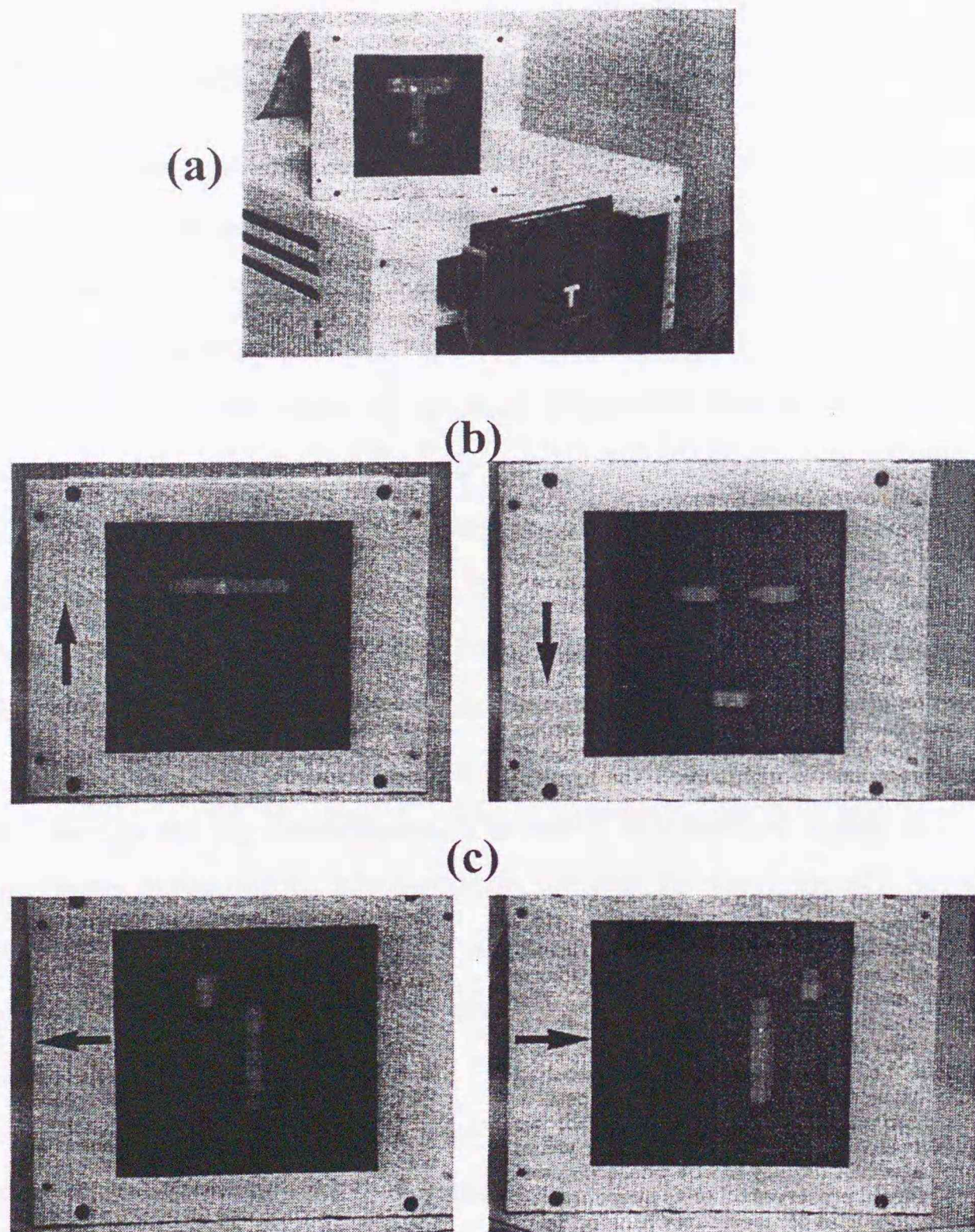
Figure 3.6: Selective detection of vectorial edge components of a letter image for application to pattern recognition. (a) The photoreceptor detects and displays the whole image of the letter T when the optical axis of incident imaging light is periodically chopped to produce an oscillation in light intensity (b) Extraction of the horizontal upper and lower edges from the letter T under vertical oscillation of the optical axis. (c) Extraction of the vertical edge components from the letter T under horizontal oscillation of the optical axis. The arrow indicates the scanning direction of imaging light during oscillation.

assisted by a computation architecture, because the edge detection capability has already been endowed to the sensor at the material level [50].

3.2.5   On the stability of the Image Sensor

The bR-basd photoreceptor was subjected to a forced preservation to check its stabilities against light irradiation and heat. The photoreceptor sample comprising a single pixel was placed in an incubator equipped with a 6.5 KW xenon arc lamp, which white light illuminates the sample with an intensity of 85,000 lx. To simulate a situation in which the sample is left outdoors under direct solar irradiation during midsummer days, we repeated continuous irradiation for 3.8 h at regular darkness intervals of 1.0 h that corresponds to nighttime. The light-to-dark (daytime-to-nighttime) ratio of preservation time was thus 19 : 5. Temperature and relative humidity were controlled at 30 °C, 30% for the irradiation time, and 25 °C, 90% for the dark time, respectively. This forced preservation corresponds to threefold acceleration of samples left outdoors under the sunlight in summertime. The photoelectric output of the sample was monitored with a light source of a constant intensity during preservation. The result is presented in Fig. 3.7. Apparently the photoreceptor maintains its photoelectric activity for more than 4 months, i.e., 12 months as a corresponding period under ambient conditions. With respect to the fact that no output decay was detected, we assume that our device is practically useful for years.

To ensure thermal stability of the photoreceptor, we performed forced preservation tests by incubating samples continuously at temperatures ranging from 60 to 90 °C. It was revealed that, when the photoreceptor is preserved at high temperatures above 70 °C for 24 h and its photoelectric output is checked after cooling to room temperature, the photoelectric output tends to undergo an irreversible suppression by 10–50%. No significant suppression took place at temperatures as high as 70 °C. On a calorimetric basis, bR in an aqueous solution is known to undergo denaturation at temperature above 90 °C but to resist denaturation at a temperature as high as 140 °C in dry film [51]. We assume that the somewhat lower stability observed for our device against high temperatures is due mainly to the layer structure of the bR film that is tailored only by physical adsorp-
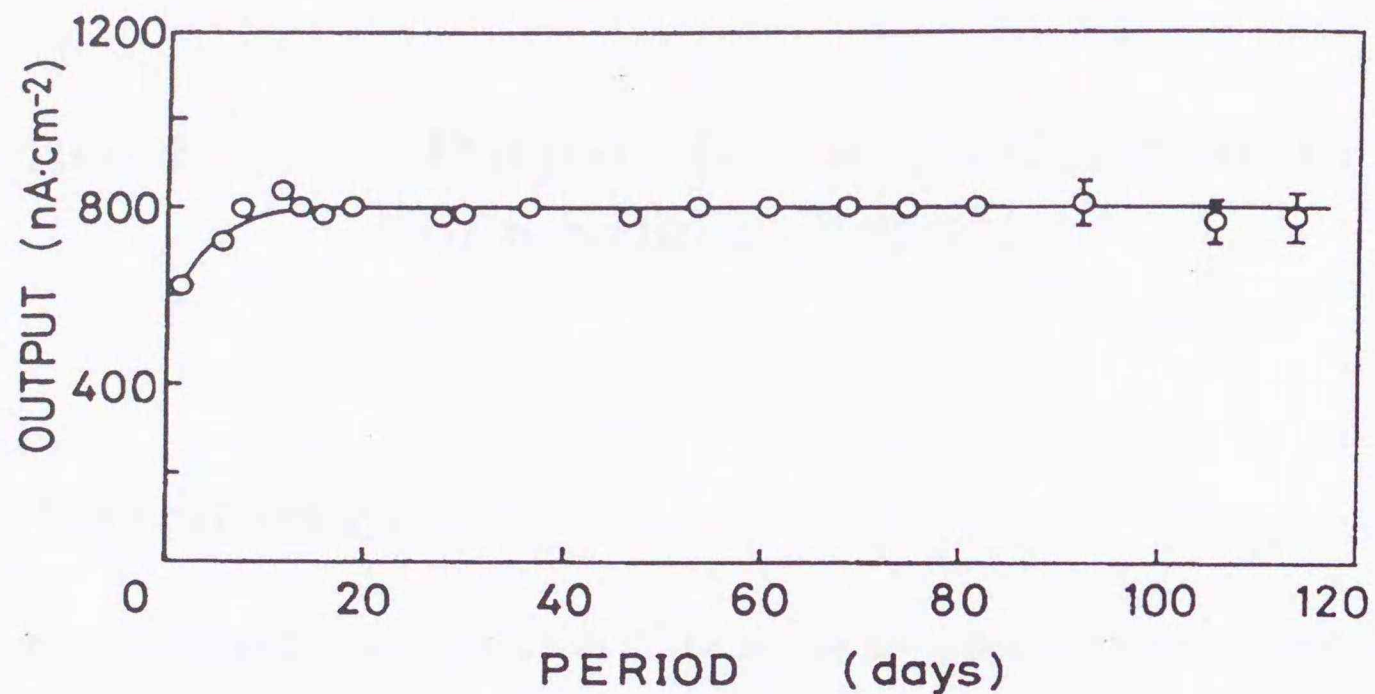
Figure 3.7: Stability of the photoelectric output of the bR-based photoreceptor against light irradiation during long-term preservation. This simulation test ensures that the photoreceptor is stable for years when it remains outdoors under sunlight.

tion without being reinforced by covalent bonding between electrode materials and bR molecules. Higher stability against heat treatment could thus be gained by improvement of the method of immobilizing bR molecules on the electrode surface. Both preservation tests on light fastness and thermal stability demonstrate that the bR-based photoreceptor is amply stable for use in light-sensing systems in ambient conditions.

3.3   Conclusion

We fabricated a unique bioelectronic image sensor by implementing 256-pixel bR-based artificial photoreceptors. The differential light responsivity endowed with the bR-based photoreceptor demonstrates that the visual information processing, such as mobile image extraction and edge detection, are performed in real time without the need of operation and computation circuits. Geometrical oscillation of imaging light, as a spatial modulation corresponding to eye movements, better assists the vectorial detection of edge components, which makes a central contribution for pattern recognition [52]. Advanced implementation of visual functions based on the present system are highly sought after as a retina model for realizing material-level, real-time processing of visual information.

Chapter 4   Purple Membrane Orientation of a Solid Substrate

4.1   Introduction

Bacteriorhodopsin (bR), the only protein in the purple membrane (PM) of *Halobacterium salinarium*, transports protons from the cytoplasm to the extracellular space by light, generating a transmembrane electrochemical gradient [2]. The amino acid sequence of the protein has been established [7] and a three dimensional model has been developed [53] which is consistent with this sequence and its diffraction data [4, 5].According to this model, the orientation of the protein in the membrane is such that the carboxyl terminus is on the cytoplasmic side and about 20 amino acid residues protrude into the cytoplasm while the amino terminus appears to exist outside of the cell membrane.

Since PM can easily be isolated without any apparent impairment in function and is extremely stable against light, attempts have been made to devise bioelectronic systems such as optical computers and memories [35, 37, 47].We have demonstrated that a liquid-junction photocell with ultra thin LB films of PM has differential responsivity to light intensity, which is characteristic of vertebrate photoreceptors [42].This bR photocell was shown to be capable of detecting and processing optical information in a manner similar to that found on visual functions [48].

Such artificial systems have been thought to exhibit photoelectric activity only when the incorporated bR molecules are non-randomly oriented so that unidirectional currents can be produced upon illumination. It has been believed that the orientation of PMs is based on physical properties of the asymmetric membrane structure, such as a difference in the surface charge densities on both sides of the membrane [23] and the permanent dipole moment associated with the surface potential of PM [54]. These asymmetrical properties raise the possibility of there being a number of procedures for controlling the

orientation of PM, such as dispersion at the air/water interface, adsorption to charged membrane filters, and electric-field application [33]. The orientation of PM has thus been postulated on the basis of the direction of the photoelectric response in the device form and the actual degree of the oriented membranes remains unknown.

Only few morphological aspects of the PM surfaces have, however, been characterized by direct observation. Fisher et al. showed that it is possible to distinguish between the two surfaces using electron microscopy with an air-dried, platinum-carbon-shadowed PM [30], suggesting that the C-terminal side was exposed to the cytoplasmic surface on the basis of a morphological comparison between the sidedness of PM fragments and freeze-fracture of whole cells. This technique, however, requires high degree of skill and a great deal of experience contingent on a delicate determination of what distinguishes 'cracked' areas and 'pitted' ones on the membrane surface, a determination that varies considerably with the drying procedure.

In the present Chapter, we report a method for detecting a specific side of PM fragments based on immuno-gold labeling that utilizes a monoclonal antibody labeled with colloidal-gold particles, as illustrated in Fig. 4.1.
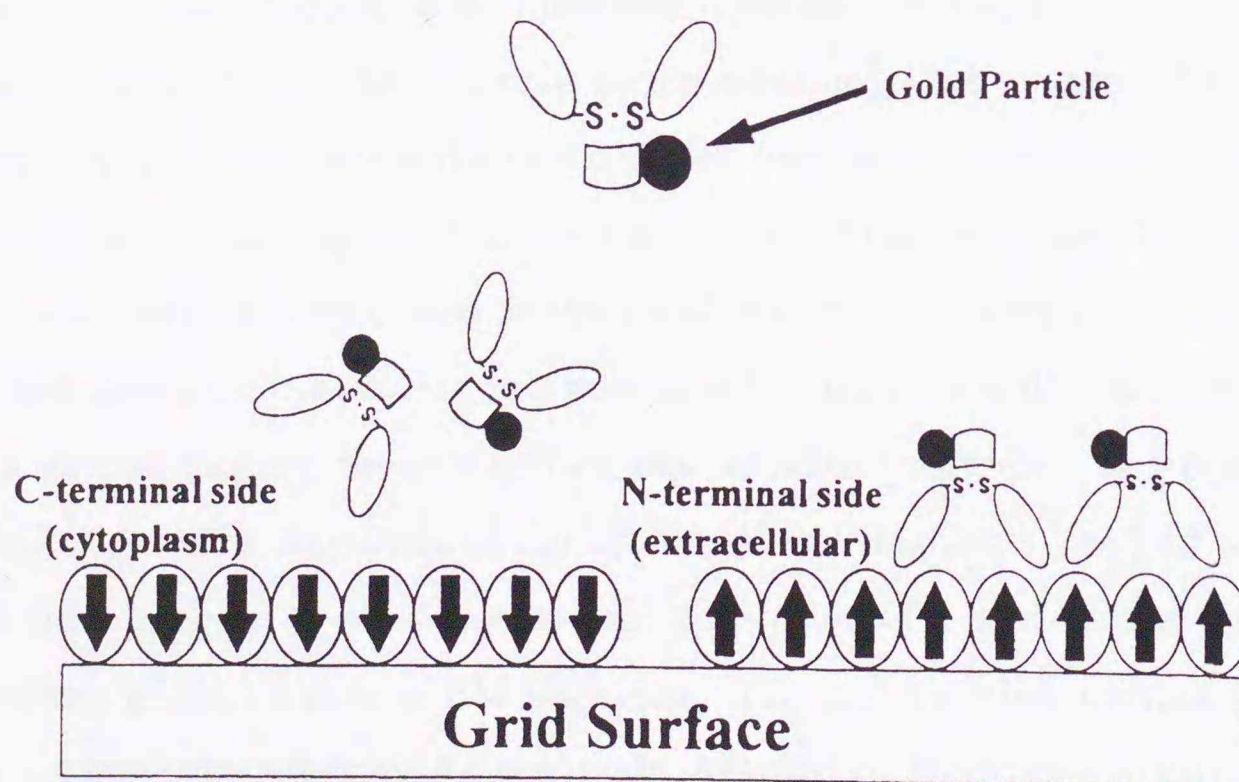
Figure 4.1: Diagram of the immuno-gold labeling experiments.

4.2   Materials and Methods

Purple membrane (PM) fragments were isolated from *Halobacterium salinarium* strain S9 using the standard procedure [39]. and were suspended in pure water (pH 7) to give an optical density of about 5 (570 nm). Peptides comprising the C- and N-terminal sequences of bR were synthesized on an ABI 430A peptide synthesizer, coupled to Keyhole-limpet haemocyanin (KLH) and used to immunize mice. Inhibition experiments and immunoblot analyses are described in the figure legends.

PM monolayer (LB) films were prepared as described in Chapter 2 [55]. In short, a pure water suspension of PM fragments was mixed with hexane and dimethyl formamide (DMF) and emulsified by agitation on a Voltex mixer. A monolayer of PM fragments spread on a neutral aqueous subphase was transferred onto a solid substrate either by neutral dipping of the substrate across the interface or by the horizontal attachment thereof on the supernatant fragments. ELISA in this experiment was carried out as follows. PM film deposited on a glass plate through the dipping method was incubated with an anti-bR antibody and then with horseradish peroxidase (HRP) coupled goat anti-mouse IgG (Sigma). Antibodies labeled with gold particles were prepared by mixing colloidal gold solution (approx. 5 nm diameter, BioCell) with IgG in borax-HCl buffer at pH 9 and adding thereto BSA (bovine serum albumin) after 10 min, to yield a final concentration of 1%. The antibody-gold complex was centrifuged for 40 min, and the resultant precipitate was suspended in small amounts of PBS containing 1% BSA and the suspension was used for immunoblot analysis and electron microscopy.

For electron microscopy, a grid (nickel) was coated with a carbon film just before use. In the case of vertical dipping, the grid surface was rendered hydrophilic by treatment with electric discharge. After deposition of the LB film of PM fragments, the grid was treated with 0.1% BSA in order to avoid non-specific adsorption of a gold-labeled antibody on the grid surface in the absence of PM fragments. The grid was then incubated with the solution containing the antibody-Au conjugate, followed by shadowing it with platinum, and it was observed with an electron microscope (JEM 2000FX).

4.3   Results and Discussion

4.3.1   Preparation of Monoclonal Antibodies

Monoclonal antibodies against bR have already been prepared by immunizing either intact bR or defined fragments to mice for studying the surface topography of bR [56, 57]. The use of these antibodies confirmed the earlier conclusion that the carboxyl terminus is exposed to the cytoplasmic site.

To produce monoclonal antibodies capable of recognizing the respective sides of bR, we chose two peptides as antigens, the one of which is 9 residues of (pyr)Glu-1 to Glu-9 (bR-N peptide) as an extracellular side, the other being 18 residues of Gly-231 to Ser-248 (bR-C peptide) as a cytoplasmic side. The two peptides were prepared with a peptide synthesizer and then, were conjugated with KLH as a carrier protein. After these conjugates were separately immunized in mice, seven stable hybridoma cell lines for bR-N peptide and 8 for bR-C peptide were established through the conventional procedure. We selected the monoclonal antibodies secreted by these cells, N7-3 (IgG1) for bR-N peptide and C3-2 (IgG2a) for bR-C peptide, for further investigations because they have relatively high binding affinity.

In an attempt to localize the epitope in the amino acid sequence, we studied the binding capability of each antibody to several truncated peptide analogs by a competitive inhibition assay. The epitope of N7-3 was found to exist between (pyr)Glu-1 and Ile-4, that of C3-2 lying between Gly-231 and Glu-234 (Fig. 4.2). Replacement of (pyr)Glu with Glu at the N-terminus did not affect the binding affinity with N7-3. Both epitopes are generally small (3 or 4 amino acid residues) in length, although Lerner et al. [58] suggested that monoclonal antibodies recognize a minimum of 7 residues. However, Hodges et al. recently reported that monoclonal antibodies directed to the cytoplasmic carboxyl terminus of bovine rhodopsin recognized residues confined to small linear epitopes ranging from 4 to 11 residues [59], which is consistent with our results. The binding specificity of the two antibodies was examined using the immunoblotting technique (Fig. 4.3). Treatment of bR with chymotripsin specifically cleaves at Phe-71 to form two fragments, C1 (72-246 amino acids) and C2 (1-71 amino acids) [60], which were located at the 16 kD and

8 kD regions, respectively, as determined by Coomassie Blue-stained SDS-PAGE analysis (Fig. 4.3 (B), lane 1). The bands were transferred to the PVDF (polyvinyliden difluoride) membrane and treated with a monoclonal antibody labeled directly with colloidal gold, either C3-2 or N7-3 (Fig. 4.3 (B), lanes 2 and 3).

The C2 part (containing N-terminus) was stained with gold labeled N7-3 in lane B, while C1 part (containing C-terminus) was stained with gold labeled C3-2 in lane C. In addition, bR prepared by papain digestion [8], which lacks approximate 17 amino acids from the COOH terminus, did reacted with N7-3, but not with C3-2 (data not shown). Hence, it was found that the two monoclonal antibodies had specificity sufficient to evaluate the surfaces of the PM.

4.3.2 Visualization of PM Surface by Immuno-gold Labeling

First, we used ELISA to estimate the ratio of the surfaces (C-, or N-terminal side) of a PM monolayer film on a glass substrate prepared by the LB method [55]. Two types of PM-LB films, the so-called Z- and X-type films were prepared by vertical and horizontal dipping of a plate, respectively. On the assumption that the C-terminal side of the PM film on the aqueous surface orients to the aqueous phase by hydrophilic interactions due to the asymmetry of surface charge densities [23], the C-terminus side of a PM-LB film should be exposed to the air on an X-film; on the other hand, the orientation of PM should be opposed on a Z-film. The films deposited on the glass plate were reacted with either N7-3 or C3-2 as a probe, and then incubated with an HRP conjugated goat anti-mouse antibody in order to determine the proportion of the respective surfaces. The ratio of the amounts of the C-terminus in the Z- film to that in the X-type film was 1 : 1.4 with the use of C3-2, whereas that of the N-terminus was 1 : 0.8 with N7-3. These results reveal that there is actually on a slight tendency for the the C-terminus to orient to the aqueous subphase. This fact conflicts with the hypothesis that the C-terminal side of PM exclusively orients to the water subphase.

Further, we have attempted to visualize the surface of PM by using immuno-gold labeling and electron microscopy for determining the sidedness of the membrane precisely. The antibody-Au conjugate was prepared by mixing the colloidal gold solutions with either

Epitope of mAb specific for the bR N-terminal peptide

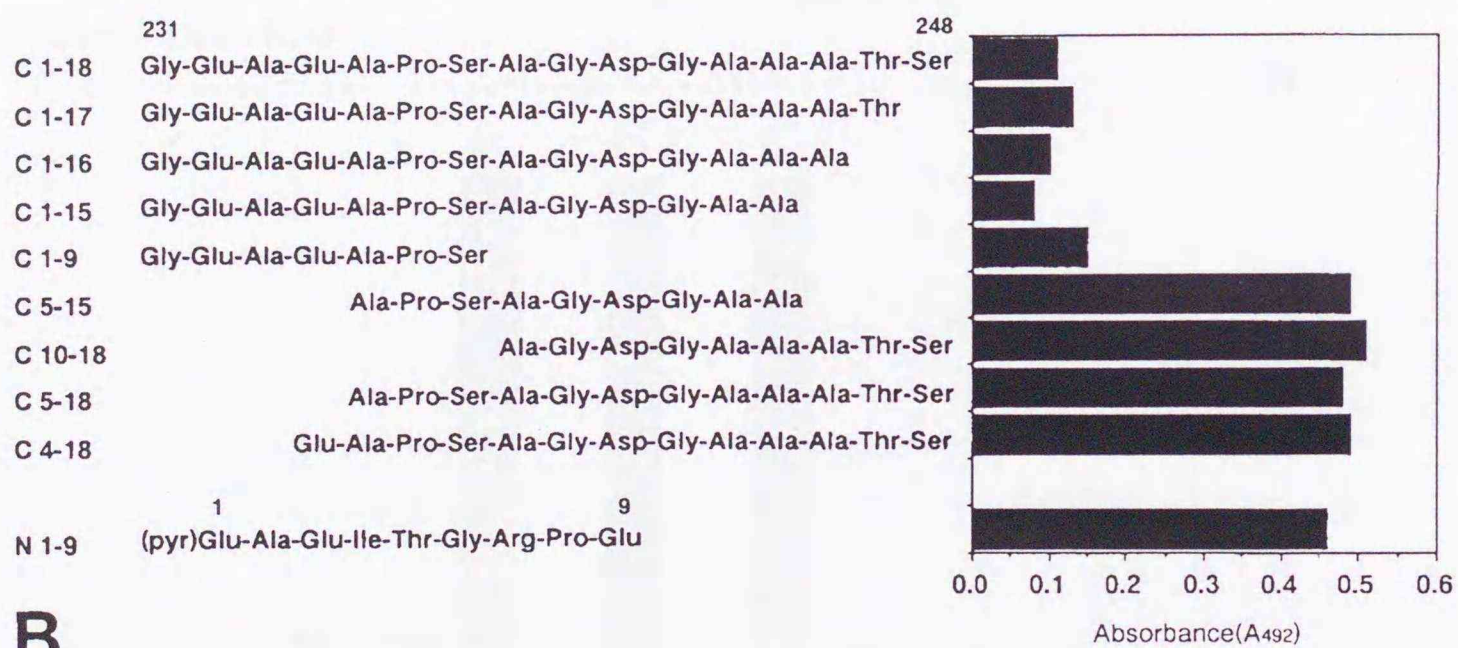|		
N1-9	(pyr)Glu-Ala-Gln-Ile-Thr-Gly-Arg-Pro-Glu	[1 ... 9]
N Glu1-9	Glu-Ala-Gln-Ile-Thr-Gly-Arg-Pro-Glu	
N 1-5	(pyr)Glu-Ala-Gln-Ile-Thr	
N 5-9	Thr-Gly-Arg-Pro-Glu	
C 1-18	Gly-Glu-Ala-Glu-Ala-Pro-Ser-Ala-Gly-Asp-Gly-Ala-Ala-Ala-Thr-Ser	[231 ... 248]

Absorbance(A₄₉₂): axis 0.0 0.2 0.4 0.6 0.8 1.0
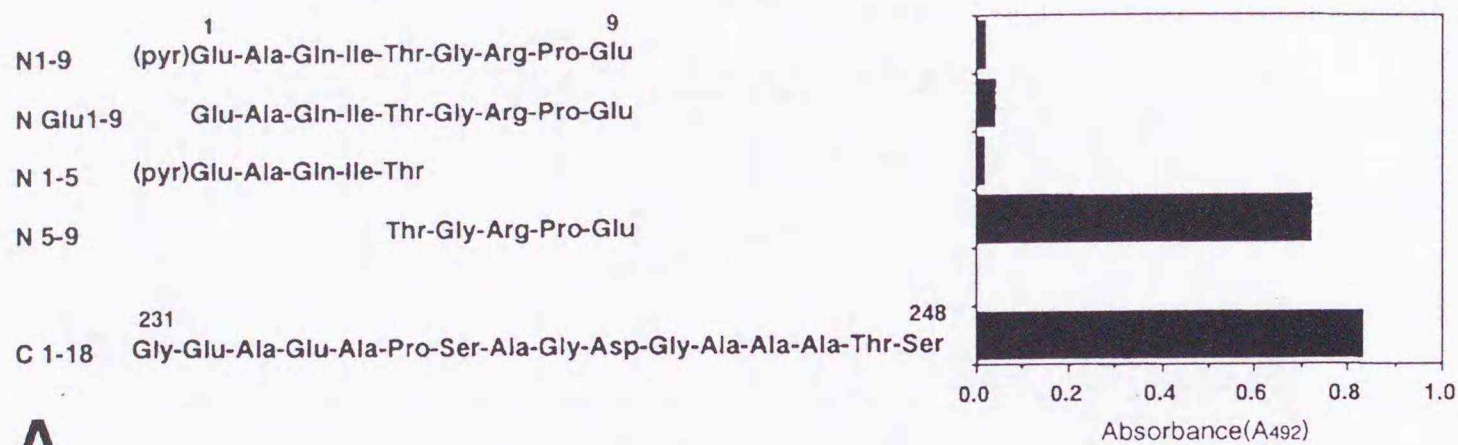
A

Epitope of mAb specific for the bR C-terminal peptide

C 1-18	Gly-Glu-Ala-Glu-Ala-Pro-Ser-Ala-Gly-Asp-Gly-Ala-Ala-Ala-Thr-Ser	[231 ... 248]
C 1-17	Gly-Glu-Ala-Glu-Ala-Pro-Ser-Ala-Gly-Asp-Gly-Ala-Ala-Ala-Thr	
C 1-16	Gly-Glu-Ala-Glu-Ala-Pro-Ser-Ala-Gly-Asp-Gly-Ala-Ala-Ala	
C 1-15	Gly-Glu-Ala-Glu-Ala-Pro-Ser-Ala-Gly-Asp-Gly-Ala-Ala	
C 1-9	Gly-Glu-Ala-Glu-Ala-Pro-Ser	
C 5-15	Ala-Pro-Ser-Ala-Gly-Asp-Gly-Ala-Ala	
C 10-18	Ala-Gly-Asp-Gly-Ala-Ala-Ala-Thr-Ser	
C 5-18	Ala-Pro-Ser-Ala-Gly-Asp-Gly-Ala-Ala-Ala-Thr-Ser	
C 4-18	Glu-Ala-Pro-Ser-Ala-Gly-Asp-Gly-Ala-Ala-Ala-Thr-Ser	
N 1-9	(pyr)Glu-Ala-Glu-Ile-Thr-Gly-Arg-Pro-Glu	[1 ... 9]

Absorbance(A₄₉₂): axis 0.0 0.1 0.2 0.3 0.4 0.5 0.6

B

Figure 4.2: Three and eight peptides analogs of varying lengths of the native bR-N and the bR-C peptides, respectively, were synthesized and examined with the anti-bR antibodies by competitive inhibition assay. Microtiter plates were coated with 50 μg/ml of bR in 0.1M carbonate-buffered saline at pH 8.5. The plates were rinsed in phosphate-buffered saline (PBS) containing 3% bovine serum albumin (BSA) prior to use. Competitive assays were carried out by preincubating serial concentrations (10^{-4}–10^{-8}M) of the synthetic peptide antigen with 1 μg/ml of IgG N7-3 or C3-2 in PBS for 2 hrs at 37°C, followed by adding 50 μl of the mixtures to the bR-coated plates. The plates were incubated for 1 hr, washed in PBS containing 0.05% Tween-20 and treated with a secondary anti-mouse goat IgG conjugated with horse radish peroxidase (HRP). After 1 hr, the plates were again washed in PBS and then developed with the peroxidase reaction to measure the absorbance at 492nm. (A) The competition assay of bR-N peptide analogs with the N7-3 antibody. (B) The competition assay of bR-C peptide analogs with the C3-2 antibody.
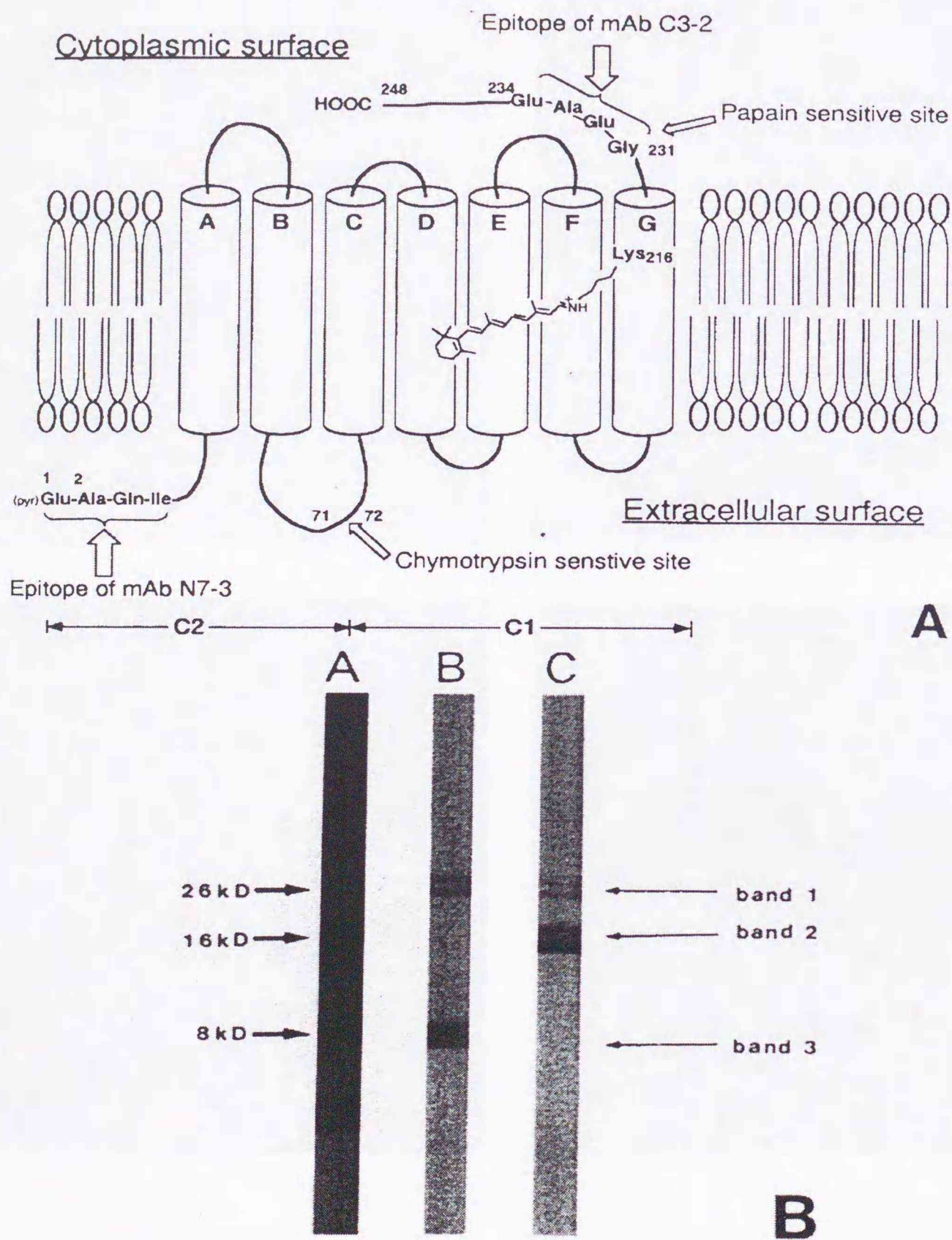
Figure 4.3: (A) Secondary structure model for bR. Chymotrypsin cleaves bR into two fragments, C1 (72-248 amino acids) and C2 (1-71 amino acids). Papain removes about 17 amino acids from the COOH terminus of bR. (B) Immunoblot analyses of bR fragments cleaved with chymotripsin. Products digested by chymotripsin were subjected to SDS-PAGE (10%) and blotted to a PVDF membrane (Millipore) using a transblot apparatus. The filters were blocked with BSA and incubated with the respective gold-labeled antibody. Lanes: 1, SDS-PAGE analysis of bR fragments, Coomassie Blue-stained gel; 2, immunoblot from a duplicate gel, stained with the anti-bR-N antibody (N7-3, 5 nm colloidal gold labeled); 3, stained with the anti-bR-C antibody (C3-2, 5 nm colloidal gold labeled).
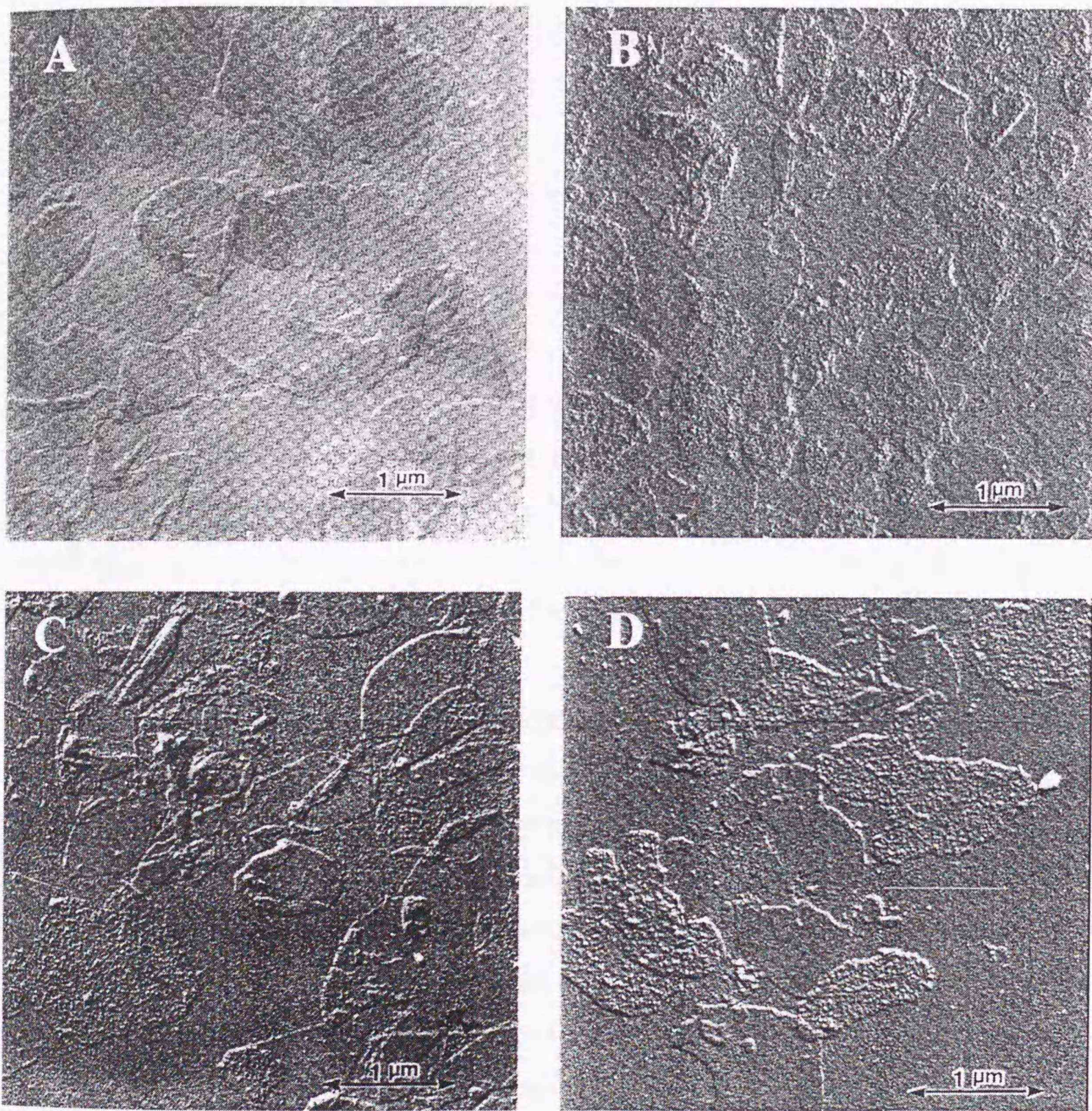
Figure 4.4: Electron micrograph of a PM monolayer. PM fragments prepared by a LB method or spontaneous adsorption were deposited on an electron microscope grid and treated twice with BSA solution. It was then transferred to the labeling buffer containing N7-3-Au conjugate for 10 min. at 37°C, rinsed in phosphate buffer and in pure water. After shadowing with platinum, it was observed with an electron microscope. (A) A monolayer of PM on a grid prepared by the LB method without immuno-gold labeling. Neither the 'cracked' nor 'pitted' areas shown by Fisher et al. appear in the LB film[30]. (B) Immuno-gold labeling with N7-3-Au conjugate of the PM film transferred by horizontal dipping, (C) by vertical dipping and (D) of PM fragments adsorbed spontaneously on a grid in concentrated PM suspension. Rough regions, which are covered with gold particles, indicate the extracellular side of PM.

N7-3 or C3-2 (Fig. 4.3(B)). The two types of LB films of PM were prepared using the same procedure described above. Fig. 4.4(A) shows the platinum-shadowed PM monolayer film transferred on the grid by the horizontal attachment method prior to immuno-gold staining. Each film on a grid was pre-treated with BSA, and incubated with the solution containing the antibody-Au conjugate. After platinum-shadowing treatment, the glid was subjected to electron microscope observation. The N7-3-Au conjugate clearly distinguished the surface morphology of PM where the extracellular surface is exclusively labeled with gold particles, while the C3-2-Au conjugate was somewhat less distinct than the N7-3-Au conjugate under various conditions. This difference is probably because the binding affinity of C3-2 is lower by one order of magnitude than that of N7-3. Figures 4.4 (B) and (C) compare the morphologies of the PM surfaces obtained by horizontal and vertical dipping, respectively, and reacted with the N7-3-Au conjugate. In each case, we conclude that the surface orientation of the PM monolayer is substantially random, which is in agreement with the results in ELISA.

As a reference, a PM film underwent no specific treatment for orientation was prepared by allowing a grid for spontaneous adsorption of PM from a highly concentrated PM suspension. As shown in Fig. 4.4(D), PM fragments were adsorbed on the grid leaving much vacancy because they were not compressed on the aqueous surface. Apparently, no orientation is recognized. this fact confirms that the LB film of PM fragments are randomly oriented. These results ensure that the orientation of PM can hardly be controlled at hydrophobic/hydrophilic interfaces such as an air/water interface with the successful assistance of a difference in the surface charge densities [52].

4.4   Conclusion

The results presented in this study demonstrate that immuno-gold labeling techniques provide a very useful and direct means of detecting the sidedness of biological membrane proteins such as bR, and that controlling the orientation of PM fragments at the air/water interface is essentially difficult. Nevertheless, it is of interest that the LB film prepared by spreading PM at the air/water interface results in a photoelectric response which

is highly rectified [38, 40, 42, 61]. Mechanistic studies of photocurrents arising from randomly oriented PM fragments are currently being investigated.

Chapter 5 Highly Oriented Purple Membrane by Antibody Techniques

5.1 Introduction

Bacteriorhodopsin (bR) is the sole protein found in the purple membrane (PM) in *Halobacterium salinarium*. Uniformly oriented bR molecules in PM perform unidirectional pumping of protons from the cytoplasm to the extracellular space during the photocycle, thereby forming an electrochemical gradient across the membrane. The three-dimensional structure and photocyclic reaction of bR have been well-elucidated by Henderson and co-workers [4, 5, 53] and Khorana and co-workers [62, 63, 64].

The photocycle of bR and its rapid optical change [9] exhibits versatile photophysical functions in vitro; these functions can provide components that critically important in the design of molecular electronic devices [37, 47] and optical memories [35, 45]. We have verified that a PM-immobilized liquid-junction photocell exhibits differential electrical responsivity to light intensity, a function characteristic of vertebrate photoreceptors [42, 55]. One potential application for this responsivity is in the manufacture of an artificial retina that could detect and process optical information in a manner closely approximating certain visual functions [48].

In bR-based photoelectric devices, a truly integrated unidirectional–and thus highly efficient–electric response can only be obtained when the bR molecules have a nonrandom orientation. In this respect, efforts thus far to control the orientation of PM included such means as dispersion at the air-water interface, on charged membrane surfaces, in an electric field, and so forth [33]. However, in most cases, PM orientation is deduced on the basis of the direction and intensity of the photoelectric response of the PM monolayer after it has been incorporated into a device system. This sort of indirect approach frequently leads to conclusions that are confusing or contradictory [33].

The reason for this ambiguity is that no direct method has ever been devised that provides a precise means for controlling and determining the orientation of PM fragments.

We have established an immuno-gold labeling technique that provides a highly accurate means of determining the ratio of orientation of PM sheets [65].

In this section, we describe a method to establish the perfect re-orientation of bR through use of bispecific (BS) antibodies that simultaneously recognize both a phospholipid hapten and a specific side of the bR molecule, as shown in Fig. 5.1. Our antibody technique is used to clarify the effect of orientation of bR on bR-generated photoelectric events and to conclusively demonstrate the inherent advantages that the ability to precisely control PM orientation holds for the design of molecular devices [66].

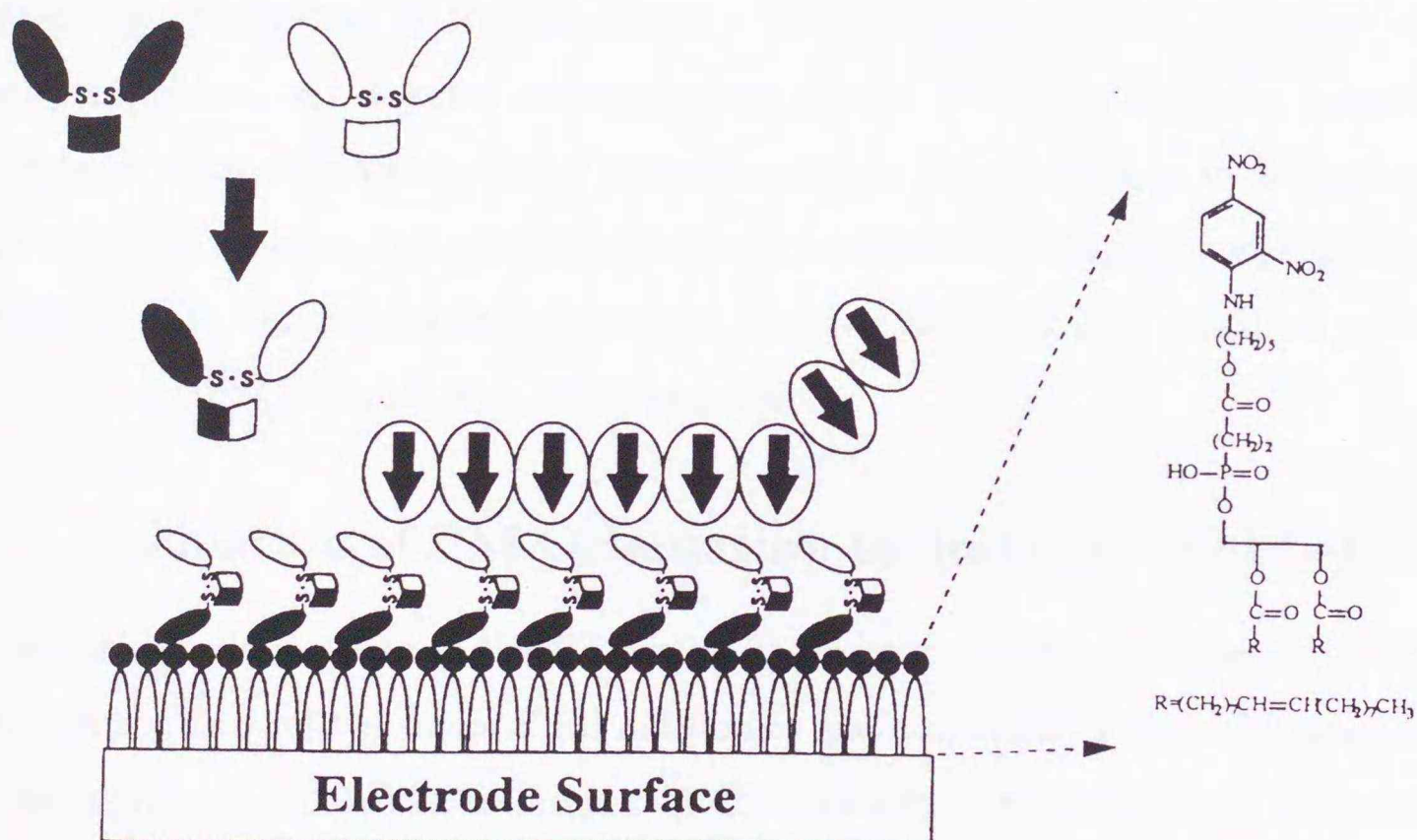Figure 5.1: The principle of rational orientation of PM using BS antibodies.

5.2 Results and Discussion

5.2.1 Preparation of Bispecific Antibodies

N-(2,4-Dinitrophenyl)aminocaproyl phosphatidylethanolamine (DNP-cap PE, obtained from Avanti Polar Lipids, Inc. USA) was selected as an amphipathic hapten phospholipid. This phospholipid has been used previously by Uzgiris and Kornberg [67] to form

a two-dimensional monolayer. An antibody to DNP [immunoglobulin (IgG$_1$)], a mono-clonal antibody to the hapten site of the phospholipid (2,4-dinitrophenyl group, DNP), was produced by immunizing mice with 2,4-dinitrobenzene sulfonic acid conjugated with Keyhole-lympet haemocyanin (KLH).

Mice were immunized with peptide-KLH conjugates to obtain monoclonal antibodies for each side of the bR molecule. Through this process we obtained two antibodies, C3-2 (IgG$_1$), which recognizes a carboxyl terminus portion of bR, and N7-3 (IgG$_{2a}$), which recognizes an amino terminus portion of bR. The epitope and the specificity of the antibodies have been established as described in [65]. The BS antibodies were prepared by modifying the method of Brennan *et al.* [68]. As shown in Fig. 5.2, each of the resulting antibodies was digested with pepsin to obtain an F(ab')$_2$ fragment, which was then reduced with dithiothreitol and reacted with an Ellman's reagent for protection of the mercapto groups. The resulting antibody to DNP Fab' fragment was chemically reassociated with antibody to bR fragments (derived from C3-2 or N7-3) to yield BS antibodies to DNP-C3-2 and DNP-N7-3, respectively.

5.2.2   Evaluation of PM Orientation by Immuno-gold Labeling

To examine the effectiveness of the BS antibody, we prepared a monolayer array of PM oriented on the array of two kinds of BS antibodies and evaluated its degree of orientation with the immuno-gold labeling technique. A CHCl$_3$ solution of dimyristoyl phosphatidyl choline (DPPC) containing 7% hapten phospholipid (DNP-cap PE) was, under a con-trolled surface pressure of 30 mN/m, applied on a surface of pure water in a Langmuir film balance to form a monolayer, and the hapten monolayer was deposited onto an elec-tron microscope grid. The grids were treated for 30 min at 37°Cwith an aqueous solution containing the above-prepared BS antibody to DNP-C3-2 or BS antibody to DNP-N7-3 (100 μg/ml), respectively, and incubated with a PM suspension (0.4 mg/ml) isolated from the S-9 strain of *Halobacterium salinarium* with the conventional method [39]. Each grid-deposited monolayer film was treated with 0.1% solution of bovine serum albumin to prevent nonspecific adsorption of a gold-labeled antibody on the grid surface in the absence of PM fragments. In the final step, the grid was then incubated with a solution
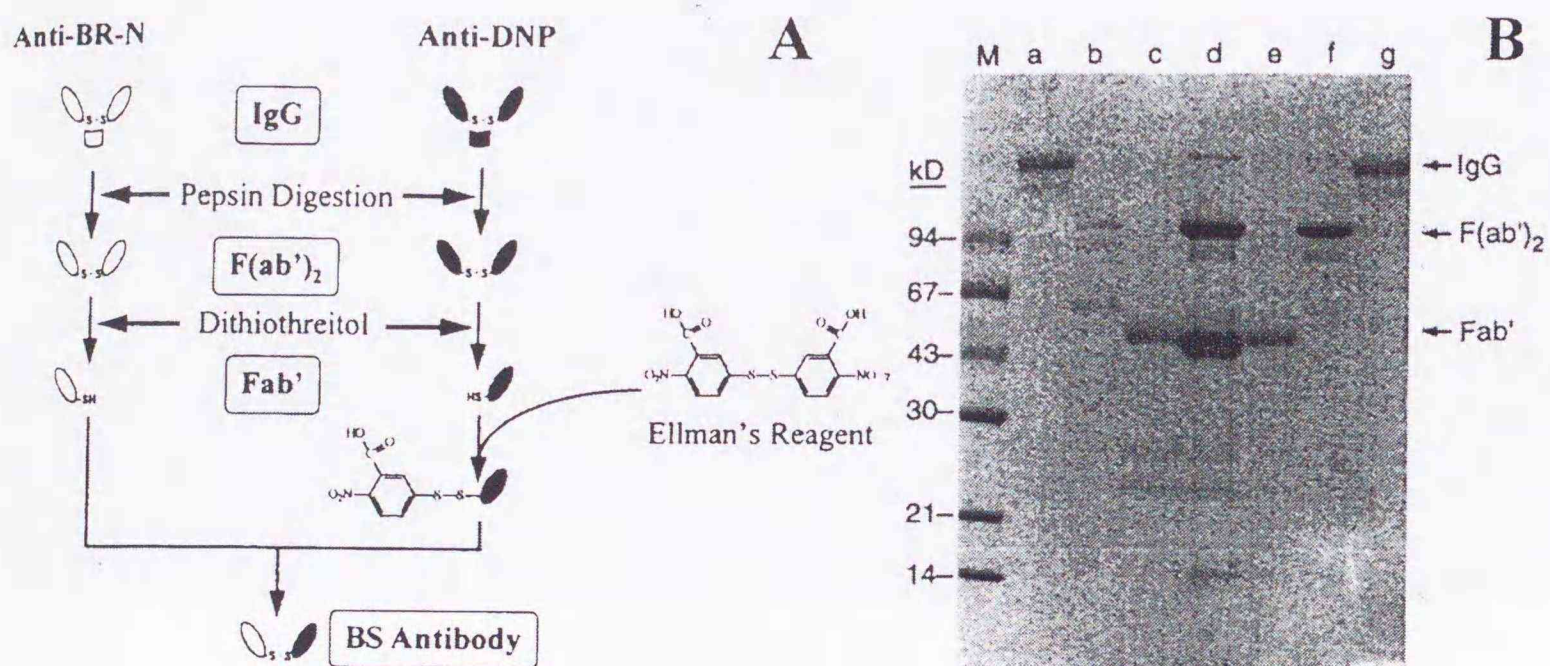
Figure 5.2: (A) Diagram of a method for synthesizing a BS antibodies. (B) The processes involved in the formation of a BS antibody by SDS-polyacrylamide gel electrophoresis analysis. Lanes a and g, antibodies of C3-2 or N7-3 and anti DNP, respectively; lanes b and f, digested antibodies $F(ab')_2$ derived from their intact antibodies; lanes c and e, Fab' reduced with dithiothreitol; lane d, a BS antibody reassociated with Fab' from C3-2 or N7-3 and from anti-DNP; lane m, prestained molecular weight markers. The obtained BS antibody was purified by high performance liquid chromatography (HPLC).

containing an N7-3-Au conjugate that recognizes the extracellular surface of PM only. After platinum-shadowing treatment, the grids were observed under an electron microscope (Figures 5.3(A) and (B)). A randomly oriented PM monolayer film spontaneously adsorbed on a grid, is included here as a reference (Fig. 5.3(C)).

As can be seen in Figures 5.3, the PM monolayer treated with BS antibody to DNP-C3-2 is almost completely covered with gold particles ($\geq 85\%$), whereas the PM monolayer treated BS antibody to DNP-N7-3 is devoid of labeling ($\leq 5\%$). In both cases, the orientation of the PM monolayer is precisely defined. In the first case, the cytoplasmic surface of the PMs is exclusively directed toward the substrate, as indicated by the total covering with gold particles. In the second case, the cytoplasmic surface is inversely directed, as evidenced by the lack of labeling. These results show that the properties of BS antibodies can be harnessed to precisely control the orientation of the PM monolayer.
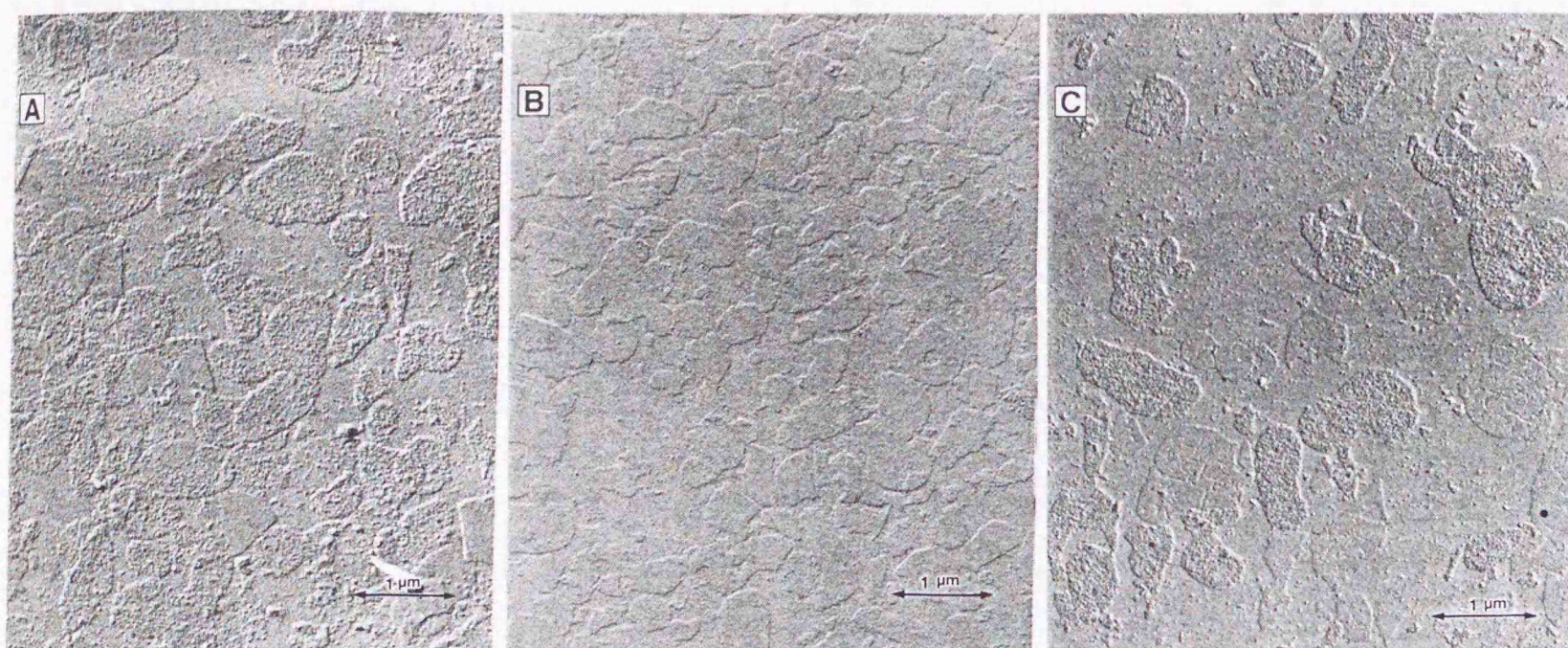
Figure 5.3: Surface morphology of PM films as observed using electron microscopy. (A) The cytoplasmic side of PM fragments treated with BS antibodies to DNP-C3-2 faces the grid surface. (B) The extracellular side of PM fragments treated with BS antibodies to DNP-N7-3 faces the grid surface, (C) Random orientation of PM fragments adsorbed spontaneously on a grid.

5.2.3   Photoelectric Response from Highly Oriented PM Films

We next examined the photoelectric response of these antibody-mediated PM films. A sandwich-type photoelectric device [42, 55] was used to obtain a photocurrent response from the PM monolayers. A conductive SnO_2 electrode that captures the charge displacement current of bR served as a common substrate for the PM monolayer. As described above, the cytoplasmic and extracellular sides of the PM monolayer were oriented toward the electrode (substrate) by using, respectively, the BS antibodies to DNP-C3-2 and DNP-N7-3.

Visible light irradiation of the PM film caused the production of photocurrent signals with characteristic differential response profiles; the direction of the flow of electrons is always rectified from the electrode to electrolyte side. A comparison of the photocurrent signals obtained from the three sources, the two antibody-mediated PM monolayer films and the randomly oriented reference (LB film) is shown in Fig. 5.4. Exactly the same light intensity was used with all three samples to eliminate the influence of light intensity, which has a linear relationship with light intensity [42, 55].
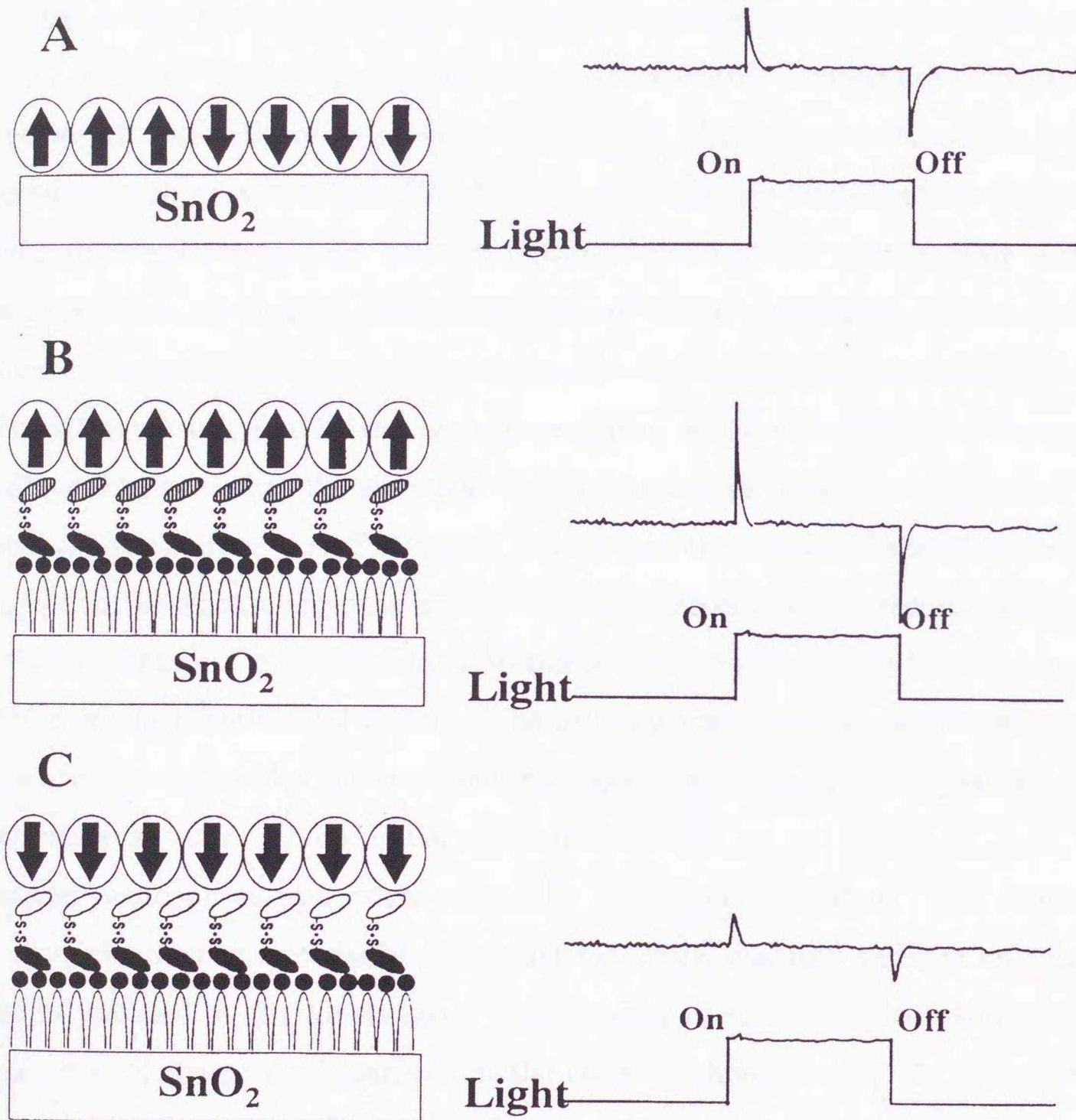
Figure 5.4: Comparison of the typical photoelectric response from a sandwich-type photocell. (A) Photoelectric response from a monolayer PM film prepared using the LB method, which is randomly oriented. (B) An oriented monolayer PM film with the cytoplasmic side facing the SnO₂ electrode. (C) An oriented monolayer PM film with the extracellular side facing the SnO₂ electrode. The arrows indicate the orientation of bR along the direction of proton pumping.

The peaks of the transient photocurrents produced upon the onset of light irradiation indicate the response strength of each of the tested PM monolayers. The most intense response was produced by the sample with the cytoplasmic (carboxyl terminus) side of PM directed to the electrode (SnO_2), whereas the weakest response was produced by the sample oriented in the opposite direction. As expected, a moderate response was produced by the randomly oriented sample (LB film), although no antibody layers are inserted between the electrode and PM. Because the response mechanism in this device does not involve electron transfer between electrode and PM and photocurrent is solely induced electrostatically through charge displacement within an assembly of bR molecules, the influence of a separating layer (hapten and antibodies) is assumed to be less significant.

An important finding is that the electric response, which corresponds to a positive charge displacement towards the electrode surface, is maximal when the cytoplasmic side is oriented to the electrode side. This result implies that the positive charge displacement contributing to the electric response is inverse to the direction of the proton transfer. A similar relation has been postulated for PM-immobilized dry photocells [69, 70]. Apparently, based on our experimental evidence, the primary event of vectorial charge transfer in the bR photocycle should occur in a direction opposite to proton pumping which occurs in a time range far later than the initial structural change.

A rectified photocurrent still exists when PM orientation is random. This result indicates an electrochemical interfacial effect that externally controls, through an electrostatic field developed in the double layer, the efficiency of charge displacement through the suppression of charge displacements in the cathodic direction [40]. In these charge displacements, the part of the charge that flows in the direction of the electric field has a major effect in the charge transfer. This charge transfer induces a current in the electrode. For charge displacements in the opposite direction, the displacements are electrostatically suppressed. In fact, no inverse current is induced even using the inversely oriented PM sample as shown in (Fig. 5.4(C)). Accordingly, a trace response survived in the inversely oriented sample because a few cathodically responsive PM fragments remain. This lack of a response indicates that the most significant photoelectric response and the maximum charge displacement effect can be elicited from a PM-based photoelectric device in which

a highly organized, effective array of PM films is used [71, 72].

5.3   Conclusion

Our studies demonstrate that the preparation of precisely oriented, molecularly regulated bR films can now be accomplished through treatment with BS antibodies [66]. We believe that the key to the design of bR-based molecular electronic devices may very well be found in the ability to control the molecular orientation of bR and the potential applications of this ability to the formation of two-dimensional molecular crystals. Typically, a two-dimensional pixelized image sensor constructed around a PM film [48] can be highly qualified as a retina model because pixel size can be minimized while still maintaining equal sensitivity between small pixels. Particularly promising is the extension of the techniques in the preparation of three-dimensionally crystals of functional proteins, starting with self-assembling of a protein multilayer on a highly oriented two-dimensional base. Solid crystals of bR-antibody with a three-dimensionally oriented network of retinal chromophore can be obtained as intelligent materials for incorporation into optoelectronic and non-linear optical applications [52].

Chapter 6   Response Mechanism I: Relation between Photoresponse and Retinal Isomers

6.1 Introduction

Bacteriorhodopsin (bR) contains retinal as its chromophore. The pioneering studies of Henderson and co-workers using electron microscopy provide a three-dimensional model of PM in which the bR molecules are arranged in a hexagonal lattice with the polypeptide chain forming seven helix segments spanning the membrane [5].

After light excitation, bR undergoes rapid retinal-isomerization from all-trans to 13-cis and then thermally relaxes through a number of intermediates. Each intermediate exists for a different time scale (ranging from a few picoseconds to 10 ms) corresponding to different protonation states of the Schiff base and several key amino acids. In the conversion from the **L** to **M** intermediates, the proton on the Schiff base is transferred to Asp-85 with subsequent proton release from Glu-204 into the extracellular side [15]. When the **M** state decays, the Schiff base is reprotonated from Asp-96. At the end of the photocycle, Asp-85 is deprotonated and the reisomerization of retinal occurs.

During this photocycle, potential change due to the proton transfers takes place, thus causing rapid photoelectric signals across electrodes attached to PM. Generating such signals is the key in using bR in some electrical devices, and therefore many systems have been proposed over the past decade [33, 73]. We previously showed that a liquid-junction photocell which immobilizes thin PM films produces a differential electric response to light-intensity changes, similar to the response of the vertebrate retina [42]. An artificial photoreceptor made of this photocell can detect and process optical information in a method similar to the visual function system [48].

It is well known that PM exists in two spectroscopically distinct states, called the dark- and light-adapted forms, which have absorption maxima at 558 and 568 nm, respectively [2]. In the light-adaptation form, bR contains all-trans retinal only. When PM is kept in the dark for an extended period, the absorption maximum shifts slowly to 558 nm, which

is thought to be the result of a mixture of all-trans and 13-cis retinal. The isomer ratio of this mixture was estimated to be approximately 50 : 50 by several different methods.

Accurate estimates of the isomer ratio were difficult to obtain because they required absolute absorption spectra of each species, which are difficult to obtain [11, 74, 75]. The HPLC (high-performance liquid chromatography) method in the early studies had several drawbacks such as the possibility of isomerization during extraction and the large variations of the ratio [10, 76, 77]. However, Scherrer et al. proposed that the ratio of 13-cis to all-trans retinal was 66 : 34 by using an improved method that combined HPLC with fast extraction [78]. Previous methods to characterize bR during its photocycle, specifically its retinal isomer ratio and isomerization process, have produced contradictory results, which have led to controversy about the isomer ratio of bR in the dark.

A sandwich-type electrochemical cell with PM gives a transient and unidirectional photocurrent [42]. When we kept this cell in the dark, the peak amplitude of the current was approximately one half that for the same PM after it was adapted to light. This peak reflects the chromophore ratio in the dark. We thus used the photoelectric response from a bR-based electrochemical cell to accurately estimate the 13-cis/all-trans isomer ratio in the dark adaptation of PM.

Here, we describe this direct and simple method for determining the 13-cis to all-trans retinal ratio in dark-adapted PM in which the photoelectric response of PM is measured in an electrochemical cell. We measured this photoelectric response at different pHs (2–12) and temperatures (5–48°C) of the electrolyte in the cell to determine the rate constants of the isomerization. These measurements showed that the isomerization rate is due to the fraction of the protonated state of Asp-85.

6.2   Materials and Methods

PM fragments were isolated from *Halobacterium salinarium* strain S9 using the standard procedure [39]. The fragments were centrifuged several times in deionized water to obtain a suspension of pure PM.

The working and counter electrode were 20×18 mm glass slides coated on one side with a 450 nm-thick conducting layer of transparent tin-oxide (SnO_2). PM was immobilized on the electrode by a casting method in which 100 μl of a suspension of PM (about 0.5 mg/ml) was pipetted onto about a 1 cm^2 area of the electrode surface and dried at room temperature. This casting method gave the same results obtained by the Langmuir–Blodgett (LB) method described previously [55]. The film take a statistically random orientation toward the electrode as was confirmed by the immuno-gold labeling technique [65, 66].

The PM-coated SnO_2 electrode was set in a sandwich-type electrochemical cell containing 100 mM KCl as an electrolyte, together with a counter electrode. To maintain the pH between 2 and 12, a mixture of buffers (sodium citrate, sodium phosphate, sodium borate, Mes, Hepes, and Mops), each at 20 mM, was used. The pH was adjusted by the addition of either 1 N HCl or 1 N NaOH. The distance between the working and counter electrode was 8 mm, which is filled with electrolyte.

Measurements were taken at various temperatures, from 5°C to 48°C. For the temperature-dependence experiments, we incubated the cell containing PM for 3 h at $\geq$24°C, 18 h at 15°C and 5 days at 5°C in the dark to ensure complete dark adaptation. For pH-dependence experiments, the cell was stored for 1 h at <pH 4, 6 h at pH 5~10, and 48 h at pH 11 in the dark at 24°C. A 150 W xenon arc lamp was used as a light source in combination with a green band-pass filter (HOYA, G550) and IR-cut filter (Toshiba IRA-05); the incident power was 10 mW/cm^2 at the working electrode.

Photocurrents produced in the cell were converted to a voltage mode that was amplified in a circuit (Bioelectric amplifier MEG 1200, Nihon Koden Co.) and finally displayed on a digital storage oscilloscope (Gould model 420).

The absorption spectrum change of the PM film on the SnO_2 electrode in the dark was monitored using a spectrophotometer (Hitachi U-3000).

6.3 Results

6.3.1 Retinal Isomer Ratio

Figure 6.1(L) shows a typical photoresponse pattern from the light-adapted cell at pH 7.0. The peak amplitude gradually decreases as the time in the dark increased, and finally reached that for the dark-adapted cell (D) in Fig. 6.1. The difference in the amplitude of the transient response between light- and dark-adaptation corresponded to the amount of 13-cis retinal in the dark [79].

This time-dependent decrease in the amplitude correlates well with the change in visible absorption for a dark adapted cell (Fig. 6.2). Repetitions of photoelectric measurements for both light- and dark-adaptations using the same cell showed that the chromophore
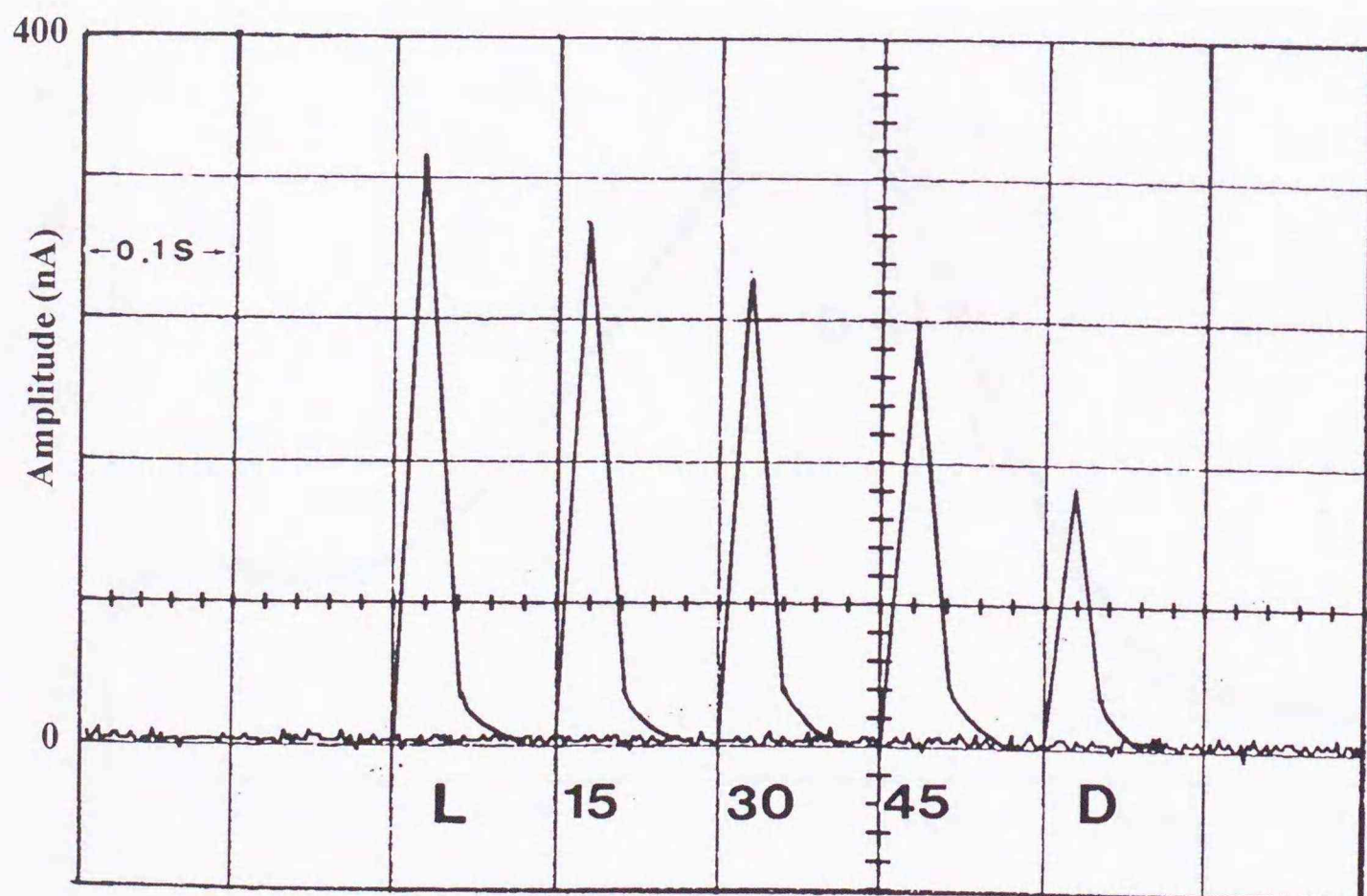

Figure 6.1: Photoresponse patterns of light-adapted (L) PM films at 15, 30, and 45 min after illumination and of dark-adapted (D) PM films. The films were on an SnO_2 electrodes in an electrochemical cell at pH 7.0 at 24°C. Comparison of peak amplitude between light adapted (L) and dark adapted (D) PM always gave the ratio of 1 : 0.45. The cell was used repeatedly and still gave the same isomer ratio.

ratio in the dark was 55±2% 13-cis and 45±2% all-trans retinal. The value is consistent with that obtained by Váró and Bryl [80] in which they used a dry cell with a thick layer (O.D.>10) of electrodeposited PM . This ratio was also previously determined by using HPLC, suggesting that 13-cis retinal in the dark was from 50% to 60% [10, 76, 77].

Recently, Scherrer et al. proposed that the isomer ratio in the dark is 66~67% 13-cis and 33~34% all-trans retinal by HPLC analysis in combination with an improved extraction technique in which up to 70% of the retinal in PM is extracted within 4 minutes [78]. This result conflicts with our data obtained by the photoelectric response method. Smith et al. [81] determined 13-cis isomer to be ~60% by NMR spectroscopy. Although, resonance Raman and FTIR spectroscopy can give qualitative information on the isomer ratio, quantifying the ratio is not so easy [82, 83].
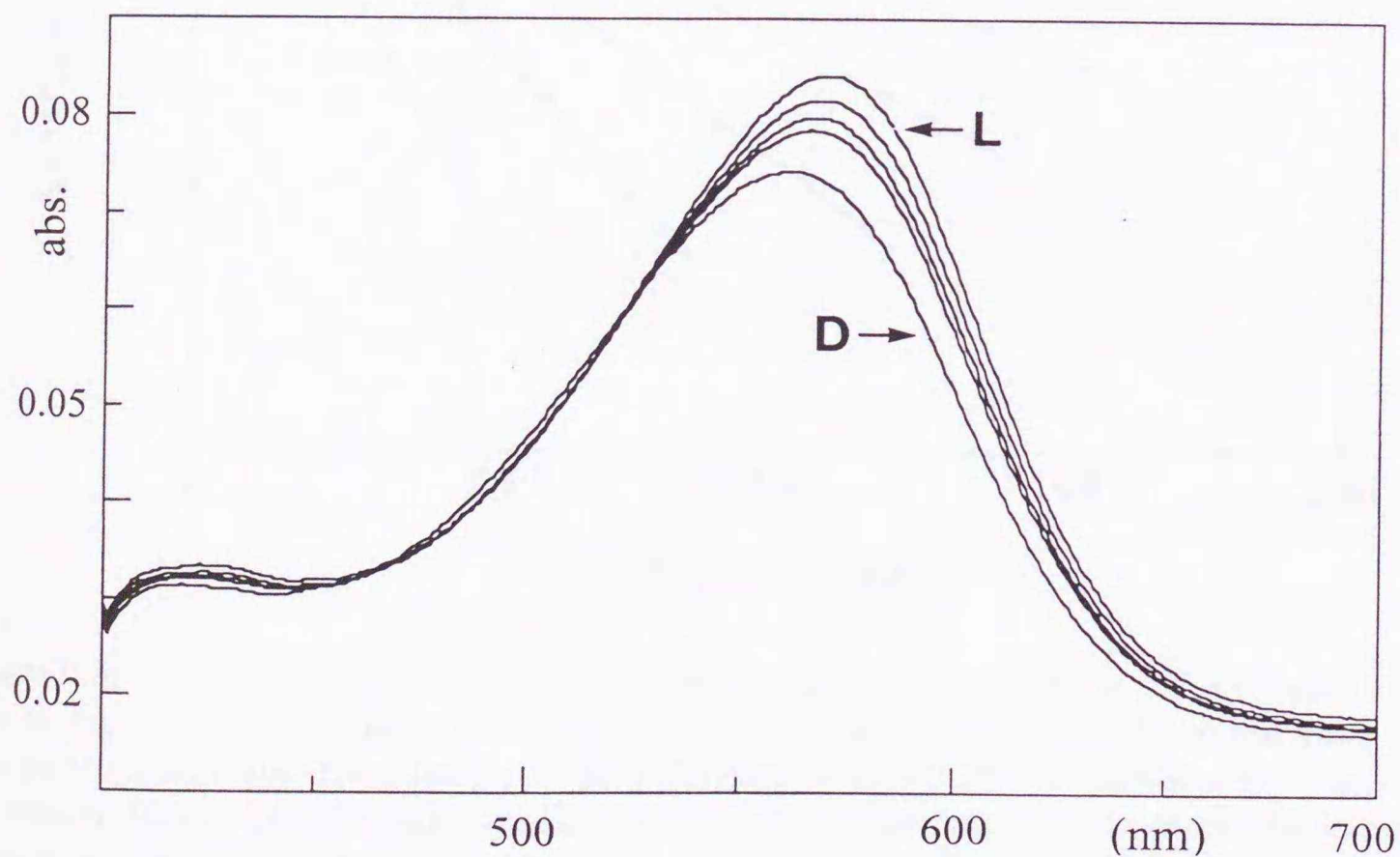

Figure 6.2: Time-dependent absorption spectra of an electrochemical cell with PM in the dark at pH 7.0 at 24°C after illumination. The magnitude of the absorption at 570 nm decreased with time. The light adapted cell (the uppermost trace, L), 15 min, 30 min, 45 min, and the dark-adapted cell (D). This absorption change corresponds to the peak amplitude shown in Fig. 6.1.

6.3.2   Temperature Effect on the Isomerization Rate

Figure 6.3 shows the time courses of the dark-adapted cell measured for various temperatures at pH 7.0. The isomerization rate strongly depended on the temperature, giving a lifetime (half-life) of 25 h, 5 h, 35 min, and 10 min at 5°C, 15°C, 30°C, and 48°C, respectively, whereas the ratio of the isomers was almost independent of the temperature in the range from 5°C to 48°C. This data agrees with the rates determined by Ohno et al. [84] in which the formation of the M intermediate was measured.
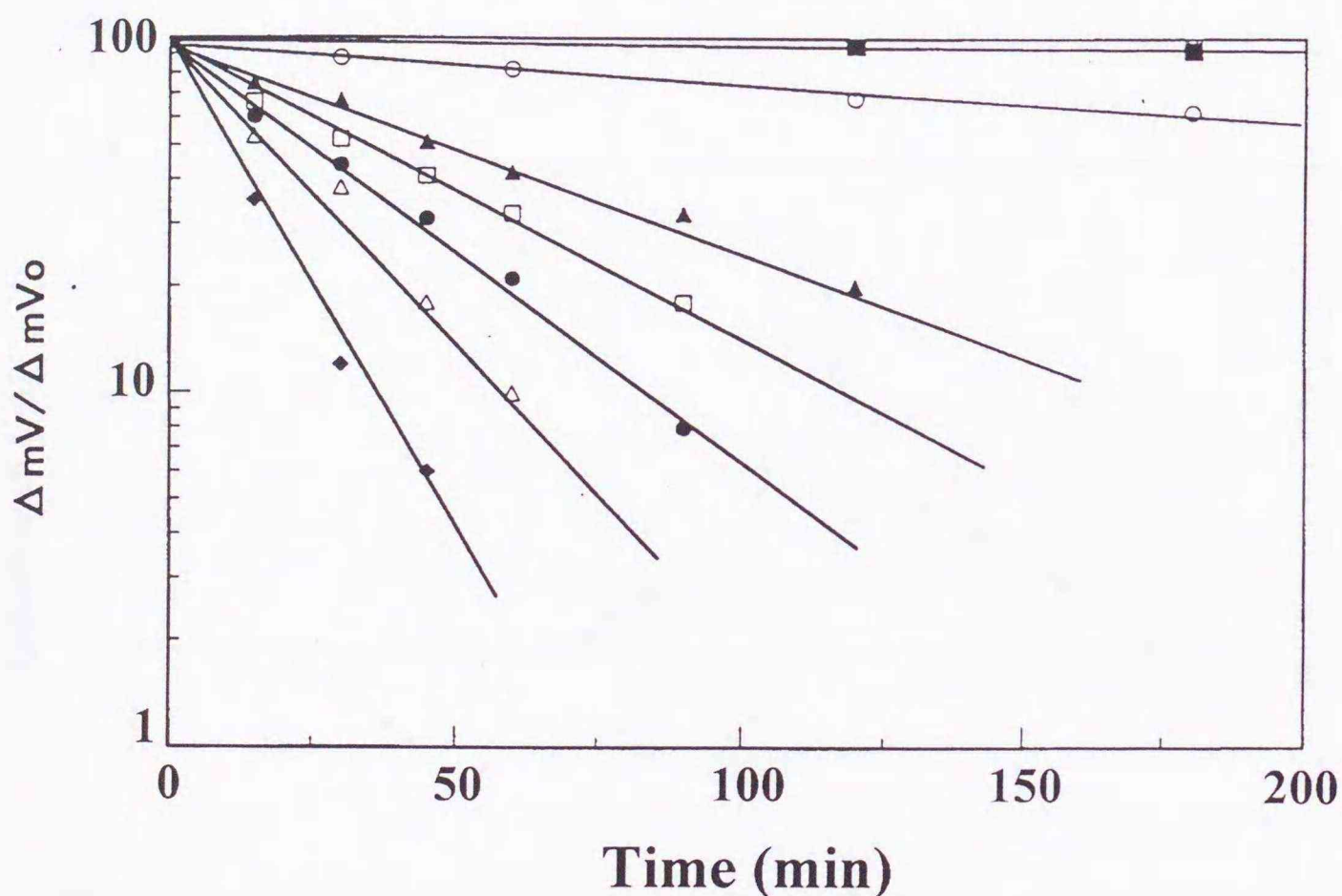

Figure 6.3: Kinetics of the dark-adaptation at various temperatures at pH 7.0 based on the data in Fig. 6.1. The amplitude changes ($\Delta mV/\Delta mV_0 \times 100$) are plotted versus time (min) on a logarithmic scale. Here ΔmV_0 is the difference in amplitude between the light-and dark-adaptations (L and D). The value of ΔmV is the value of the amplitude at each time minus the value of the amplitude of the dark-adaptation (D). Symbols: (■) 5°C; (○) 15°C; (▲) 24°C; (□) 30°C; (●) 34°C; (△) 38°C; (◆) 48°C.

6.3.3   pH Effect on the Isomerization Rate

Figure 6.4 shows the response profile at different pHs at 24°C, which is similar to that obtained by Robertson and Lukashev [85]. The amplitude and direction (or sign) of the

photoresponse strongly depended on pH. Figure 6.5 shows kinetics of dark-adaptation at different pHs at 24°C. Below pH 4.0, all-trans retinal is quickly isomerized to the 13-cis form in the dark and reached equilibrium. In the pH range of 5.0–10.0, the isomerization rate gradually decreased with increasing pH, becoming negligible at pH 11.0. The kinetic data at pHs 2, 5, and 11 (where the responses were small) were taken by electrically amplifying the response. The agreement between our data for the pH-dependence of the isomerization rate and the data obtained by Balashov et al. [86] using spectroscopy confirms that the photoelectric response in our cell is a direct measure of the isomer composition.
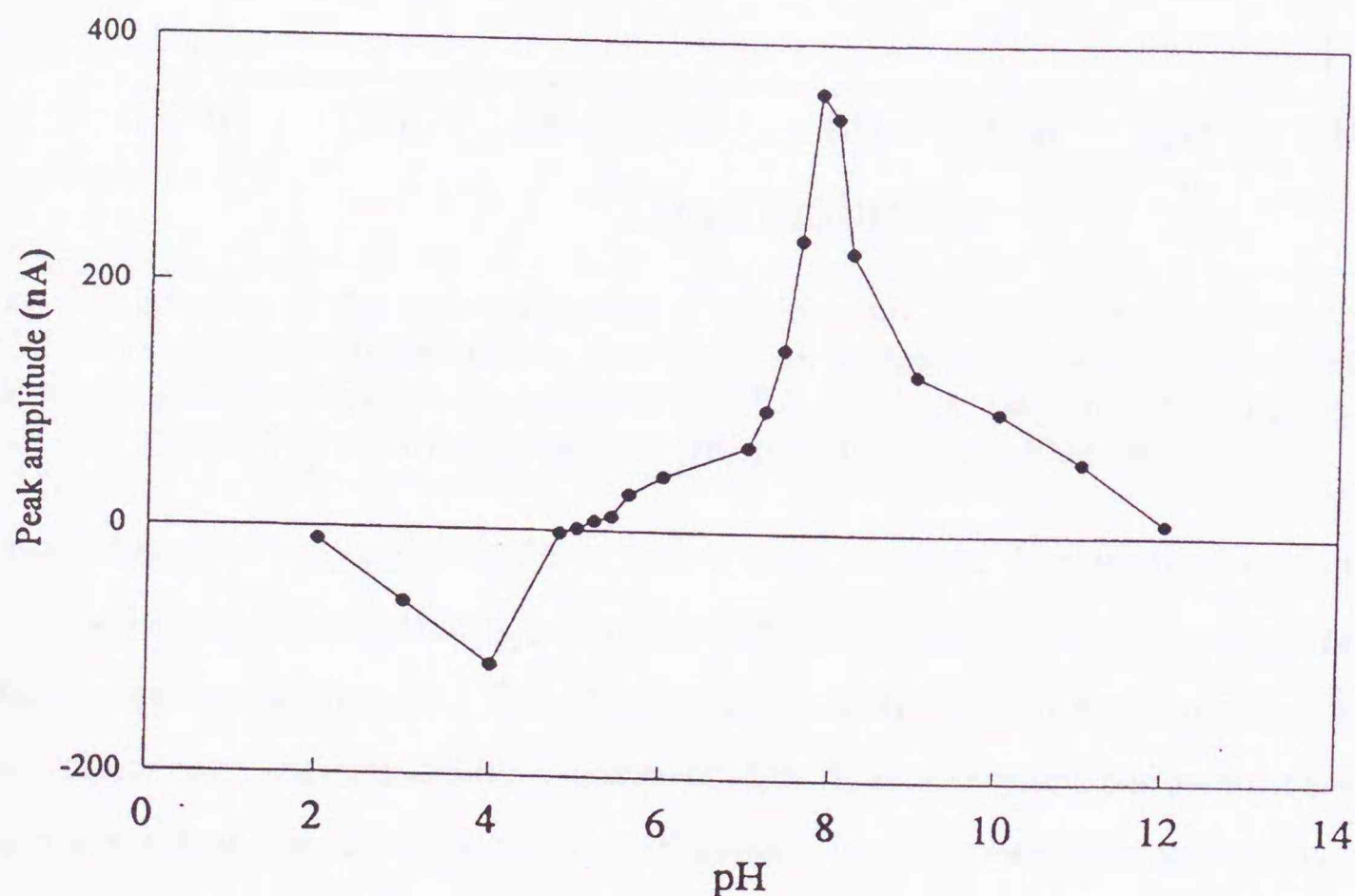

Figure 6.4: pH dependence of the peak amplitude of photoresponse from a electrochemical cell with PM at 24°C. The electrolyte was 0.1 M KCl with a mixture of buffers. The sign changes at between pH 4.8 and pH 5.0.

6.4 Discussion

In connection with the mechanism of the transient photocurrent, Robertson and Lukashev pointed out that the differential response of the photocurrents results from a surface
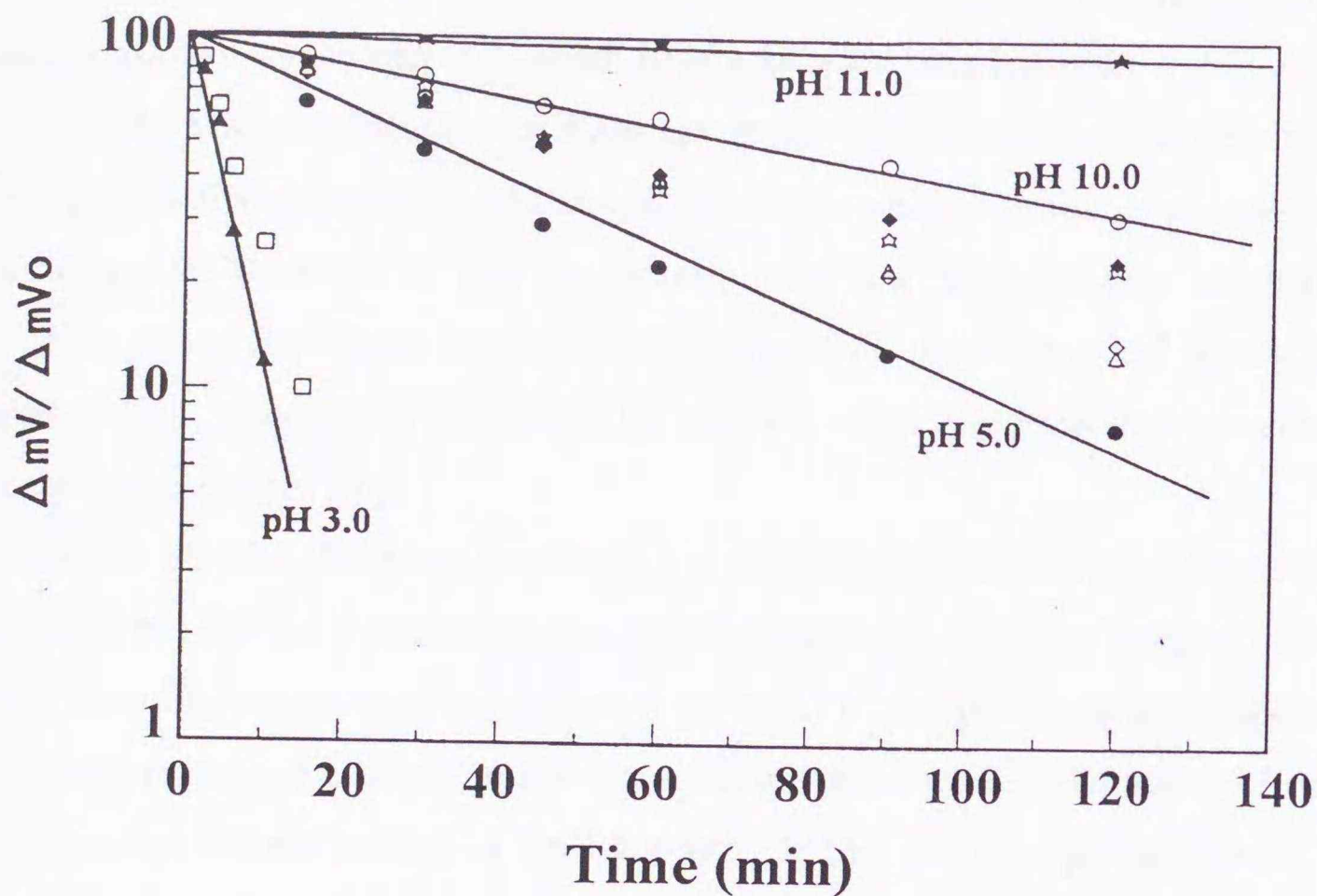
Figure 6.5: Kinetics of the dark-adaptation at different pH at 24°C. The amplitude changes ($\Delta mV/\Delta mV_0 \times 100$) are plotted versus time (min) on a logarithmic scale, where ΔmV_0 and ΔmV are the same as defined in the legend in Fig. 6.3. Symbols: (▲) pH 3.0; (□) pH 4.0; (●) pH 5.0; (△) pH 6.0; (◇) pH 7.0; (☆) pH 8.0; (◆) pH 9.0; (○) pH 10.0; (★) pH 11.0.

potential change of the oxide electrode rather than a charge displacement current [85]. Their experiments showed that a potential shift of the SnO_2 surface occurs when the proton concentration changes. The interpretation of Robertson and Lukashev is that proton release from the extracellular surface of PMs directed toward the electrode surface changes the pH at the electrode surface. However, a strong response still exists in our previous experiments where PMs are highly oriented with the cytoplasmic side directed to the electrode surface by using the antibody techniques [66].

The rate constant of thermal isomerization in the dark at <pH 4 is much faster than that at >pH 5 (Fig. 6.5), which is consistent with the protonation of Asp-85 being involved in catalyzing thermal isomerization process in bR. The data by Balashov et al. [86] suggests that thermal isomerization of the chromophore in the dark proceeds through a transient protonation of Asp-85, which is part of the counter ion of the Schiff base. In other word, the isomerization rate of all-trans to 13-cis in the dark is dependent on the

fraction of blue membrane in PM. The pH dependence of the isomerization rate for dark adaptation has two transitions [84], which have estimated pKa 2.9 and 9.6 [87].

According to evidence obtained by Balashov et al. [86], the pKa of Asp-85 is linked with the protonation state of the amino acid residue in which a proton is released to the extracellular side. Brown et al. [15] has recently identified this residue as Glu-204. The values of the pKa of Asp-85 are 2.6 and 7.5 when Glu-204 is protonated and deprotonated, respectively [88]. The pKa of Glu-204 is 9.7 and 4.8 when Asp-85 is deprotonated and protonated, respectively [16].

As shown in Fig. 6.4, the peak amplitude has a maximum value at pH 7.9 and almost zero between pH 4.8 (very small negative response) and pH 5.0 (very small positive response). This may reflect that the direction (or sign) of the photoresponse depends on the protonation state of Glu-204 in the active state (probably $L \longrightarrow M$ state) of bR. As Glu-204 does not release protons at <pH 4, proton uptake precedes proton release. This uptake elicits the negative photoresponse at the electrode.

Our results for the pH-dependence in the isomerization rate agree with the those by Balashov et al. [86], who shows that the pKa of Asp-85 has two values depending on the protonation state of Glu-204 and that the rate constant in the dark is directly proportional to the fraction of protonated Asp-85.

It is known that bR containing 13-cis retinal is not directly involved in the photocycle but can be photoisomerized to all-trans retinal via an another route [2]. Photoresponse of dark-adapted bR must originate from the all-trans retinal form of the pigment only, which undergoes to the photocycle. Thus, we determined the isomer ratio of retinal in bR in the dark.

6.5   Conclusions

Our photoelectric response method is simple and reliable, because the difference in the peak amplitude between in the light-and dark-adaptation is quite large (Fig. 6.1), thus making it easy to detect, and because a photocell with PM can be used repeatedly, thus saving time.

Our measurements using this method demonstrate that (a) the peak amplitude of the photoresponse of PM is related to the protonation state of Glu-204 and (b) the rate constant in the dark at different pHs is closely associated with the fraction of protonated Asp-85.

Chapter 7   Response Mechanism II: Relation between Photoresponse and Proton Translocation

7.1   Introduction

The retinal protein bacteriorhodopsin (bR) utilizes visible-light energy for the active transport of protons across cell membranes. Retinal is covalently bound to Lys-216 of the protein through a protonated Schiff base, forming a chromophore that absorbs at 570 nm. Initiated by the photoisomerization of the retinal from all-trans to 13-cis, bR passes through a number of spectroscopically distinct intermediates and returns to the initial state on the msec time-scale. During this cyclic reaction, the net unidirectional transfer of protons is accomplished by a geometrically controlled sequence of protonation and deprotonation of specific amino acids [13, 89]. Site-directed mutagenesis has proved to be a powerful means to reveal the molecular mechanism of the proton transfers. It was established that Asp-85 is the proton acceptor from the protonated Schiff base in the L to M transition of the photocycle. In about the same time range as the protonation of Asp-85, a proton is released to the extracellular protein surface via deprotonation of another amino acid residue, while Asp-85 remains protonated until the retinal reisomerizes to all-trans in the last step of the cycle [90]. In the reprotonation of the Schiff base during the M to N state transition Asp-96 acts as the proton donor from the cytoplasmic side.

It appears therefore, that acid-base equilibria involving a few amino acid residues strongly affects the photocycle and the proton transfers. At neutral pH, light-induced proton release to the extracellular surface takes place on the submillisecond time scale (in the L to M reaction), and proton uptake occurs in several milliseconds (in the M to N reaction). At higher pH, the proton uptake becomes slower because the reprotonation of Asp-96 (decay of N) is pH dependent. It has recently been suggested that the residue that releases the proton into the extracellular side on the formation of the M state is Glu-204 [15, 91]. In the unphotolyzed state, the pKa of Glu-204 is about 9 [87], but in the photocycle (during the L to M transition), it changes to about 6 [92]. At pH much

lower than 6, Glu-204 is therefore expected to remain protonated. Proton release is indeed delayed in the photocycle until the final O to bR transition. Asp-85, Asp-96 and Glu-204 thus function as key amino acids which participate in the proton pumping, together with several other residues in the retinal binding pocket [93, 94].

Charge transfer events of bR and mutants have been extensively studied by means of photoelectric measurements of oriented films [33], in which the protein was incorporated in lipid bilayer membranes separating two aqueous solutions [95, 96], adsorbed on a solid support in contact with aqueous solutions [97, 98], or electrodeposited on a conductive electrode to constitute a dry sandwich cell [99]. Light-induced voltage or current responses on various time scales have been obtained, which are ascribed to charge displacements during the photocycle. Wavelength-selected excitation of photocycle intermediates, such as M state, also yields electric response and its potential applications to optical information sensing have been studied [47]. We have studied photocurrent generation by thin Langmuir-Blodgett films of purple membranes (PM) immobilized at the electrode-aqueous electrolyte interface. Unidirectional transient photocurrents of time-differential responsivity were obtained which have been applied to fabricate optical sensors and a bR-based artificial photoreceptor [42, 48, 100].

In this Chapter, we report the results of photocurrent measurements conducted with bR mutants in which amino acids with major participation in proton pumping are replaced. Our particular interest in this study is to elucidate, with the electrochemical method, the origin of proton release on the extracellular surface which is coupled to the protonation of Asp-85. It was recently reported that the mutation of bR by replacing Glu-204 with Gln deactivates the proton release [15]. Glu-204 was therefore a strong candidate for the terminal proton release group. Our experiment using the mutant E204Q provides independent confirmation for this idea [101]. In addition to Glu-204, this measurement system suggested that another proton release group might be existed at the extracellular side.

7.2 Materials and Methods

The site-specific residue replacements D85N, D96N, E204Q, and E194Q were introduced in the bop gene and expressed in Halobacterium salinarium with a vector based on a halobacterial plasmid [102, 103]. The purple membranes (PMs) containing these mutants, as well as natural PM with wild-type bR, were purified by a standard method [39].

Construction of electrochemical cells that immobilize thin films of these samples basically follows our previously reported method [42], except for the film preparation process. PMs were suspended in deionized water at a concentration of about 1 mg/ml, and a thin film of PM was formed on the surface of a tin oxide electrode (40 nm-thick conductive SnO_2 layer coated on a glass support) by allowing a drop of a suspension spreaded on the surface to dry. These films have a random orientation of PM fragments on the electrode, and may be regarded as structurally equivalent to Langmuir-Blodgett films formed on the same kind of electrode [65], which is known to yield a sufficiently high photocurrent response in the method used here [66]. The PM-immobilized SnO_2 electrode and a counterelectrode (SnO_2-coated or platinum-coated glass) were in contact with an aqueous electrolyte containing 0.1 M KCl. The distance between the working electrode and the counterelectrode was 8 mm, which is filled with electrolyte. To maintain the pH between 2 and 12, a mixture of buffers (sodium phosphate, sodium borate, Mes, Hepes, and Mops) in deionized water, each at 20 mM, was used. The pH of the electrolyte was adjusted by the addition of HCl or NaOH.

As a light source to illuminate the sandwich-type thin electrochemical cell above, a 150W Xenon arc lamp in combination with an infrared cut-off filter and a band-pass filter was employed, which provided green light with an intensity maximum at 530 nm, a half-band width of 65 nm and an incident power at the electrode of about 10^{-2} W/cm^2. In kinetic investigations, a Nd-YAG pulse laser (Continuum, Surelite I), at 532 nm, with a light pulse width of 7 ns was employed.

For photocurrent measurements, a circuit comprising an operational amplifier in combination with a resistor (1 MΩ) was used to convert a small transient current into a dc voltage. Voltage signals were monitored on a Gould Model 420 and/or Hewlett Packard

Model 54520C digital storage oscilloscope. The RC time constant of the net circuit which limits the response time of the present measurement system was less than 20 μs. For laser pulse excitation, a current-voltage conversion circuit with a time constant less than a μs was used. All electrochemical measurements were performed under aerobic conditions at room temperature, using light-adapted bR samples unless otherwise stated.

7.3   Results and Discussion

7.3.1   Kinetic Profiles and the Origin of the Response

Illumination of the photocell with continuous light of constant intensity caused transient photocurrents with time-differential profiles. It has been previously confirmed that, in the potentiostatic condition using the three electrode system, the response of photocurrents is strongly rectified in the cathodic direction (the direction of electron transfer from the electrode to electrolyte side). This is true in the pH range 5-10, and within an extensive range of the electrode potential applied to the bR-coated SnO_2 [55]. This situation is unchanged in the present cell in which the bR-coated SnO_2 electrode is free of potentiostatic regulation. The observed photocurrent was maintained as cathodic in the pH range of 5-10. Its amplitude was shown to be proportional to the incident light intensity (number of incident quanta), as found previously [42]. With illumination at a constant intensity, the current is rapidly reduced to the zero level and turning off of light causes a transient negative spike of current whose amplitude is essentially equal to that of the positive one. A typical profile of photocurrent response for a bR film under green light excitation is shown in 2.2(b). The amplitude of the transient is a linear function of light intensity. The action spectrum of such photocurrents gave a peak around 560-570 nm and coincided with the optical absorption of bR, reproducing our previous observation [42].

As shown in Fig. 6.1, a comparison of a sequence of transient photocurrents have experienced different extents of dark adaptation. The bR-immobilized electrode was exposed to intense 530 nm light to establish a light adapted state of bR by monitoring saturation of the photocurrent output [80]. For completion of dark adaptation, it was kept in darkness at room temperature until its photoresponse amplitude was found to reach a minimum

value. The result shows that the photocurrent amplitude of a light-adapted electrode decreases with the time of dark adaptation until it is reduced to the level of 45% of the initial value. This change was reversible. The value 45% obtained by the prolonged dark adaptation is in good agreement with the 13-cis/all-trans isomer ratio of retinal in the dark-adapted state that is 45:55 [10, 11, 80, 84]. This coincidence, together with the fact that light-adapted bR contains virtually only all-trans retinal, indicates that the origin of the photoresponse is the all-trans retinal chromophore and the 13-cis isomer has little contribution to the signal.

Balashov et al. [86] suggested that thermal isomerization of the chromophore in the dark proceeds through a transient protonation of Asp-85, which is part of the counter ion of the Schiff base. In other words, the isomerization rate of all-trans to 13-cis in the dark is dependent on the fraction of blue membrane in PM. The pH dependence of the isomerization rate for dark adaptation has two transitions, which have estimated pKa's of 2.9 and 9.6 [26]. We have confirmed these phenomena by measuring the photoresponse in various pH in the dark [79].

In Fig. 7.1, time courses of the transient response measured after laser pulse excitation are exhibited for different pH values in the electrolyte. At neutral pH the response arises with a half time of about 100 μs, followed by a slower, millisecond range decay. When the electrolyte is alkaline (pH 10), both the rise and decay become several times slower than those measured at neutral pH. The observed rise time 100 μs at neutral pH closely corresponds to the time range 70-100 μs of the **L** to **M** state transition in the photocycle [92]. The **L** to **M** transition is also coupled with the release of proton on the extracellular surface which occurs in a similar time range of 71+4 μs [104]. The millisecond scale slow decay of response, on the other hand corresponds to the last step of the cycle involving the proton uptake process, **M** to **N** state transition of the time range 1 ms. These two processes in the photocycle are the consequences of proton transfers in the same direction. The directions of the current changes we measure, however, are opposite to each other.

As for the mechanism of the transient photocurrent, a recent paper of Robertson and Lukashev [85] pointed out that the differential response of the photocurrents is the result of a surface potential change of the oxide electrode rather than a charge displacement cur-
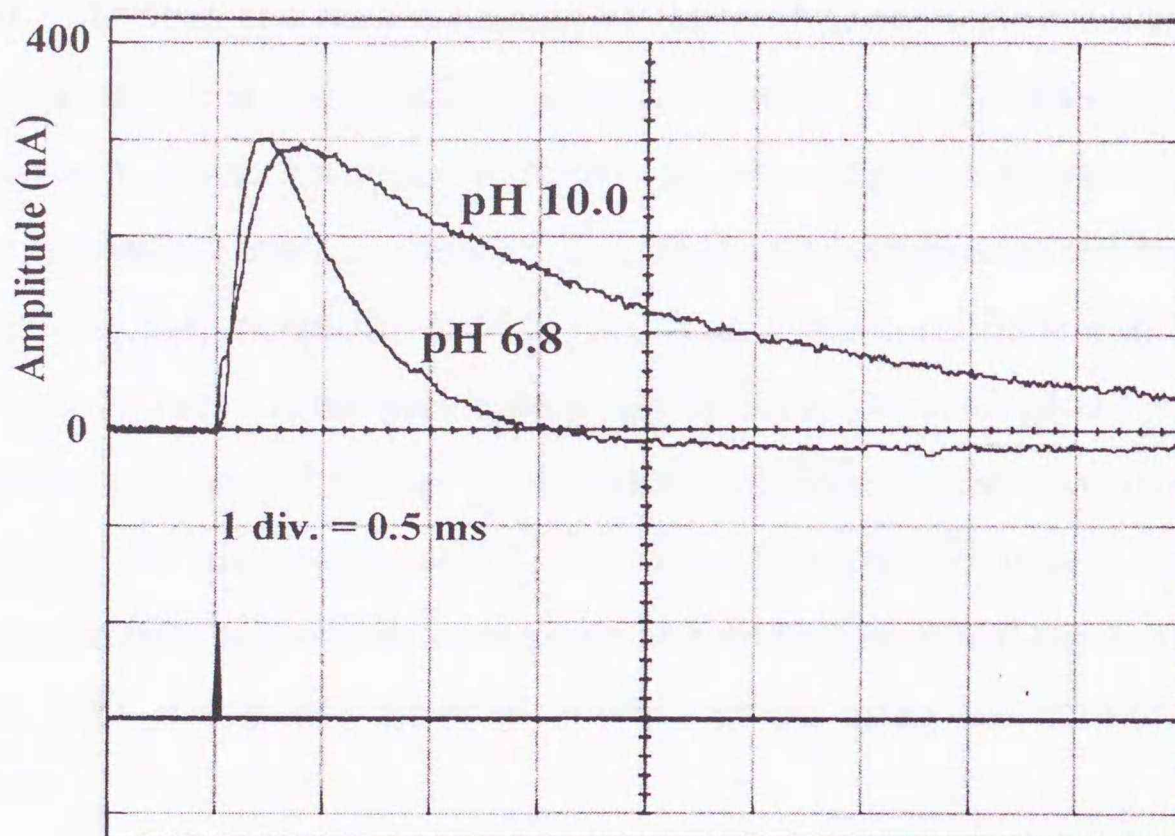
Figure 7.1: Comparison of kinetic profile for PM films at pH 6.8 and 10.0. The photocell was irradiated with laser light (a Nd-YAG pulse laser, at 532 nm) and the response was monitored with a digital storage oscilloscope.

rent, to which we had ascribed the mechanism. Their experiments showed that a potential shift of the SnO_2 surface occurs when the proton concentration changes, according to the Nernst equation, and they attributed the differential-type response of current to this. The mechanism for why the proton concentration change induces a transient current in the consequence of a surface potential change of an oxide electrode is the well established phenomenon that any oxide surface of metal and metal oxide electrodes undergoes a surface potential shift of the theoretical slope -59 mV/pH according to the Nernst equation. In photoelectrochemistry, this phenomenon has long been used to regulate the efficiency of dye-sensitized photocurrents on SnO_2 electrode. The interpretation of Robertson and Lukashev is that proton release from the extracellular surface of PMs directed toward the electrode surface changes the pH at the electrode surface. However, a strong response still exists in our previous experiments where PMs are highly oriented with the cytoplasmic side directed to the electrode surface by using the antibody techniques [66].

The results indicate the involvement of an electrochemical mechanism for current generation other than electrostatic charge displacement effects, which is independent of the

orientation of PM. That the time constants of rise and decay components in transient response correspond to the proton release and uptake steps, and that the signs of current change in these components are opposite, suggest an effect of proton concentration change around bR molecules on these components. The transient changes arise not from a spatial difference involving the orientation of PMs, but from a temporal difference between release and uptake. In Fig. 7.1, the prolonged decay of the response at pH 10 is most likely associated with the slowing of proton uptake that is reflected in the photocycle kinetics. More evidence that the photoresponse is a reflection of the transient proton concentration is confirmed by the simultaneous measurements of photoresponse and absorption changes of the protein [105] and is also provided in experiments using the mutants of bR, as described below.

7.3.2   Response Behavior of Mutant Systems

Fig. 7.2 shows a comparison of photocurrent response profiles obtained with the mutant proteins, D96N, D85N, E204Q and E194Q, measured at neutral pH. The films generated positive spikes of transient photocurrents upon onset of continuous illumination with green light, except for E204Q and E194Q. In the D96N mutant, an amply high response with a slow decay occurs on illumination but its negative response on switching off light is significantly reduced. This observation coincides with those of Robertson and Lukashev [85] using the same mutant. Suppression of the negative (anodic) response is consistent with their interpretation that the D96N with very slow proton uptake function does not cause a sufficiently rapid decrease of proton concentration to effect the transient capacitive current and thereby diminishes the response.

Charge displacement mechanisms, which have extensively been used to explain bR-induced photocurrents and voltages in bR-based photoelectric systems, should be also considered because such displacements actually exist in our samples. But, their contribution is not significant when the orientation of the PM is random. We obtained a response profile for a wild-type bR film in the alkaline condition similar to D96N. In the latter, the slow response is accelerated when azide is added, consistent with the more rapid decay of M under these conditions [106]. In the wild-type as well as in the mutant, the nega-
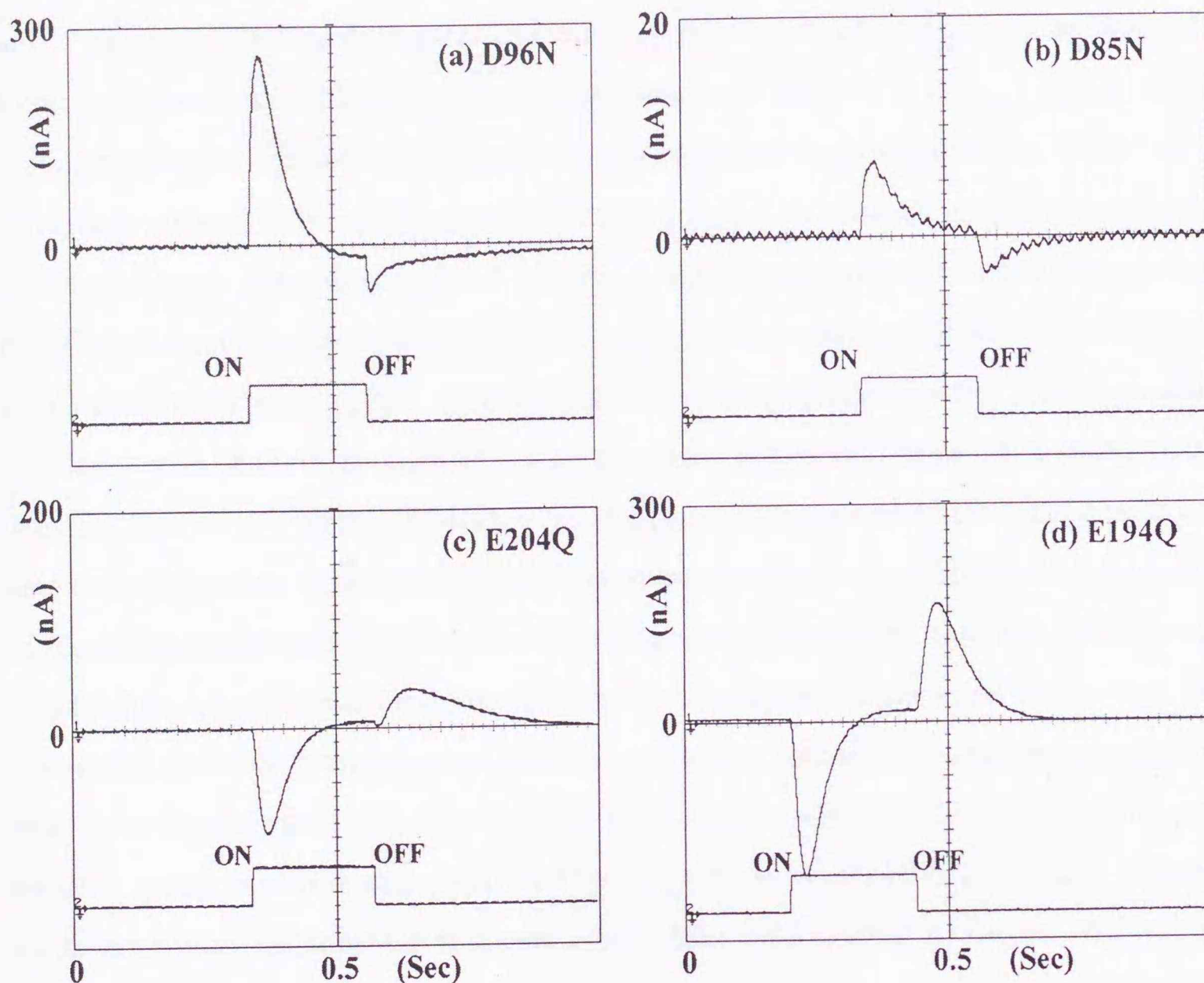
Figure 7.2: Response profiles of mutant proteins immobilized at the SnO₂/electrolyte interface at pH 7.8. Conditions are the same as shown in Fig. 2.2. (a) D96N, (b) D85N, (c) E204Q and (d) E194Q. The profile of wild-type is shown in Fig. 2.2(b).

tive response is also characterized as a slow current change of the millisecond time scale, corresponding to the proton uptake step in the bR photocycle.

The negative spike upon turning off the light originates from proton uptake by the protein that decreases the proton concentration of the electrolyte at the SnO₂ electrode-electrolyte interface. Thus, a pH increase that results from proton uptake yields a positive potential shift of SnO₂ surface which causes as a capacitive effect a transient anodic current (negative response), and vice versa: a pH decrease by proton release causes a transient cathodic current (positive response).

The mutant D85N gave only a weak response both in positive and negative regions

at the neutral pH (Fig. 7.2(b)). In D85N, the result is compatible with the fact that although proton transport does not occur, a small extent of proton release does, either from the cytoplasmic [12, 93] or the extracellular side [98].

In contrast, the mutant E204Q gave a quite different response pattern. First, its photoresponse proved to be in the opposite (anodic) direction with an amplitude comparable to the wild-type. Second, the photoresponse as well as the cathodic response on switching off light are considerably slower compared to the normal response of wild-type bR. In Fig. 7.2(c) the time course of the anodic transient photoresponse for the E204Q mutant is compared with that of the cathodic photoresponse of the wild-type. It is noted that the response time of the mutant E204Q is in a range of milliseconds which corresponds to the time range of proton uptake reaction in the photocycle [15]. This finding indicates, based on the above mentioned assignment of the response components, that the initial reaction in the light-excited E204Q is proton uptake. Such reaction occurs when the proton release process is inhibited in the mutant E204Q. According to the time-resolved spectroscopic analysis by Brown et al. [15], Glu-204 may be the origin of the postulated terminal proton releasing group, which is also confirmed by theoretical calculations [107]. Our photoelectric investigation collaborates this conclusion from independent evidence. We will show further evidence for this with the pH dependence data of the mutant photoresponse which follows.

7.3.3 pH Dependences of the Photoresponses of bR and the Mutants

Figure 7.3 shows the dependence of the peak amplitude of transient photocurrent on the pH of the electrolyte for wild-type bR and the mutants, D85N and E204Q. The profile of D96N is similar to that of wild-type as shown by Robertson and Lukashev [85]. The wild-type bR exhibits a maximum photocurrent at around pH 8 and almost zero between pH 4.8 (very small negative response) and pH 5.0 (very small positive response).

In acidic conditions of pH<5, photoresponse is changed to negative values. In the highly acidic region (<pH 3), the so-called blue membrane is formed, in which Asp-85 (pKa is about 2.6) is protonated. The protonated state of Asp-85 prevents the formation

of M intermediate and blocks the proton release. According to Balashov et al. [86] and Richter et al. [91], the pKa of Asp-85 is closely linked with the protonation state of the amino acid residue in which a proton is released to the extracellular side. In titration experiments in the absence of photoexcitation the values of the pKa of Asp-85 were found to be 2.6 and 7.5 when Glu-204 is protonated and deprotonated, respectively. The pKa of Glu-204 was 9.7 and 4.8 when Asp-85 was deprotonated and protonated, respectively [16, 91]. At pH below 5, Glu-204 is not capable of deprotonation in the photocycle. This is responsible for suppression of proton release in low pH region [92]. In highly alkaline conditions Glu-204 (pKa = 9.7 in the ground state) undergoes deprotonation, which again prevents release protons. As a result, the photocurrents decreases as the pH is increased above 8. The consequence of these pH dependencies for the wild-type is a complex pH effect on the photocurrent we observe that is in agreement of those previously measured for other photoelectric systems [85, 95, 108].

The mutant D85N showed a very weak response in all pH ranges (Fig. 7.3(b)). Although its pH dependence is obscured by suppressed response, its profile resembles the wild-type except for an reverse response region at high pH. The reduction of response amplitude comes from the deactivated photocycle, as explained above, due to the absence of the Schiff base proton acceptor. The reverse response occurring at increased pH, if any, may be attributable to the species with unprotonated Schiff base that becomes protonated after its photoexcitation [12], and thus would show transient proton uptake rather than release.

The mutant E204Q and E194Q showed a quite different dependence profile as shown in Fig. 7.3(c) and (d). Cathodic (positive) photoresponse is found only in the alkaline region of pH 9-12 although it is weak in amplitude. In other pH ranges, including the acidic region, photocurrent response with relatively high amplitude occurred in the anodic (negative) direction. This evidence corroborates our concept that the residues Glu-204 and Glu-194 function as the terminal proton releasers in bR. In E204Q, because there is assumed to be no terminal release group on the extracellular side, proton uptake occurs first [91] and it appears as a distinct anodic response as observed here. The weak cathodic response in the alkaline region is a sign of early proton release which is recovered at high

pH. An origin of this proton release may be cytoplasmic rather than extracellular side. In this regard, Tittor et al. [96], based on their experiments, proposed a possible inversion of proton translocation in some mutant systems. In the system where the proton release is entirely blocked on the extracellular side, the bR molecule would take other molecular mechanism to recover a part of proton transfer activity. This phenomenon, if it is the case, may be detectable only in the PM sample that lacks Glu-204.
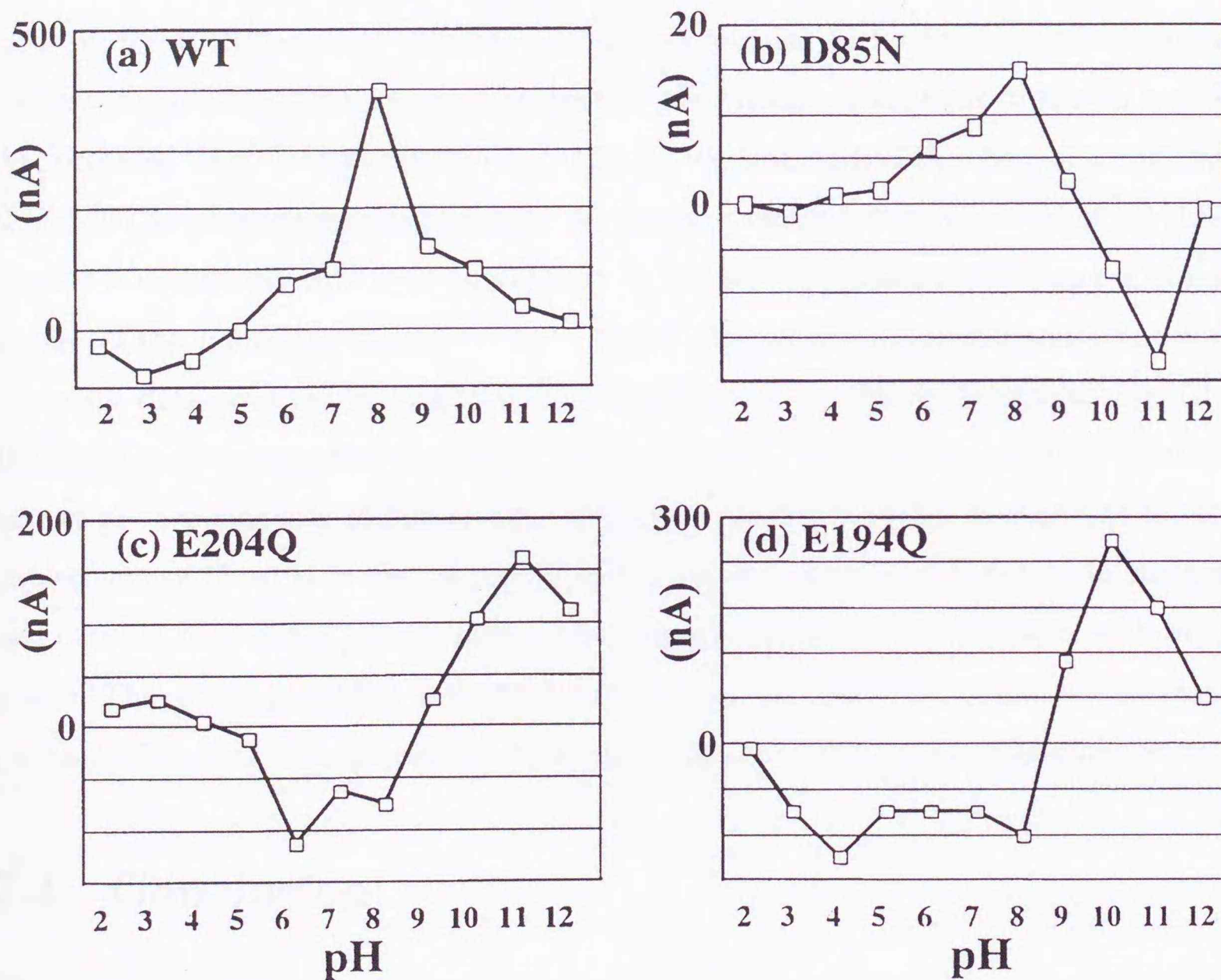

Figure 7.3: pH dependences of the response amplitudes of wild-type and several mutant proteins. The measurements were done by replacing the electrolyte with buffer solutions at different pHs (24 °C) in the photocell. (a) Wild-type, (b) D85N, (c) E204Q and (d) E194Q.

7.3.4   Another Proton Releasing Group

At low pH, protonation of Asp-85 is not accomplished by fast proton release. Instead, release takes place in the last step of the photocycle [92], after proton uptake occurs during the preceding $N \longrightarrow O$ transition, which corresponds to the negative response of wild type as shown in Fig. 7.3. The switch between the two types of proton release, "early", which correlates with the $L \longrightarrow M$ transition, and "late", which correlates with $N \longrightarrow O$ transition, depending on the pKa of the proton release group.

As shown in the previous Section, E204Q was revealed to be a proton release group because it shows negative response at neutral pH, which corresponds to proton uptake that precedes "late" proton release (Fig. 7.2(c)). We investigated the effect of a mutation of Glu-194 on photoelectric responsivity. In the most recent structure model of bR [109], Glu-194 is in the loose turn terminating helix F. The E194Q mutant shows features similar to that of the E204Q as shown in Fig. 7.2(d). This result is basically consistent with the recent data obtained by using the E194C-mutant [110]. This fact suggests that Glu-194, like Glu-204, is part of the proton release complex, which is also assumed from the data of pH dependencey shown in Fig. 7.3. There are two possible mechanisms for the involvement of Glu-194 in the process of proton release, direct and indirect. In the first case Glu-194 may directly participate in proton transfer and share a proton with other groups. The second possibility is that Glu-194 controls the pKa of the proton release group (probably Glu-204), through control of the conformation of this group, or its environment.

7.4   Conclusion

The mechanism for generation of photocurrent can be interpreted by considering the timing of proton release and uptake of bacteriorhodopsin at the interface in the electro-chemical cell, as shown in Fig. 7.4. First, oxide electrodes like SnO_2 are known to function as a pH sensor. This function is based on a surface potential shift obeying the Nernst equation as discussed in previous Section. For example, pH decrease causes a positive potential change that causes a cathodic current. When the light is turned on, bR releases protons and the proton concentration at near the electrode is raised rapidly. This causes

to generate a photocurrent. After that, bR starts to uptake protons. Under continuous illumination, the proton release and uptake are balanced and the current is offset to the zero level. Once the light is switched off, however, bR stops to release protons immediately but continues to uptake protons. This produces a response in the opposite direction.
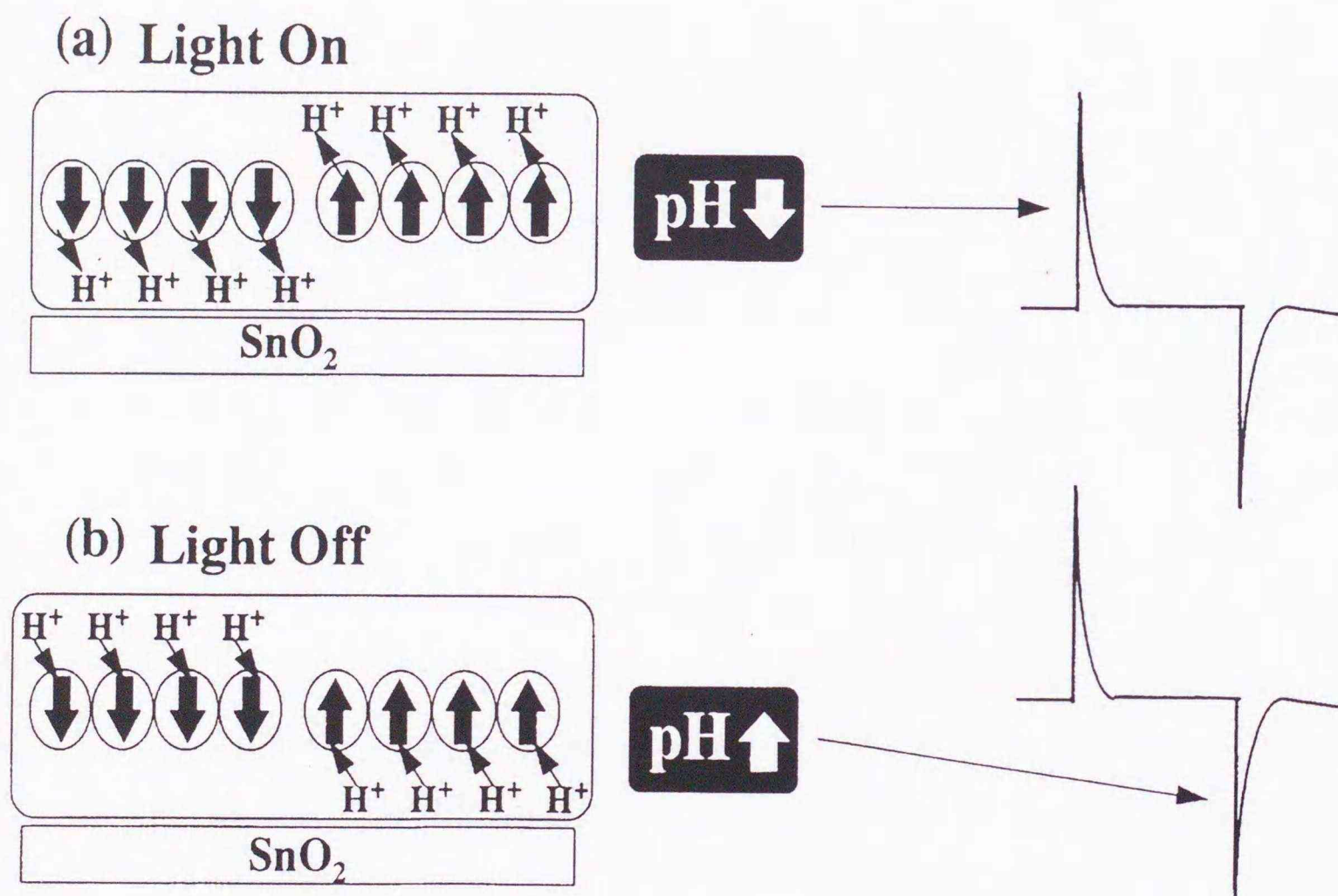

Figure 7.4: A possible mechanism for rectified photoresponse from a bR-based electrochemical cell. (a) When the light is turned on, the pH decreases at the electrode because bR releases protons. (b) When the light is turned off, the pH increases at the electrode because bR takes protons up after proton release is stopped.

By detecting transient currents at the electrode-electrolyte interfacial film of photoexcited bR and its mutants, the photoelectrochemical method is proving to be a useful means to elucidate the molecular mechanism of proton release and uptake processes in these proteins. The pH dependences of the amplitude and the sign of photocurrent, as well as their response kinetics, reflect independent activities of key proton releasing and uptaking residues. Our response measurements using the mutants E204Q and E194Q indicate that both Glu-204 and Glu-194 act as the key terminal proton releasing groups

in the extracellular side. Extension of this study to analysing the behavior of the E204Q and E194Q mutants in extreme conditions may be promising for elucidating side reactions that are supplementary to the main proton transfer process.

Chapter 8   Concluding Remarks

The results investigated in this thesis are summarized and are concluded as follows:

In Chapter 2, it was shown that visible light irradiation of an electrochemical cell containing PM produces a transient photocurrent with a peak value and direction dependent on the differential of the change in the light intensity. This function makes possible various types of optical image processing, such as mobile image extraction and edge detection, that are essential for visual information processing. This differential responsivity is in fact similar to the function of light sensing found in our visual reception.

In Chapter 3, to examine the visual information processing abilities of the cell, a similar sandwiched cell on a lithographycally patterned pixel network of Indium-tin oxide electrode, which has 256 pixels in a single electrode on a glass plate, was fabricated. Electric signals at the photoreceptor were amplified and finally output to a display panel having a 256-pixel array of light emitting diodes (LEDs). Using this system, optical images captured and processed by the photoreceptor are simultaneously visualized by forwarding the signals to a 2-dimensional display.

A unique function of the bR-based photoreceptor in image sensing is rapid and selective detection of a moving object. The photoreceptor can sense various optical images that impinge on or are scanned across the pixel array. Edge detection and contrast enhancement, which are significant steps in executing pattern recognition, are immediate applications of this sensing system. The oscillation of an image that is incident on the photoreceptor, thus simulating the eye movement in visual perception, has been investigated and shown to be capable of sensing still objects. The bR-based artificial photoreceptor can also function as a speed sensor and direction sensor. For example, direction sensing is done by vectorially distinguishing the edge component extracted from a moving image. Such technologies could evolve into the fabrication of light-receptive chips for blind people, which can be

73

referred to as visual prostheses [111].

In Chapter 3, a monoclonal antibody technique for determining the surface morphology of PM has been developed. Two types of antibodies for distinguishing the extracellular surface and the cytoplasmic surface of PM were produced by immunizing the corresponding synthetic peptides to mice. The LB method was employed to form a single-layer two-dimensional array of PM fragments on an electron microscope grid. The LB film was then treated with the antibodies which had been labeled with labeled with colloidal gold particles. Electron microscope observation revealed the orientation of PM, visualizing the morphology of the two surfaces of PM to be rough and smooth regions, respectively.

In Chapter 4, a rational method for constructing highly oriented films of PM has been established by using two kinds of bispecific (BS) antibodies with different antigen-binding sites, one binding a specific side of bR and the other a phospholipid hapten. A hapten monolayer deposited on a metal electrode was treated with a BS antibody solution and incubated with a PM suspension to produce a highly oriented PM film, as confirmed by electron microscopy in which immuno-gold labeling technique was used. This antibody-mediated PM monolayer was then used in the construction of a light-sensing photoelectric device.

Another promising extension of the antibody technique is in the preparation of the three dimensionally ordered crystal of bR molecules, starting with highly oriented two-dimensional bases. Multifunctional devices for optical information processing, including those endowed with nonlinear optical properties, will be within the scope of potential applications using three-dimensional oriented assemblies of bR.

In Chapter 5, It was revealed that the photoresponse was originated from all-trans retinal in the photocycle, that is, 13-cis retinal did not contribute to the response. The composition of retinal isomers in bR in PM was determined by photoelectric response measurements using a sandwich type electrochemical cell. The measured amplitude of the photocurrent obtained from a dark-adapted sample was 55% lower than that from a light-adapted sample. This ratio, 55 : 45, would correspond to the 13-cis/all-trans isomer ratio of retinal in the dark if the 13-cis form of the pigment did not give a response. The isomer ratio in the dark depended only weakly on the temperature of the electrolyte,

whereas the retinal isomerization rate strongly depended on the temperature and the pH of electrolyte in the cell. These results indicate that photoelectric response is elicited only by a species originating from bR containing all-trans retinal and that the behavior of the response in the dark is associated with the pKa of proton release kinetics of Asp-85.

In Chapter 6, light-induced transient photocurrents of bR (wild type) and its mutants Asp96→Asn (D96N), Asp85→Asn (D85N), Glu204→Gln (E204Q), and Glu194→Gln (E194Q) were measured at the interface of an electrode and the aqueous solution in an electrochemical cell. The ratio of the response amplitude between the light and dark adapted samples is constant indicating that only the all-trans retinal containing species are responsible for the photocurrent. The response time after laser pulse excitation (532 nm) was estimated to be about 100 μs. This fact suggests that the response may be due to the **L** to **M** transition in the photocycle. Transient positive (cathodic) photocurrents and negative (anodic) currents of randomly oriented films upon the onsets of continuous illumination and of turning off light, respectively, were investigated at different pH values. At pH < 5 the profile with the wild type is inverted. This pH dependence and the observed suppression of the response in the mutant D85N, and the lack of negative response in the mutant D96N, showed that the positive signal originates from the proton release and the negative one from proton uptake. Therefore, the response is dependent on the proton concentration near the electrode. Illumination of the mutant E204Q that lacks a protonatable residue at position 204 yielded a negative response, which suggests that in this protein proton uptake precedes proton release. This observation confirms measurements made earlier with pH indicator dyes, and indicates that terminal proton release depends on the Glu-204 residue.

However, in the course of these experiments, we found another proton release group. Substitution of Glu-194, a residue on the extracellular surface of bR, with glutamine (E194Q) showed a response profile similar to that of E204Q. This indicates that Glu-194 is a critical component of the proton release complex.

In summary, our studies demonstrate that the preparation of molecularly regulated bR monolayer films can be accomplished by using bispecific antibodies. The author believes that these techniques are key to the design and construction of more sensitive artificial

photoreceptors. The 2-dimensional pixelized image sensor described here can serve as a good retina model because the pixel size can be reduced if the sensitivity per pixel is increased. Our final goal is to produce an eye chip that can be surgically implanted into the eye, as shown in Fig. 8.1. Further development of such a chip may provide light perceptivity again to people who suffer from certain forms of blindness. This can be referred to as a visual prosthesis [111]. I hope that such a chip will be successfully used some day.
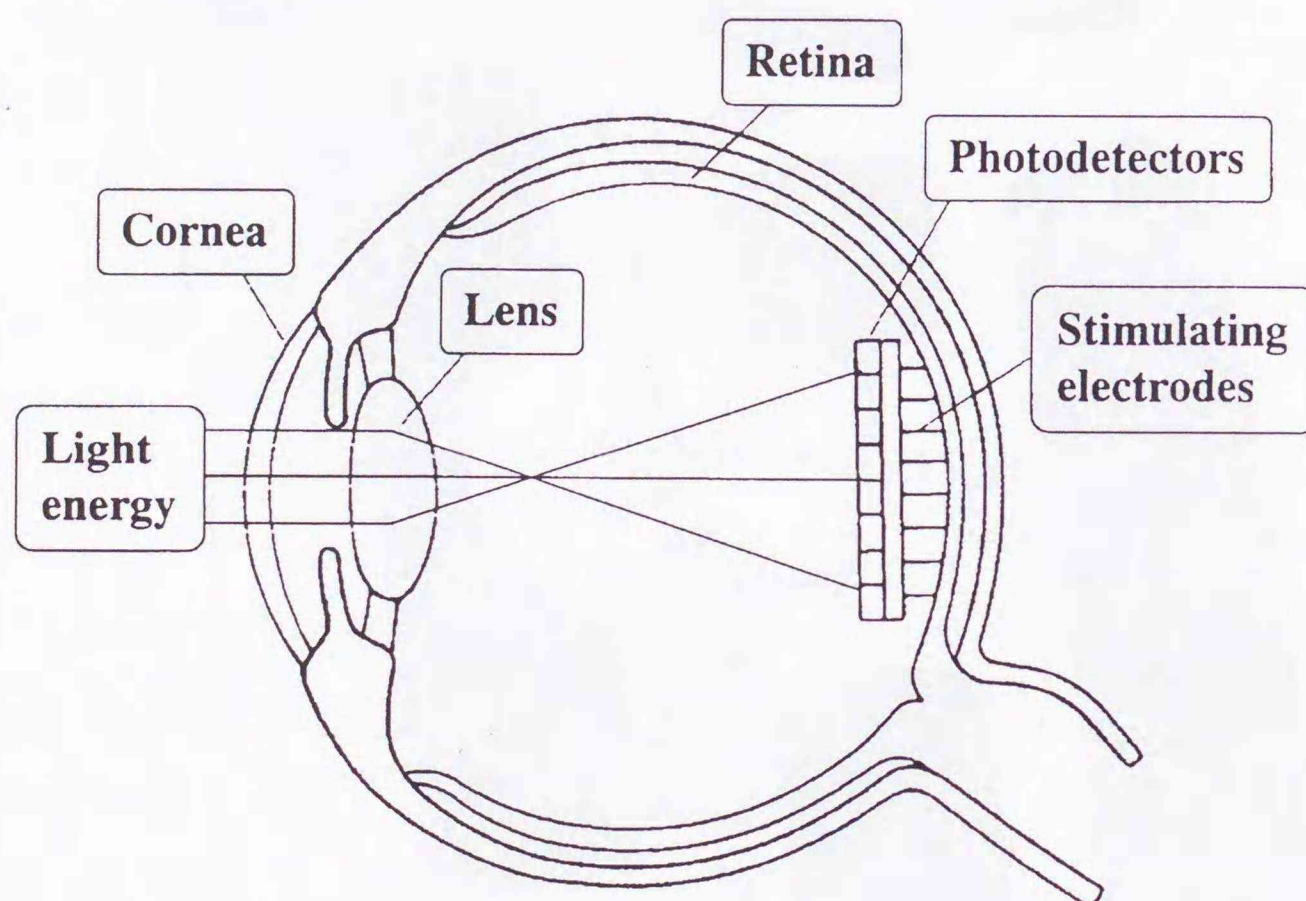
Figure 8.1: Eye chip: light-sensitive chip that can be surgically implanted into the eye to restore basic sight to people suffering from certain forms of blindness could bypass damaged photoreceptors in the retina.

In the basic aspects, photoelectric measurements of bR have proven to be very fruitful in elucidating the molecular mechanisms of light-driven proton pump. An excellent signal to noise ratio of this experiment system gave a clear discrimination between proton release and uptake of bR. By using this system, we have found Glu-194 participates in early proton release at the extracellular side, suggesting a possible new pathway for the proton translocation, as shown in Fig. 8.2. This approach is just coming into vogue and promises further insights into the molecular interactions between the chromophore and the protein.

A next interesting line of research concerns the comparison of bR to other retinal proteins, such as halorhodopsin [112, 113] and phoborhodopsin [114]. In fact, we have demonstrated that halorhodopsin acts as a proton pump in the presence of sodium azide, which will be published elsewhere [115].
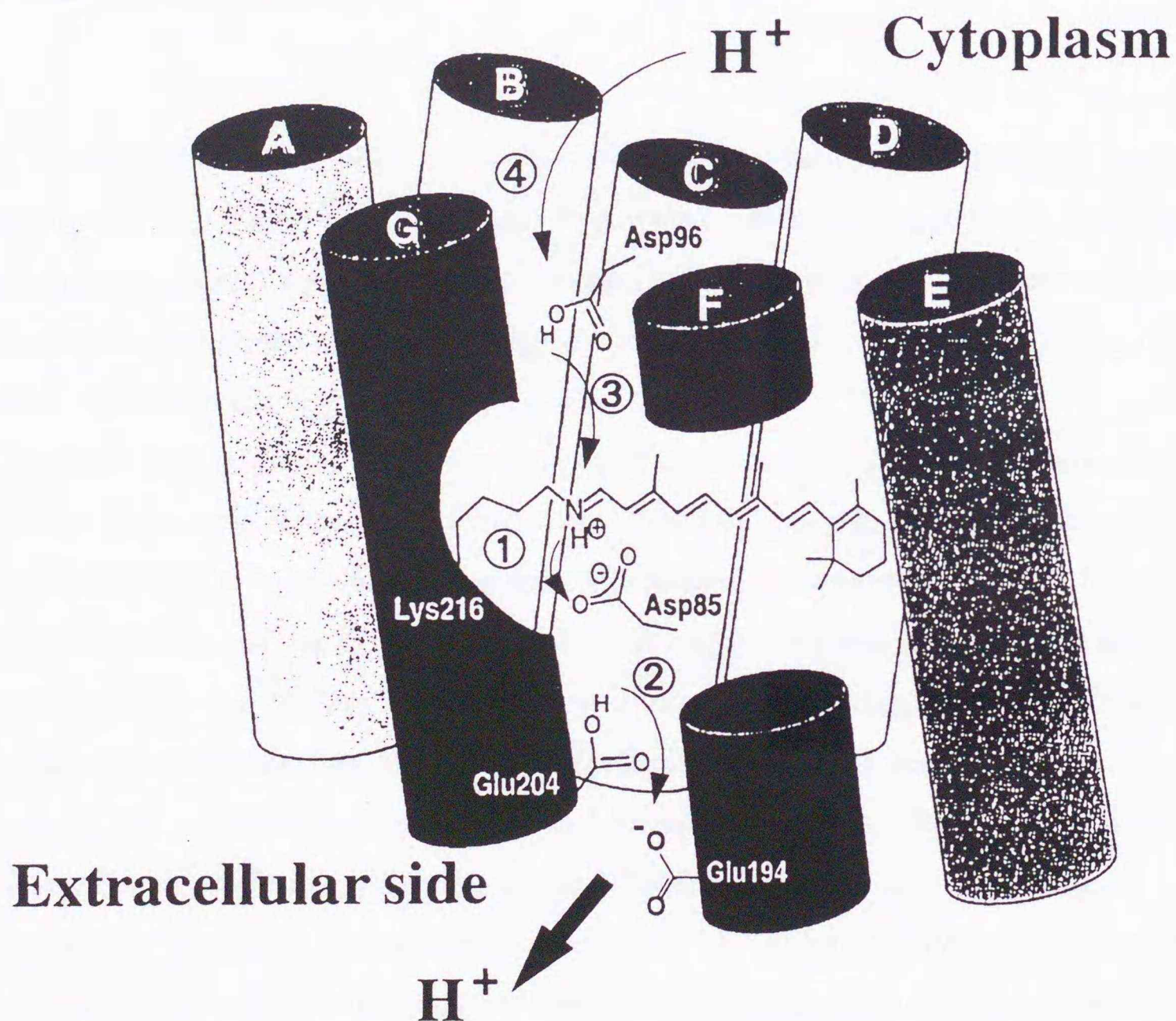

Figure 8.2: Schematic structure of a novel pathway for proton translocation in bR including the key amino acid residues.

This photoelectric method described in this thesis provides not only a novel artificial photoreceptor but does also a non-destructive analytic method capable of clarifying the function of ion transporting proteins. The author wishes this thesis contributes to the further development for constructing more sophisticated devices and to elucidate the mechanism of light-sensitive and ion transporting proteins.

Acknowledgements

References

[1] D. Oesterhelt and W. Stoeckenius, *Nature New Biol.* **233**, 149–152 (1971).

[2] W. Stoeckenius, R. H. Lozier, R. A. Bogomoloni, *Biochim. Biophys. Acta* **505**, 215–278 (1979).

[3] P. Mitchell, *Nature* **191**, 144–148 (1961).

[4] R. Henderson and P. N. T. Unwin, *Nature* **257**, 28–32 (1975).

[5] R. Henderson, J. M. Baldwin, T. A. Ceska, F. Zemlin, E. Beckman, K. H. Downing, *J. Mol. Biol.* **213**, 899–929 (1990).

[6] N. Grigorieff, T. A. Ceska, K. H. Downing, J. M. Baldwin, R. Henderson, *J. Mol. Biol.* **259**, 393–421 (1996).

[7] R. Dunn, J. McCoy, M. Simsek, A. Majumdar, S. H. Chan, U. L. RajBhandary, H. G. Khorana, *Proc. Natl. Acad. Sci. USA* **78**, 6744–6748 (1981).

[8] M.-J. Liao and H. G. Khorana, *J. Biol. Chem.* **259**, 4194–4199 (1984).

[9] L. Song, M. A. El-Sayed, J. K. Lanyi, *Science* **261**, 891–894 (1993).

[10] A. Maeda, T. Iwasa, T. Yoshizawa, *J. Biochem. (Tokyo)* **82**, 1599–1604 (1977).

[11] W. Sperling, P. Carl, C. Rafferty, N. Dencher, *Biophys. Struct. Mech.* **3**, 79–94 (1977).

[12] M. Kataoka, H. Kamikubo, F. Tokunaga, L. S. Brown, Y. Yamazaki, A. Maeda, M. Sheves, R. Needleman, J. K. Lanyi, *J. Mol. Biol.* **243**, 621–638 (1994).

[13] J. K. Lanyi, *Biochim. Biophys. Acta* **1183**, 241–261 (1993).

[14] H. G. Khorana, *Proc. Natl. Acad. Sci. USA* **90**, 1166–1171 (1993).

[15] L. S. Brown, J. Sasaki, H. Kandori, A. Maeda, R. Needleman, J. K. Lanyi, *J. Biol. Chem.* **270**, 27122–27126 (1995).

[16] S. P. Balashov, R. Govindjee, E. S. Imasheva, S. Misra, T. G. Ebrey, R. K. Crouch, D. R. Menick, *Biochemistry* **34**, 8820–8834 (1995).

[17] K. Racker, *Biochem. Biophys. Res. Commun.* **55**, 224–230 (1973).

[18] K. Singh, H. Korenstein, H. Lebedeva, S. R. Caplan, *Biophys. J.* **31**, 393–402 (1980).

[19] S. R. Caplan and G. Fisher, *J. Membrane Sci.* **16**, 391–405 (1983).

[20] E. P. Lukashev, S. Y. Zaitcev, A. A. Kononenko, V. P. Zubov, *Stud. Biophys.* **132**, 111–118 (1989).

[21] F. T. Hong, *BioSystems* **19**, 223–236 (1986).

[22] S. Y. Liu and T. G. Ebrey, *Biophys. J.* **54**, 321–329 (1988).

[23] S.-B. Hwang, J. I. Korenblot, W. Stoeckenius, *J. Membrane Biol.* **36**, 115–135 (1977).

[24] M. C. Blok, K. J. Hellingwerf, K. Van Dam, *FEBS Lett.* **76**, 45–50 (1977).

[25] L. A. Drachev, A. D. Kaulen, S. A. Ostroumov, V. P. Skulachev, *FEBS Lett.* **39**, 43–45 (1983).

[26] S. Kunugi, H. Yamada, Y. Nakamura, F. Tokunaga, A. Tanaka, *Polym. Bull.* **18**, 87–90 (1987).

[27] H.-W. Trissl, *Biochim. Biophys. Acta* **806**, 124–35 (1985).

[28] G. Váró, *Acta Biol. Acad. Sci. Hung.* **32**, 301–310 (1981).

[29] E. Bamberg, N. A. Dencher, A. Fahr, M. P. Heyn, *Proc. Natl. Acad. Sci. USA* **78**, 7502–7506 (1981).

[30] K. A. Fisher, K. Yanagimoto, W. Stoeckenius, *J. Cell Biol.* **77**, 611–621 (1978).

[31] A. Fahr, P. Lauger, E. Bamberg, *J. Membrane Biol.* **60**, 51–62 (1981).

[32] K. Nagy, *Biochem. Biophys. Res. Commun.* **85**, 383–390 (1978).

[33] H.-W. Trissl, *Photochem. Photobiol.* **51**, 793–818 (1990).

[34] Z. Chen and R. R. Birge, *TIBTECH* **11**, 292–300 (1993).

[35] R. R. Birge, *Annu. Rev. Phys. Chem.* **41**, 683–733 (1990).

[36] C. Bräuchle, N. Hampp, D. Oesterhelt, *Adv. Mater.* **3**, 420–428 (1991).

[37] H. Takei, A. Lewis, Z. Chen, I. Nebenzahl, *Appl. Opt.* **30**, 500–509 (1991).

[38] T. Furuno, K. Takimoto, T. Kouyama, A. Ikegami, H. Sasabe, *Thin Solid Films* **160**, 145–151 (1988).

[39] D. Oesterhelt and W. Stoeckenius, *Methods Enzymol.* **31**, 667–678 (1974).

[40] T. Miyasaka and K. Koyama, *Chem. Lett.* 1645–1648 (1991).

[41] T. Miyasaka, Y. Maekawa, K. Koyama, *Thin Solid Films* **180**, 73–75 (1989).

[42] T. Miyasaka, K. Koyama, I. Itoh, *Science* **255**, 342–344 (1992).

[43] T. Miyasaka and K. Koyama, *FUJIFILM R & D* **39**, 105–112 (1994).

[44] A. A. Kononenko, E. P. Lukashev, S. K. Chamorovsky, A. V. Maximychev, S. F. Timashev, A. B. Rubin, L. N. Chekulaeva, *Biochim. Biophys. Acta* **892**, 56–67 (1987).

[45] N. Hampp, D. Bräuchle, D. Oesterhelt, *Biophys. J.* **58**, 83–93 (1990).

[46] R. Simmeth and G. W. Reyfield, *Biophys. J.* **57**, 1099–1101 (1990).

[47] D. Haronian and A. Lewis, *Appl. Opt.* **30**, 597–608 (1991).

[48] T. Miyasaka and K. Koyama, *Appl. Opt.* **32**, 6371–6379 (1993).

[49] C. M. A. Pennartz and W. A. van de Grind, *Vision Res.* **30**, 1223–1234 (1990).

[50] T. Miyasaka and K. Koyama, *Oyobuturi* **61**, 1053–1067 (1992).

[51] Y. Shen, C. R. Safinya, K. S. Liang, A. F. Ruppert, K. J. Rothschild, *Nature* **366**, 48–50 (1993).

[52] K. Koyama, *Gendai Kagaku* **July**, 24–31 (1995).

[53] D. M. Engelman, R. Henderson, A. D. McLachlan, B. A. Wallace, *Proc. Natl. Acad. Sci. USA* **77**, 2023–2027 (1980).

[54] Y. Kimura, M. Fujisawa, A. Ikegami, *Biophys. J.* **45**, 615–625 (1984).

[55] T. Miyasaka and K. Koyama, *Thin Solid Film* **210/211**, 146–149 (1992).

[56] K. Kimura, T. L. Mason, H. G. Khorana, *J. Biol. Chem.* **257**, 2859–2867 (1982).

[57] Y. A. Ovchinnikov, N. G. Abdulaev, R. G. Vasilov, I. U. Vturina, A. B. Kuryatov, A. V. Kiselev, *FEBS Lett.* **179**, 343–349 (1985).

[58] R. Lerner, J. G. Sutcliff, T. M. Shinnick, *Cell* **23**, 309–310 (1981).

[59] R. S. Hodges, R. J. Heaton, J. M. R. Parker, L. Molday, R. S. Molday, *J. Biol. Chem.* **263**, 11768–11775 (1988).

[60] K.-S. Huang, M.-J. Liao, C. M. Gupta, N. Royal, K. Biemann, H. G. Khorana, *J. Biol. Chem.* **257**, 8596–8599 (1982).

[61] S.-B. Hwang, J. I. Korenblot, W. Stoeckenius, *J. Membrane Biol.* **36**, 137–158 (1977).

[62] M. S. Braiman, T. Mogi, T. Marti, L. J. Stern, H. G. Khorana, K. J. Rothschild, *Biochemistry* **27**, 8516–8520 (1988).

[63] T. Mogi, L. J. Stern, T. Marti, B. H. Chao, H. G. Khorana, *Proc. Natl. Acad. Sci. USA* **85**, 4148–4152 (1988).

[64] H. Otto, T. Marti, M. Holz, T. Mogi, M. Lindau, H. G. Khorana, M. P. Heyn, *Proc. Natl. Acad. Sci. USA* **86**, 9228–9232 (1989).

[65] N. Yamaguchi, Y. Jinbo, M. Arai, K. Koyama, *FEBS Lett.* **324**, 287–292 (1993).

[66] K. Koyama, N. Yamaguchi, T. Miyasaka, *Science* **265**, 762–765 (1994).

[67] E. E. Uzgiris and R. D. Kornberg, *Nature* **301**, 125–129 (1983).

[68] M. Brennan, P. F. Davison, H. Paulus, *Science* **229**, 81–83 (1985).

[69] A. McIntosh and F. Boucher, *Biophys. J.* **60**, 1–7 (1991).

[70] A. McIntosh and F. Boucher, *Biochim. Biophys. Acta* **1056**, 149–158 (1991).

[71] K. Koyama, *Nihon Yukagakkaishi* **45**, 715–722 (1996).

[72] K. Koyama, N. Yamaguchi, T. Miyasaka, *Adv. Mater.* **7**, 590–594 (1995).

[73] F. T. Hong, *Retinal proteins in photovoltaic devices, in: "Molecular and Biomolecular Electronics", Edited by R. R. Birge (ACS Advances in Chemistry Series No. 240, pp. 527-559* (Americal Chemical Society, Washington, DC, 1994).

[74] D. Oesterhelt, M. Meentzen, L. Schumann, *Eur. J. Biochem.* **40**, 453–463 (1973).

[75] K. Ohno, Y. Takeuchi, M. Yoshida, *J. Biochem. (Tokyo)* **82**, 1177–1180 (1977).

[76] M. J. Pettei, A. P. Yudd, K. Nakanishi, R. Henselman, W. Stoeckenius, *Biochemistry* **16**, 1955–1959 (1977).

[77] M. Tsuda, M. Glaccum, B. Nelson, T. Ebrey, *Nature* **287**, 351–353 (1980).

[78] P. Scherrer, M. K. Mathew, W. Sperling, W. Stoeckenius, *Biochemistry* **28**, 829–834 (1989).

[79] K. Koyama, *Photochem. Photobiol.* **66**, 784–787 (1997).

[80] G. Váró and K. Bryl, *Biochim. Biophys. Acta* **934**, 247–252 (1988).

[81] S. Smith, H. De Groot, R. Gebhard, M. Courtin, J. Lugtenburg, J. Herzfeld, R. Griffin, *Biochemistry* **28**, 8897–8904 (1989).

[82] L. Eisenstein, S. Lin, G. Dollinger, J. Odashima, K. Termini, K. Konno, N. Ding, K. Nakanishi, *J. Am. Chem. Soc.* **109**, 6860–6862 (1987).

[83] J. B. Ames, S. R. Bolton, M. M. Netto, R. A. Mathies, *J. Am. Chem. Soc.* **112**, 9007–9009 (1990).

[84] K. Ohno, Y. Takeuchi, M. Yoshida, *Biochim. Biophys. Acta* **462**, 575–582 (1977).

[85] B. Robertson and E. P. Lukashev, *Biophys. J.* **68**, 1507–1517 (1995).

[86] S. P. Balashov, E. S. Imasheva, R. Govindjee, T. G. Ebrey, *Biophys. J.* **70**, 473–481 (1996).

[87] S. P. Balashov, R. Govindjee, M. Kono, E. S. Imasheva, E. Lukashev, T. G. Ebrey, R. K. Crouch, D. R. Menick, Y. Feng, *Biochemistry* **32**, 10331–10343 (1993).

[88] S. P. Balashov and T. G. Ebrey, *The Spectrum* **7 (3)**, 1–8 (1994).

[89] M. P. Krebs and H. G. Khorana, *J. Bacteriol.,* **175**, 1555–1560 (1993).

[90] O. Bousché, S. Sonar, M. P. Krebs, H. G. Khorana, K. J. Rothschild, *Photochem. Photobiol.,* **56**, 1085–1095 (1992).

[91] H. T. Richter, L. S. Brown, R. Needleman, J. K. Lanyi, *Biochemistry* **35**, 4054–4062 (1996).

[92] L. Zimányi, G. Váró, M. Chang, B. Ni, R. Needleman, J. K. Lanyi, *Biochemistry.* **31**, 8535–8543 (1992).

[93] Y. Cao, G. Váró, A. L. Klinger, D. M. Czajkowsky, M. S. Braiman, R. Needleman, J. K. Lanyi, *Biochemistry* **32**, 1981–1990 (1993).

[94] R. Govindjee, S. Misra, S. P. Balashov, T. G. Ebrey, R. K. Crouch, D. R. Menick, *Biophys. J.,* **71**, 1011–1023 (1996).
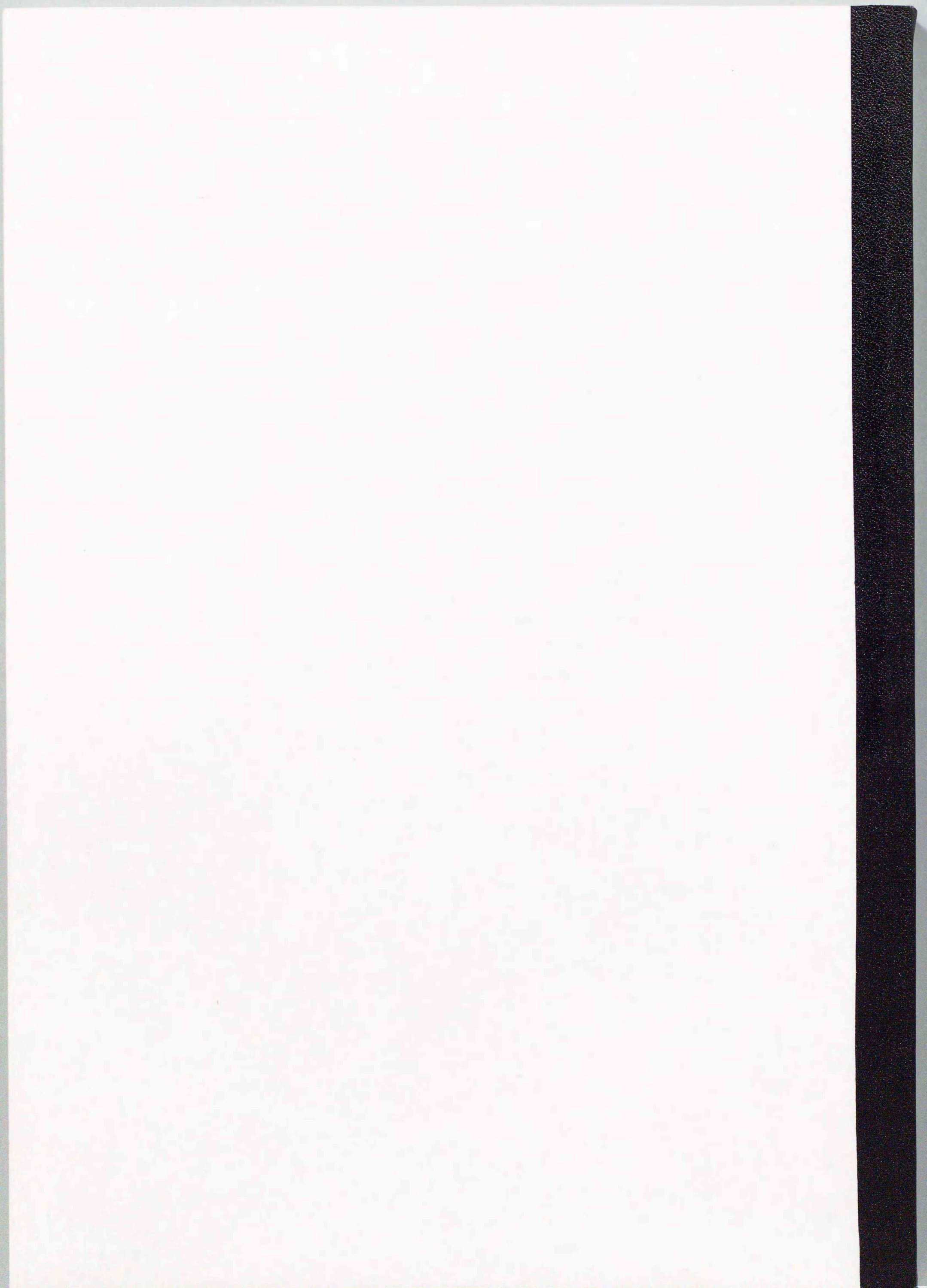
[95] F. Hong, *IEEE Eng. Med. Biol.* **13**, 75–93 (1994).

[96] J. Tittor, U. Schweiger, D. Oesterhelt, E. Bamberg, *Biopys. J.* **67**, 1682–1690 (1994).

[97] S. Y. Liu, *Biophys. J.* **57**, 943–950 (1990).

[98] S. Moltke, M. P. Krebs, R. Mollaaghababa, H. G. Khorana, M. P. Heyn, *Biophys. J.,* **56**, 1085–1095 (1995).

[99] G. Váró and L. Keszthelyi, *Biophys. J.* **43**, 47–51 (1983).

[100] T. Miyasaka and K. Koyama, *The Spectrum* **6 (1)**, 13–16 (1993).

[101] K. Koyama, T. Miyasaka, R. Needleman, J. K. Lanyi, Photoelectrochemical evidence for proton release and uptake in bacteriorhodopsin and its mutants, *Submitted to Photochem. Photobiol.*

[102] B. Ni, M. Chang, J. K. Lanyi, R. Needleman, *Gene,* **90**, 169–172 (1990).

[103] R. Needleman, M. Chang, B. Ni, G. Váró, J. Fornés, S. H. White, J. K. Lanyi, *J. Biol. Chem.,* **266**, 11478–11484 (1991).

[104] U. Alexiev, R. Mollaaghababa, P. Scherrer, H. G. Khorana, M. P. Heyn, *Proc. Natl. Acad. Sci. USA* **92**, 372–376 (1995).

[105] K. Koyama, F. Tokunaga, R. Needleman, J. K. Lanyi, Photovoltaic effects of bacteriorhodopsin and its mutants; the relationship between the photoresponse and the M intermediate, *To be submitted.*

[106] R. Miller and D. Oesterhelt, *Biochim. Biophys. Acta* **1020**, 57–64 (1990).

[107] R. V. Sampogna and B. Honig, *Biophys. J.* **71**, 1165–1171 (1981).

[108] P. Ormos, S. Hristova, L. Keszthelyi, *Biochim. Biophys. Acta* **809**, 181–186 (1985).

[109] Y. Kimura, D. G. Vassylyev, A. Miyazawa, M. Kidera, A. Matsushima, K. Mitsuoka, K. Murata, T. Hirai, Y. Fujiyoshi, *Nature* **389**, 206–211 (1997).

[110] S. P. Balashov, E. S. Imasheva, T. G. Ebrey, N. Chen, D. R. Menick, R. K. Crouch, *Biochemistry* **36**, 8671–8676 (1997).

[111] K. Cha, K. W. Horch, R. A. Normann, D. K. Boman, *J. Opt. Soc. Am. A* **9**, 673–675 (1992).

[112] G. Váró, L. Zimányi, X. Fan, L. Sun, R. Needleman, J. K. Lanyi, *Biophys. J.* **68**, 2062–2072 (1995).

[113] G. Váró, L. Brown, R. Needleman, J. K. Lanyi, *Biochemistry* **35**, 6604–6611 (1996).

[114] J. Hirayama, Y. Imamoto, Y. Shichida, N. Kamo, H. Tomioka, T. Yoshizawa, *Biochemistry* **31**, 2093–2098 (1992).

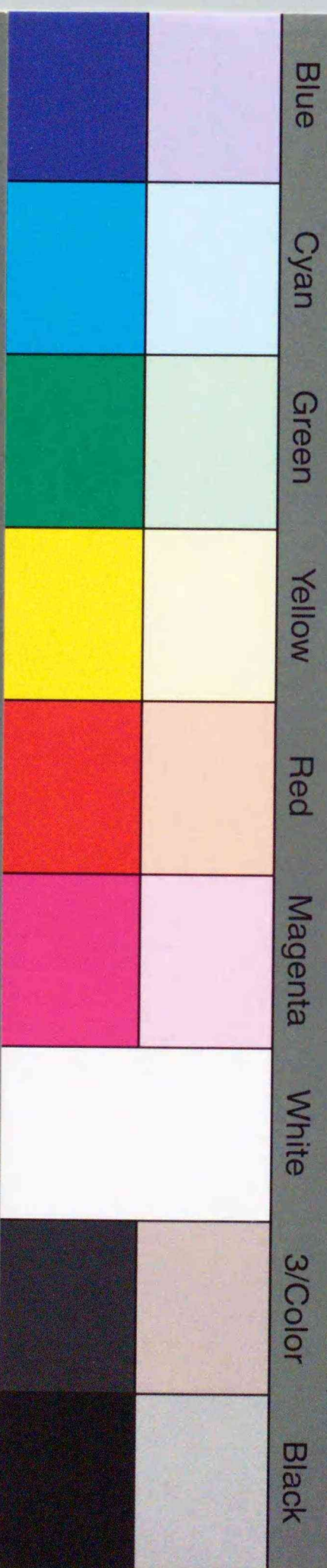[115] K. Koyama, M. Sumi, N. Kamo, J. K. Lanyi, Photoelectric response from halorhodopsin, *To be submitted*.